TECHNISCHE UNIVERSITÄT MÜNCHEN

FACHGEBIET FÜR THEORETISCHE CHEMIE

Hydrosilylation of Alkenes Catalyzed by *Bis*-N-Heterocyclic Carbene Rh(I) Complexes

A Density Functional Theory Study

Dipl. –Chem. Univ. Yin Wu

Vollständiger Abdruck der von der Fakultät für Chemie der Technische Universität München zur Erlangung des akademischen Grades eines

Doktors der Naturwissenschaften (Dr. rer. nat.)

genehmigten Dissertation.

Vorsitzender: Univ.–Prof. Dr. K. Köhler

Prüfer der Dissertation:

1. Univ.–Prof. Dr. Dr. h.c. N. Rösch, i. R.
2. Univ.–Prof. Dr. Dr. h.c. B. Rieger

Die Dissertation wurde am 14.04.2014 bei der Technischen Universität München eingereicht und durch die Fakultät für Chemie am 08.05.2014 angenommen.

Acknowledgment

First and foremost, I want to give my deepest thanks to my Doktorvater, Prof. Dr. Notker Rösch, for giving me the opportunity to do the doctoral thesis in his research group. This dissertation would not have been completed without his guidance and support. Under his supervision, I learned a lot about how to meet academic challenges. The knowledge I gained over these years is very valuable to me.

I owe a debt of gratitude to Dr. Alexander Genest, without whose help I would never have learned how to approach a scientific task and resolve essential problems. He also showed me how to communicate efficiently in a team. I am truly thankful to Prof. Dr. Rieger and all colleagues from the Wacker Institute of Silicon Chemistry for the interdisciplinary discussions. It is a pleasure to thank Dr. Virve Karttunen for providing me with the background knowledge about this interesting and complex topic, and for her patience and encouragement, especially in the initial phase of this project. I would like to thank Dr. Ion Chiorescu for helping me improve my calculation skills and for many inspiring discussions. I thank Dr. Sven Krüger for many general scientific discussions and administrative supports. I appreciate deeply administrative support by Dr. Miriam Häberle, Dr. Agnes Mirescu, Ms. Annemarie Meinel, Ms. Barbara Asam, and Ms. Elisabeth Wurm. I thank my colleagues for sharing their scientific interests with me in group seminar and other talks, and for various help with both scientific and non-scientific issues. I thank Dr. Duygu Başaran, Dr. Konstantina Damianos, Dr. Wilhelm Eger, Dr. Alena Kremleva, Dr. Alexei Matveev, Dr. Remi Marchal, Dr. Astrid Nikodem, Dr. Shane Parker, Dr. Zhijian Zhao, Dr. Shranbani Dinda, Dr. Agalya Govindasamy, Dr. Xiufang Ma, Dr. Suwit Suthirakun, Dr. Lili Zhao, Cheng-Chau Chiu, Chun-Ran Chang, Bo Li, Thomas Soini, Benjamin Chen, and Boxiao Zheng, as well as those not mentioned here.

I want to give special thanks to my friends for many memorable moments, Mrs. Katia Rodewald, Dr. Heiner Eckert, Dr. Zer-Rur Huang, Dr. Shiang-Bor Huang, Dr. Lei Lei, Dr. Yun Zhang, Dr. Bo Zhang, Yang Liu, Katharina Wussow, Xiaoxiao Du, Nan Zou, Tongyu Wang, Dr. Xiaojun Liu, Ping Lu, Hong Li, Thi-Thoa Nguyen, Gia Hoang, Daniel Nguyen, Puyee Wong, Shuomei Huang, Huiyi Loy, Will Chua, Pricilla Chua, Ying Yuan Wong, and many more. I am grateful to the Plum Village Sangha in Munich, Waldbröl, and Singapore. I also thank all sisters and brothers I met in Fo Guang Shan and Tzu Chi. My warmest thanks are due to my mother who gives me a great deal of understanding and freedom.

Finally, I gratefully acknowledge Wacker Chemie AG for awarding me a scholarship.

“Is the Master out of his mind?” she asked me.
I nodded.
“And he's taking you with him?”
I nodded again.
“Where?” she asked.
I pointed towards the center of the earth.
“Into the cellar?” exclaimed the old servant.
“No,” I said, “farther down than that.”

Jules Verne, *Journey to the Center of the Earth*

Contents

1 Introduction

Hydrosilylation is a family of catalytic transformations for the preparation of organosilicon compounds.[1] It describes the addition of a Si−H bond across unsaturated bonds, such as C−C, C−O, and C−N multiple bonds in alkenes, alkynes, ketones, and imines.[1] Among these reactions, the hydrosilylation of a C−C multiple bond is of particular interest in the context of introducing chemical functions in silicon compounds.[2] In this process, a C−Si bond is formed, which rarely occurs in nature.[3] The synthesis of such compounds make a great contribution to drug design.[4] In addition, a variety of organosilicon compounds are commercially utilized or being produced on an industrial scale, above all pressure sensitive adhesives,[5,6] binders at specific manufacturing,[6] silicon rubber,[7,8] and paper-release coatings.[9,10] Recently, synthesis of novel compounds based on an octahedral silicon center was reported.[11,12] Being a new class of structural template which can be synthesized in a straight forward fashion, the application of hydrosilylation in the field of chemical biology is highly likely.[11] Besides the generation of all the above mentioned silicon-containing final products, hydrosilylation is also an important process for preparing chemical versatile intermediates in organic synthesis, which carry the low cost and low toxic silyl moiety, one of the frequently chosen long-term protective groups.[13]

Along with the development of catalytic processes for hydrosilylation, which are predominantly homogeneous,[14,15] various mechanisms were proposed for a number of catalytic systems, e.g., the hydrosilylation of ketones by Gade's catalysts based on rhodium,[16,17] the hydrosilylation of alkynes by a series of ruthenium cyclopentadienyl complexes,[18-20] and the hydrosilylation of alkenes by ruthenium complexes bearing spectator ligands.[21-24] It is notable that for the latter group of catalytic reactions, theoretical studies have indicated that the mechanism can depend strongly on the choice of the reactant and on the ligands at the metal center.[21-24] Whereas the reactants in each catalytic process may vary as the circumstances require, the modification and improvement of transition-metal catalysts has become an extensively studied field in both experimental organometallic chemistry[25] and computational chemistry.[26]

Recently it was found that transition-metal NHC (N-heterocyclic carbene) complexes are catalytic active in several hydrosilylation processes.[1] Especially some Rh-NHC complexes turned out to be applicable catalysts in the hydrosilylation of ketones[27] and alkynes.[28,29] The NHC ligand brings along the advantage that it enables a moderately to highly enantioselective hydrosilylation of ketones when the catalyst is modified in an asymmetric

fashion.[30] The structures of chiral mono-NHC substituted rhodium complexes were studied by density functional (DF) calculations.[31]

Most recently, an analogous application of Rh–NHC complexes in the hydrosilylation of alkenes was reported.[32] If rhodium catalysts can be optimized in activity and selectivity with respect to this catalytic process, they should be more economical than the currently applied platinum catalysts.[33-36] In this thesis, hydrosilylation of alkenes catalyzed by a series of *bis*-NHC-Rh(I) complexes was studied using density functional (DF) methods. The resemblance between Rh(I) and Ru(II) complexes even extends the range of validity of such a case study to more inexpensive *bis*-NHC Ru(II) catalysts.

After presenting an extensive background on hydrosilylation and N-heterocyclic carbenes in Chapter 2 the computational details relevant in this thesis will be shown in Chapter 3. In Chapter 4, all possible pathways of the following mechanisms are explored: Glaser-Tilley (GT),[21,37] Chalk-Harrod (CH),[38] modified Chalk-Harrod (mCH),[39-44] and σ-bond metathesis (SBM),[45,46] including the induction period of the pre-catalyst and the side reaction β-hydrogen elimination. In Chapter 5, an extended set of density functionals was applied to explore a possible influence of the exchange-correlation approximation on the results in Chapter 4. The 12 chosen functionals include semi-local functionals – GGA, (gradient generalized approximation) and meta-GGA – as well as hybrid functionals. Chapter 6 deals with the problem of regioselectivity. The reaction model was extended from hydrosilylation of ethylene to the hydrosilylation of 1-butene. Besides monosilane, dimethylsilane was also considered as one of the reactants. The *bis*-NHC ligand was modified in three positions.

In summary, the current theoretical case study aims to explore the potential applicability of bidentate transition metal NHC complexes for the hydrosilylation of alkenes. A detailed study of the catalytic pathways and the factors possibly affecting the regioselectivity should provide some insight into the functionality of these model catalysts. The application of a relatively large set of DF functionals and the comparative methodological study illustrates the complexity of the encountered problems from a computational chemist's point of view.

Some aspects of Chapters 2 and 4 were in part previously dealt in my diploma thesis of the same title in 2010.[47]

2 Background

2.1 Hydrosilylation

The hydrosilylation (also called hydrosilation) of alkenes denotes the addition of a Si−H bond across C−C double bonds, forming alkyl silanes.[48] It is a fundamental chemical transformation which has been widely applied in chemical industry.[48] Along with the hydrosilylation of other unsaturated functional groups such as alkynes, imines, ketones and aldehydes (Figure 2.1), it contributes to the production of organosilicon compounds, e.g., the *α*-*ω*-functionalization of polysilanes, a class of substance which is of growing interest,[49] and various flexible organosilicon intermediates formed via consecutive desilylative oxidation,[50,51] cross-coupling,[52] proto/halodesilylation[53,54] and cycloaddition.[55] An extension of the hydrosilylation is the so-called silymetallation. In this case, a Si−M (metal) bond is added across unsaturated bonds instead of the Si−H bond, leading to the formation of versatile intermediates required in complex regio- and chemoselective reactions.[56]

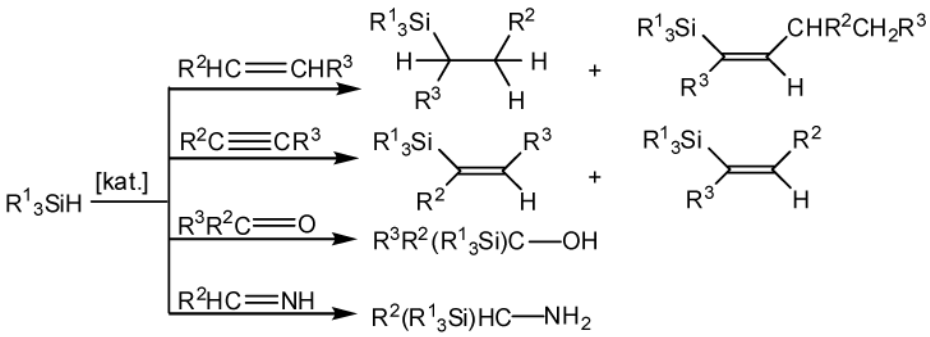

Figure 2.1. Hydrosilylation of various types of unsaturated bonds.

The first experimental record of hydrosilylation of alkene can be dated back to 1947, as the n-octyltrichlorosilane was prepared from 1-octene with trichlorosilane under catalysis by acetyl peroxide.[57] By using the same strategy, a series of novel compounds – polysilmethylenes – were synthesized and attracted great attention.[57,58] These new compounds were not only thermo- and oxidative resistant but also well soluble in organic solvents, revealing a configuration, until then unknown, consisting of the Si−CH_2−Si unit, an analogue of the well−known Si−O−Si unit of polysiloxanes.[1] Since the hydrosilylation of alkenes is often compared to the hydrosilylation of ketones and alkynes, the following paragraph will also give a brief introduction to the two related reaction types, before entering the main topic of this thesis. As background knowledge they should provide hints for context analysis regarding the whole network of hydrosilylation reactions.

The hydrosilylation of ketone is the saturation of the C−O double bond by a silane, being particularly important for the enantioselective synthesis of chiral alcohols, which are of great importance in agrochemicals and pharmaceuticals.[59,60] The significant difference between mechanisms of the hydrosilylation of ketones and alkenes is to be found in the initial stage, at the step of activation of the double bond. Due to different polarities of the double bond the hydrosilylation of ketones proceeds in a way different from the hydrosilylation of alkenes. Proposed mechanisms[61-63] predicted the ketone to be bound via the carbonyl oxygen atom to the metal center or to the silyl group. In contrast, alkenes are in most cases coordinated via a π-interaction to the metal center,[38,63,64] requiring one more coordination site. For the hydrosilylation of ketones, one of the most successful catalysts to date is Gade's catalyst, being a library of chiral oxazolinylcarbene-rhodium complexes.[16,17] Multiple reaction pathways have been studied for this catalysis system and the key intermediate was determined to be a metal silylene complex generated by double silicon-hydrogen activation, where the rhodium atom and the silicon atom are bridged via a single hydrogen atom.[65,66] This finding is apparently also applicable for other Rh based catalysts, as another experimental study on several *bis*-NHC-Rh(I) complexes also supplied evidence for the existence of the same silylene intermediate.[27]

Both the hydrosilylation of ketones and alkynes provides convenient pathways to introduce regio- and stereoselectivities into intricate multi-step chemical transformations.[20] The hydrosilylation of alkyne is commonly catalyzed by ruthenium or rhodium phosphine catalysts, e.g., reaction mechanisms were studied extensively for the ruthenium catalysts $RuHCl(CO)(PPh_3)_3$[67] and $[Cp^*Ru(MeCN)_3]^+PF_6^-$[18-20]. More recently, N-heterocyclic carbene rhodium complexes such as $[RhCl(COD)(RIm(CH_2)_3NMe_2)]$ (COD = η^4-cycloocta-1,5-diene),[28,29] and [Rh(NBD)Cl(NHC)] (NBD = 2,5-norbornadiene),[30] were also proved to be efficient and regioselective.

The hydrosilylation of alkenes can proceed under homogeneous or heterogeneous catalytic conditions.[1] As catalyst one may employ free radicals,[68] Lewis acids,[69,70] or, as in the majority of cases, transition metal (TM) complexes.[14,15] Recently, the family of N-heterocyclic carbenes was also shown to activate silicon compounds.[71] Details of the mechanisms of the homogeneous catalyzed hydrosilylation of alkenes will be discussed in separate sections in Section 2.2.

The search for appropriate transition metal based catalysts is aimed at facilitating the generally relatively difficult synthesis of organosilicon compounds.[33] Well-known industrialized catalysts in the second half of the last century are Speier's catalyst,

chloroplatinic acid − H_2PtCl_6-^{i}PrOH,[33] and the Karstedt catalyst, $Pt_2[(\eta^2\text{-}ViSiMe_2)_2O]_3$ (Me=methyl, Vi=vinyl), platinum(0)-1,3-divinyl-1,1,3,3-tetramethyldisiloxane[34,35] (Figure 2.2).

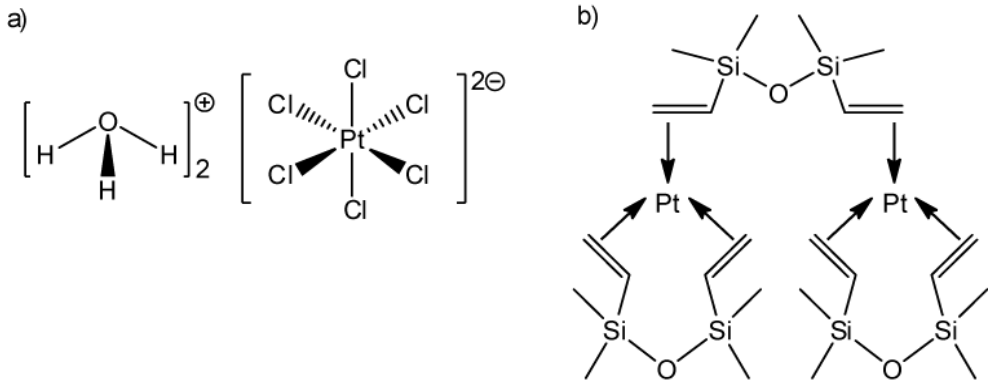

Figure 2.2. a) Speier's catalyst and b) Karstedt's catalyst. Refs. 33−35.

Furthermore platinum catalysts were synthetized and tested. The most successful ones among them are platinum-β-diketone compounds,[72] monodentate platinum-NHC complexes such as the Marko catalyst − benzimidazolylidene platinum(0),[36] and recently bidentate platinum(II)-NHC complexes.[73]

However, because of the relatively high price – currently at around 1500 US$/oz (1 oz. = 28.3 g)– of platinum, catalysts based on its neighbor transition metals gained evermore attention, e.g., ruthenium, palladium, iridium, and rhodium (Figure 2.3). Research was also extended to low price metals, such as iron, cobalt, nickel,[74] as well as early transition metals.[75] Renowned research projects are for instance the studies on the hydrosilylation of ethylene, 1-hexene, styrene and other common olefins by using cobalt(III)-Cp* (1,2,3,4,5-Pentamethylcyclopentadienyl) complex[76] and palladium(II)-1,10-phenanthroline complex;[77] iron(II) bis(imino)pyridine complexes;[78,79] a ruthenium(I)-Cp*-silylene complex;[21] an iron(II) complex with chelating Cp*-NHC ligands;[80] rhodium(III) phosphine complexes;[81,82] rhodium(I) and iridium(I) complexes with P,N−substituted indene ligands;[83-85] ruthenium(II) complexes with phosphine, acetonitrile, or cymene ligands;[22-24] and finally organo-lanthanides.[86] Two reviews provide a comprehensive overview of the latest progress in the transition metal catalyzed hydrosilylation of alkene.[87]

This thesis aims to model and study a series of rhodium complexes as potential catalysts for the hydrosilylation of alkene. Traditionally, rhodium complexes were considered rather as catalysts for the hydrosilylation of carbon-heteroatom multiple bonds than for alkenes.[88] For instance, besides Gade's catalyst, the Wilkinson catalyst, Rh(I)-tris-PPh_3 (triphenyl-phosphine) chloride, is also a preeminent catalyst for the hydrosilylation of ketones and

imines.[89] Ever since the last decade, more rhodium complexes have been reported to be catalytic active in the hydrosilylation of alkenes, most of them involving phosphine or NHC as ligands.[15] For example, the regioselectivity in the 1,4-hydrosilylation of isoprene was investigated using a series of modified Wilkinson catalysts $RhCl(PR_3)_3$ (R=Bu, Ph, *p*-MeC_6H_4, *p*-ClC_6H_4, *p*-$OMeC_6H_4$) and $RhCl(CX)(PPh_3)_2$ (X=O or S).[90] The varied electronic properties of the ligands were found to have the greatest influence on the regioselectivity, dominating over external factors such as temperature and solvent.[90] In case of Rh(I)-NHC complexes, the substituents at the imidazolium ligand play an essential role in tuning the catalytic activity and selectivity of the hydrosilylation of alkenes by triethoxysilane.[91] These catalytic species are active in the ionic liquid $BMimPF_6$ (1-butyl-3-methylimidazolium hexafluorophosphate), too, performing notably, and they can be reused apparently without loss of catalytic activity and selectivity.[91] The most recent example is an experimental study on the application of [Rh(COD)(NHC)(OH)] as catalyst for the hydrosilylation of 1-hexene by $HSiEt_3$.[32] In that study, variants of modified NHC ligands are involved, such as IPr, ICy, IDD and Ii-PrMe, which are all N-substituted unsaturated NHCs;[32] for compound abbreviations, see reference 32. The various substituents at the wingtip N-atom apparently promoted the catalytic activity and regio-control, due to the resulting different steric demand

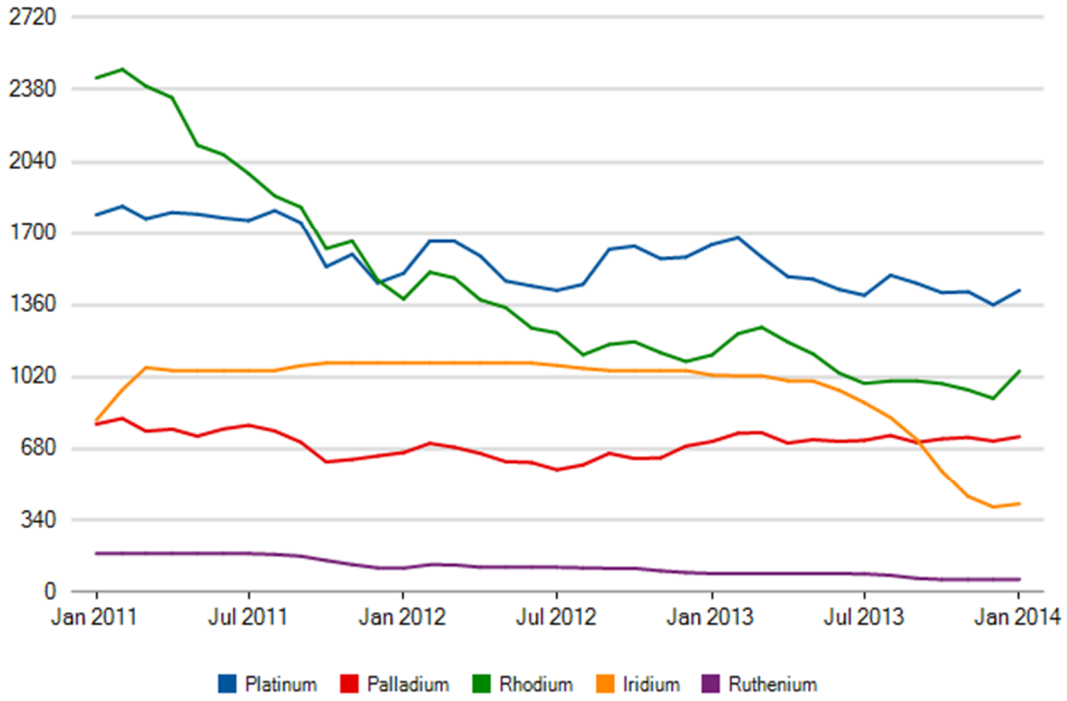

Figure 2.3. Market prices of noble metals commonly applied in catalysis (blue: platinum, red: palladium, green: rhodium, yellow: iridium, and purple: ruthenium) from January 2011 to January 2014, in US dollar per ounce (US$/oz., 1 oz. = 28.3 g). Information source: http://www.platinum.matthey.com/pgm−prices/price−charts/.

of the NHC ligand.[32] In comparison, in Chapter 6, I will present other factors of influence which dominate over the N-substituents. The difference between the experimental results and the current theoretical results can be due to one change in the catalyst structure – the ligands in the current models are bidentate instead of monodentate.

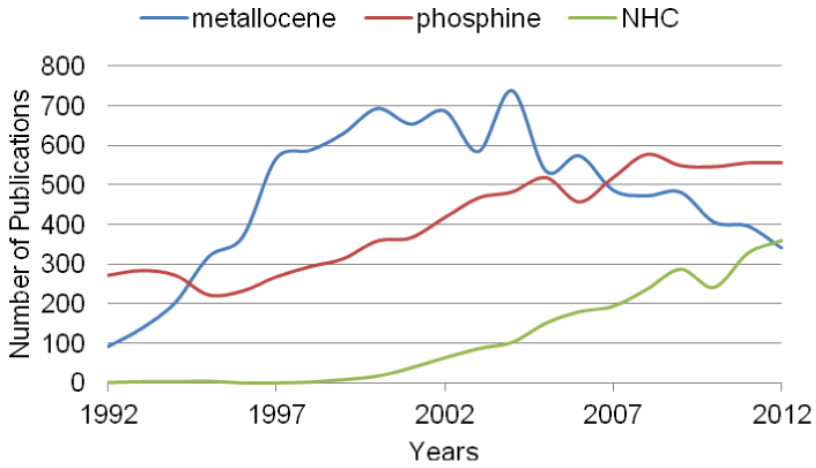

Figure 2.4. Publication trends in organometallic studies on three types of catalyst, from 1992 to 2012. Data source: ISI Web of Knowledge, Dec. 2012.

With respect to the transition metal catalyzed hydrosilylation of ketones, alkynes and alkenes, the most commonly applied ligands fall into three categories, namely cyclopentadienyl (e.g., Cp*), phosphine (e.g., PPh_3) and NHC (e.g., imidazoline) ligands. A drastically increased amount of publications on the last ligand family indicates a growing interest in the innovation of classical catalyst ligands (Figure 2.4). Recently, numerous reviews on TM-NHC complexes in the context of catalysis chemistry were published as a consequence of the rapid development in this chemistry. Among them two representative reviews are "Donor-Functionalised N-heterocyclic Carbene Complexes of Group 9 and 10 metals in Catalysis: Trends and Directions" by Normand et al.[92] and "Syntheses of Metal Complexes of N-Heterocyclic Carbenes and Recent Progress in Carbon-Carbon Multiple Bonds Hydrosilylation" by Peng et al.[74] These reviews address versatile transition metals including platinum, palladium, rhodium, cobalt, nickel, iridium, as well as ruthenium and gave extensive summaries of the application area, reviewing the research trends and directions. In Section 2.3, the synthesis, stability, bond properties of various types of NHC and several selected representing TM-NHC complexes will be introduced and discussed in detail. This intensified research on the catalysts has naturally promoted the exploration of the corresponding catalytic mechanisms. In the next chapter, I will introduce the most widely studied mechanisms of the transition metal catalyzed hydrosilylation of alkenes.

2.2 Mechanisms for the Catalyzed Hydrosilylation of Alkene

In Figure 2.5, the four most studied mechanisms for catalyzed hydrosilylation of alkenes are illustrated with their key intermediates (IM) and transition states (TS), on the example of a Rh catalyzed reaction.[93] These are the a) Glaser-Tilley[21,37] (GT), b) Chalk-Harrod[38] (CH), c) modified Chalk-Harrod[39-44] (mCH), and d) σ-bond metathesis[45,46] (SBM) mechanisms. Depending on the mechanism, the reactants silane and alkene are added consecutively (Structure **A**, **B**; Figure 2.5) or synchronous (Structure **C**; Figure 2.5) to the catalyst. In the GT mechanism, a silylene complex is formed in the initial stage, involving two hydrogen bonds between a primary silane and the metal center, followed by insertion of the C−C double bond into a Si−H bond, and replacement of the product by an additional reactant.[21] The mechanisms CH and mCH start with coupled oxidative addition of silane.[94] In the CH mechanism, first a C−H bond, then a C−Si bond is formed. The order of these bond formations is reversed in the mCH mechanism. Along both pathways, a common intermediate **D** (Figure 2.5) is formed after the stepwise bond formations. The two mechanisms CH and

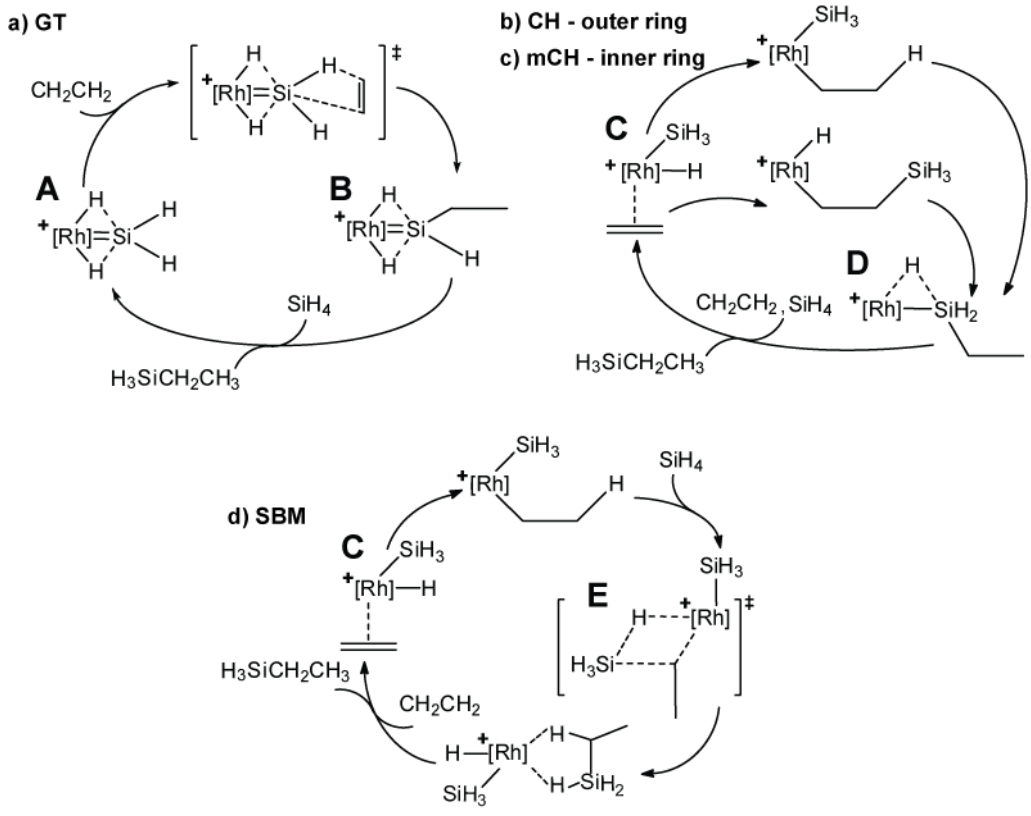

Figure 2.5. Overview of the catalytic cycles of four mechanisms of hydrosilylation: (a) Glaser-Tilley (GT); (b) Chalk-Harrod (CH); (c) Modified Chalk-Harrod (mCH); (d) σ-Bond Metathesis (SBM). Crucial intermediates and transition states are labeled by letters: GT1 – **A**, GT3 – **B**, CH1 – **C**, CH6 – **D**, and SBM5−6 – **E**. Adapted from Ref. 93.

mCH then reunite and end in a concerted elimination of the product. The SBM mechanism is characterized by the four-member transition state-**E** (Figure 2.5), where simultaneously M−H and C−Si bonds are formed, and M−C and Si−H bonds cleave to build the product. The last step occurs, similarly as in the CH and mCH mechanisms, while the product is exchanged for another alkene molecule, thus starting the subsequent catalysis cycle.

Apart from these four general mechanisms, alternative mechanisms mostly focused on variations of certain elementary steps such as the oxidative addition of reactants and hydrogen shift reactions. Among them the most successful works are the proposal of the "olefin first" mechanism for group VI metallocene catalysts,[75] and the "silyl migration" mechanism for cyclopentadienyl rhodium complexes.[95]

In the next section, an introduction is given in chronological order for the development of the four main mechanisms.

2.2.1 Chalk-Harrod Mechanism

The CH mechanism was proposed[38] to rationalize the first observed homogeneously catalyzed hydrosilylation of alkenes by Speier et al.[33] That suggestion aimed at providing a better mechanistic understanding of the catalyzed hydrosilylation reaction, which was still not fully understood at that time.

Initially, the authors were considering a general mechanism for all transition metal catalysts with a d^8 electronic configuration.[38] For that purpose, they carried out experiments not only with the original platinum(II) Speier catalyst but also with analogous iridium(I) complexes.[38] Although a coincidental coordination of silyl- and hydride fragments was not found in case of the platinum(II) complex, the corresponding iridium(III) intermediate was identified using infrared spectroscopy.[38] This evidence proved the occurrence of oxidative addition with full separation and addition of the silyl- and hydride moieties, which is an essential elementary step of the CH mechanism (Figure 2.6, upper part). The subsequent step was explored on the occasion of the laboratory observation, that the hydrosilylation reaction was accompanied by an olefin isomerization reaction in the presence of silane and the catalyst.[38] For example, the *α-β*-isomerization of 1-hexene and the *cis-trans*-isomerization of the consequently formed 2-hexene occur frequently.[38] Based on a kinetic analysis of several conceivable alternative pathways, the authors concluded that an isomerization during the hydrosilylation requires a sufficiently long lifetime of intermediate **3** in Figure 2.6, a hydride-olefin complex. This shows that the hydride moiety is added onto the olefin before the silyl moiety ("hydrogenation first"). Another hint worth noting is the relation between the rate constants of the preceding and the following elementary steps of the equilibrium between **2**

and **3** (steps **1** → **2** and **3** → **1**; Figure 2.6, lower part). A long lifetime of intermediate **3** is only possible if k_2 is notably larger than k_3, with the ratio k_2:k_3 being about 5:1 according to the ratio between the yield of olefin isomers and the introduced reactants at the beginning. This actually suggested the last step **3** → **1** to be relatively challenging from a kinetic point of view, though not stated explicitly by the authors.[38]

Later, this point was confirmed by other mechanistic studies which studied the reductive elimination in more detail for a reaction catalyzed by an iron carbonyl anion.[39,44,96] According to recent theoretical studies, this elementary step sometimes even turned out to be rate-determining with respect to the overall catalytic cycle.[22-24,37,93]

Back to the study of Chalk and Harrod, the catalytic cycle closes with species **1**. An adduct of the catalyst and the internal olefin is regenerated as the catalytic active species, after the product hydrosilane is eliminated.[38] An overview of the complete CH mechanism is analogous to the scheme shown in Figure 2.5. The proposal of the CH mechanism successfully clarified the process of oxidative addition of silanes and rationalized the formation of by-products due to an α-β-hydrogen shift.[38]

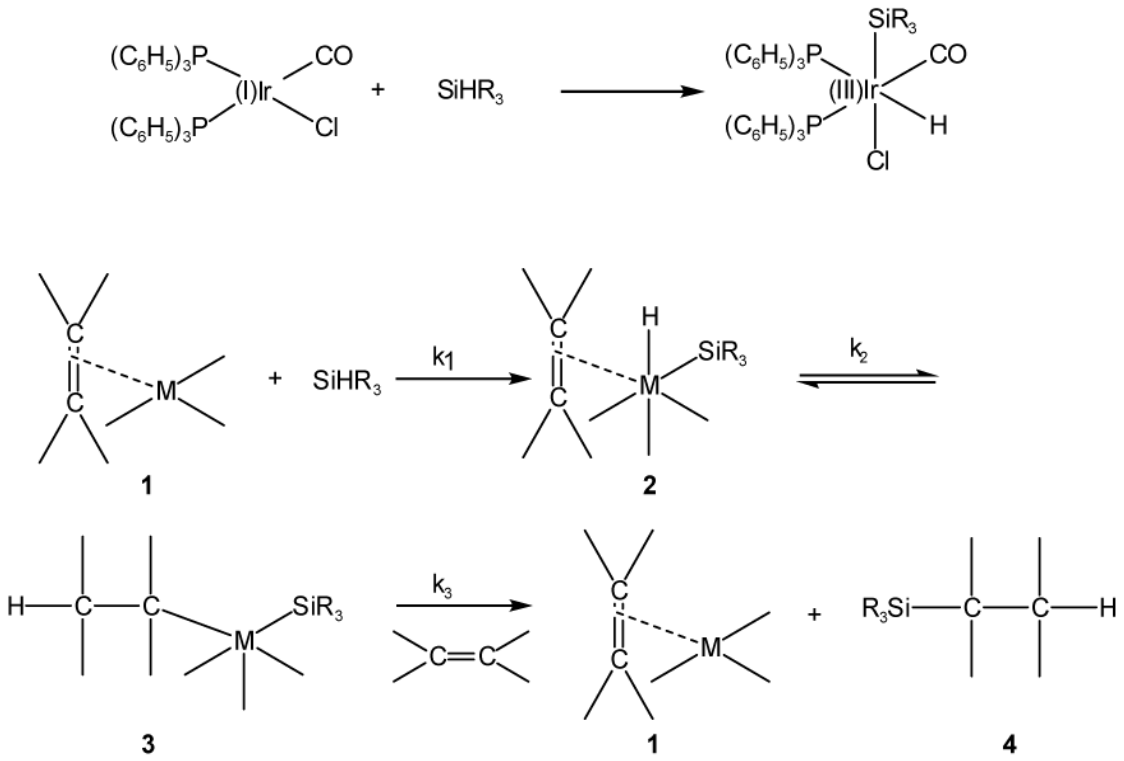

Figure 2.6. The original Chalk-Harrod Mechanism, comprising the crucial steps **1→2** oxidative addition of the silane, **2→3** formation of the C−H bond, and **3→4** reductive elimination, introducing a second ethene, Note that k_1, $k_{-2} > k_3$. The central metal can be platinum, iridium or rhodium. Adapted from Ref. 38.

2.2.2 Modified Chalk-Harrod Mechanism

One shortcoming of the CH mechanism is that it failed to rationalize the formation of alkenylsilane as side product, which also has been observed during the hydrosilylation of alkenes.[39,40,97,98] This side product is formed via the dehydrogenative hydrosilylation, while the retained C−C double bond and the C−Si bond formed suggest that the silylation step cannot be a step following hydrogenation.[44] The modified Chalk-Harrod (mCH) mechanism, also known as the Seitz-Wrighton mechanism, was suggested in 1988 to solve this problem.[44]

Originally, this mechanism was proposed for a photochemical reaction: the hydrosilylation of ethylene catalyzed by the cobalt complex $[(CO)_4Co\text{-}SiR_3]$, a follow-up study of the analogous iron complex $[(Cp^*)(CO)_2Fe\text{-}SiR_3]$.[43] It was observed that during the initial activation of the catalyst (UV-irradiation), alkenylsilane was formed (detected by gas-chromatography) instead of the expected hydrosilylation product.[44] The authors then traced this side reaction by Fourier transform infrared spectroscopy (FTIR) and, in consequence, adjusted the mechanism, Figure 2.7a.[44] They suggested that the side reaction takes place when silane is lacking. Especially, the formation of the free vinylsilane and the acyl complex $[(CO)_4Co\text{-}C(O)C_2H_5]$ (see species **4** and **7** in Figure 2.7a) indicated α-β-elimination step of the key species $[(CO)_3Co\text{-}CH_2CH_2SiR_3]$ (species **1** in Figure 2.7a), a product of the insertion of the double bonded C−C species into the Co−Si bond. In this way, the characteristic feature of the mCH mechanism − "silylation first" − was indirectly shown. Due to the instability of the cobalt alkyl complexes, the authors failed to monitor further elementary steps by FTIR to complete the catalytic cycle.[44] The proposed remaining steps of the mechanism are the result of a convincing speculation based on ^{1}H-NMR observations rather than a conclusion from concrete evidence.[44] The complete catalytic cycle is shown in Figure 2.7b.[44]

The proposal of the mCH mechanism improved the CH mechanism appreciably, as it brings up the matter of an alterable sequence of the two crucial elementary steps in a catalyzed hydrosilylation reaction, namely hydrogenation and silylation of the alkene. Together with the CH mechanism, the mCH mechanism provides reasonable rationalizations for the two experimentally most often observed side products of a transition metal catalyzed hydrosilylation of alkenes.

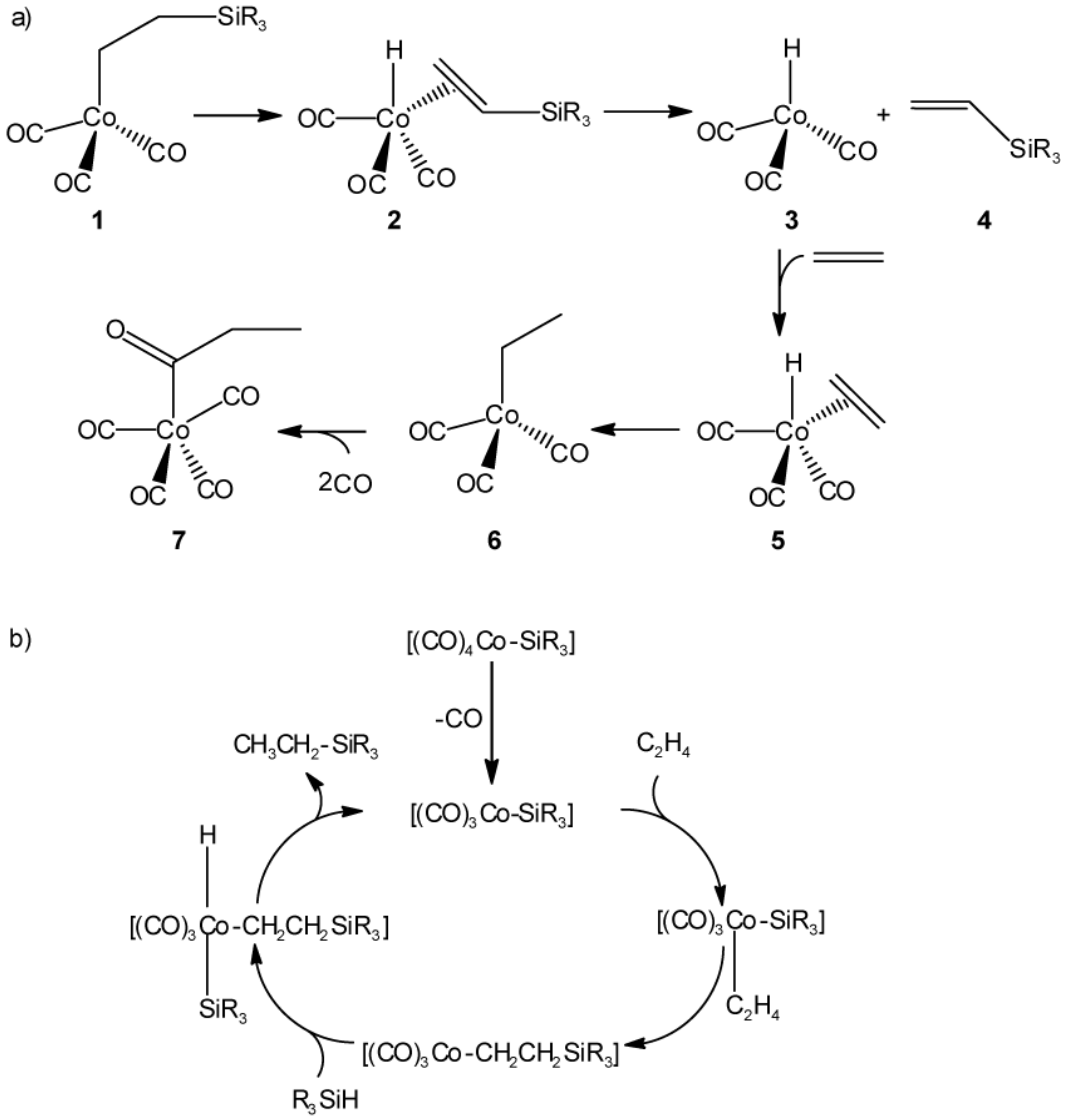

Figure 2.7. a) Mechanism of *β*-elimination – evidence for C−C insertion into the M−Si bond. b) Complete catalytic cycle of the modified Chalk-Harrod mechanism with a cobalt complex. Adapted from Ref. 44.

2.2.3 *σ*-Bond Metathesis Mechanism

The *σ*-bond metathesis (SBM) mechanism was originally proposed for the C−H activation of methane, as an alternative to the conventional oxidative addition, especially for d^0 complexes where oxidative addition is impossible.[45] The first experimental indications of the SBM mechanism were hydrogen-deuterium-isotope exchanges between the reactant methane and the catalysts, most of them being complexes of lanthanides and actinide and of early transition metals.[99] As shown in the general trajectory (cleavage of the M−X bond by a Y−H bond, Figure 2.8a), the Y−H bond was cleaved along with the M−X bond, by receiving the

electrons from the M−X bonding orbitals instead of from the metal d orbitals.[45] The SBM mechanism was adapted for a series of catalyzed chemical transformations. For instance, Tilley et al. first proposed a new route to d^0 metal silyl complexes via the SBM mechanism in the zirconium and hafnium catalyzed photochemical oligomerization of silanes.[100] Later, the SBM mechanism was suggested to rationalize the hydrosilylation reactions of alkenes.[46,101,102] Corey and Zhu studied Cp_2MCl_2/nBuLi (M = Ti, Zr, Hf), an efficient catalyst system not only for the standard hydrosilylation of alkenes but also for coupled isomerization and hydrosilylation of internal olefins and dehydrocoupling reactions.[101] They scanned all plausible pathways and obtained three main products: $RCH_2CH_2SiMePhH$, product of the hydrosilylation of olefins; $R^*CH_2CH_2SiMePhH$ (* denotes the isomerized olefin), the product of the coupled isomerization and hydrosilylation of internal olefins; as well as RCH=C(SiPhMeH)R, the product of dehydrocoupling.[101] The authors focused on enhancing the selectivity of the reaction with respect to specified products by systematically varying the reactant alkene from an electronic and steric point of view, while the other reactant was kept as the secondary silane $PhMeSiH_2$.[101] Based on their experimental findings, an overview of all interconnected alternative mechanistic pathways was proposed.[101] It ensues from the active species $Cp_2ZrHSiR_3$ (Figure 2.8b), which is generated from the original complex Cp_2ZrCl_2 (pre-catalyst) and nBuLi in the presence of PMe_3 and $PhMeSiH_2$.[101] The route of the SBM leads to the formation of species **3** (Figure 2.8b), an adduct of a metal cyclopentadienyl complex and a silane.[101] Starting from species **3** (Figure 2.8b-c), further processes follow, either hydrosilylation or dehydrocoupling/hydrogenation pathways, depending on the type of olefins added. Both variants ended with the regeneration of species **3** (Figure 2.8c)[101]

An overview over the fundamental studies on the C−H activation of alkanes (analog to the activation of Si−H in the paragraph above) has counted the metal-alkyl SBM metathesis (Figure 2.8d) as one of the most important classes.[46] Kinetic experiments were reported to support this mechanism: (*i*) the first−order rate constant of the reactions depend on the concentrations of both the metal complex and the alkane, hinting at a transition state constituted of equally participating metal complex and alkane. (*ii*) The entropy of activation is strongly negative, which is typical for associative mechanisms entailing significant organization. (*iii*) The relatively high primary kinetic deuterium isotope effect of an activated deuterated alkane substrate (k_H/k_D = 3−6) indicates significant C−H bond cleavage in the transition state.[46]

As a side remark on the SBM mechanism, note that it was initially explored for Cp-based catalytic system. The first mechanistic study assigning the SBM mechanism to a non-Cp-based catalytic system was an experiment investigating yttrium complexes catalyzed hydrosilylation of alkene.[102] In that study, the metathesis reaction was determined to be a slow process, following the fast olefin insertion into a reactive metal hydride bond.[102]

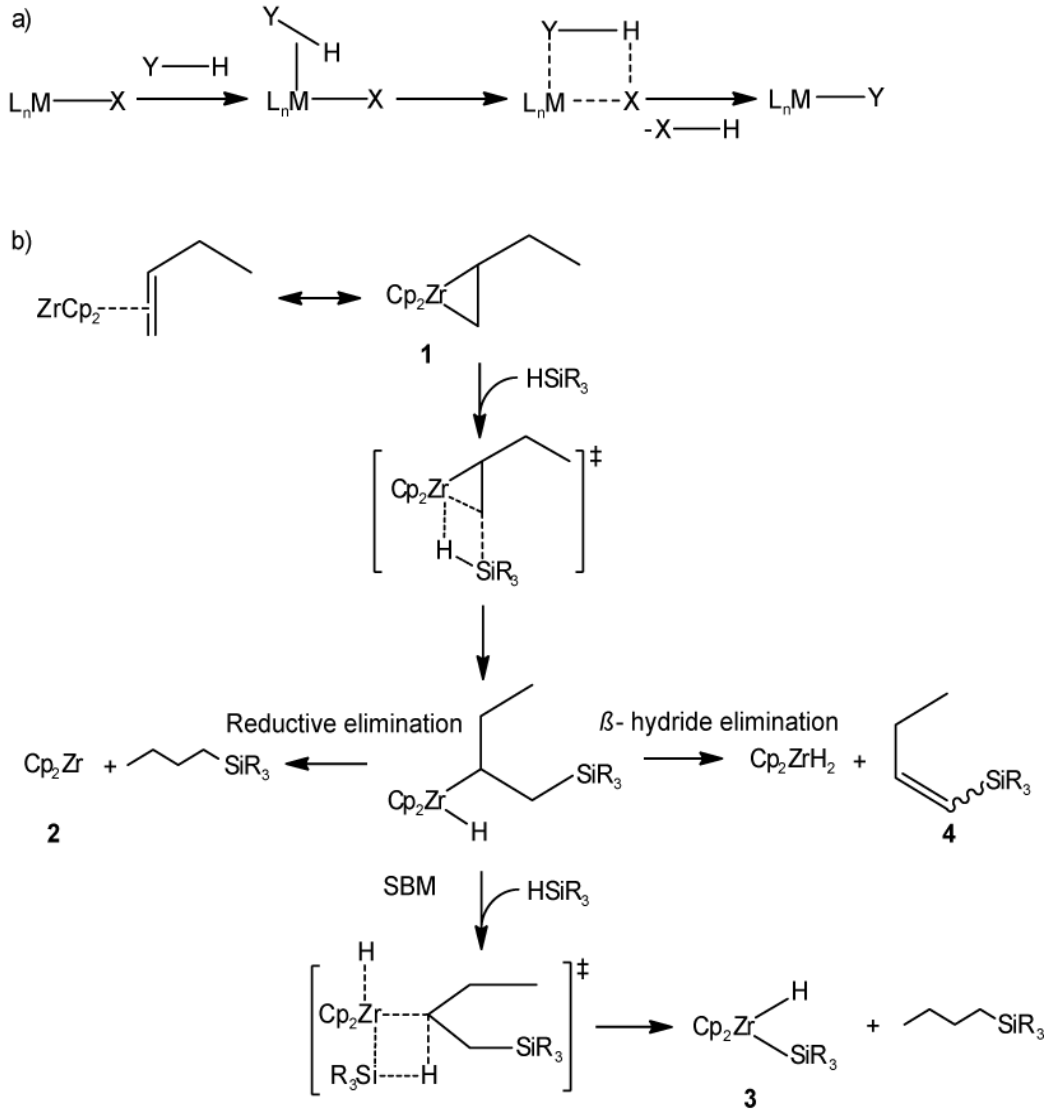

Figure 2.8. a) General procedure of σ-Bond metathesis. b) SBM as one of the alternative pathways for the zinc metallocene catalyst. Adapted from Refs. 45 and 101.

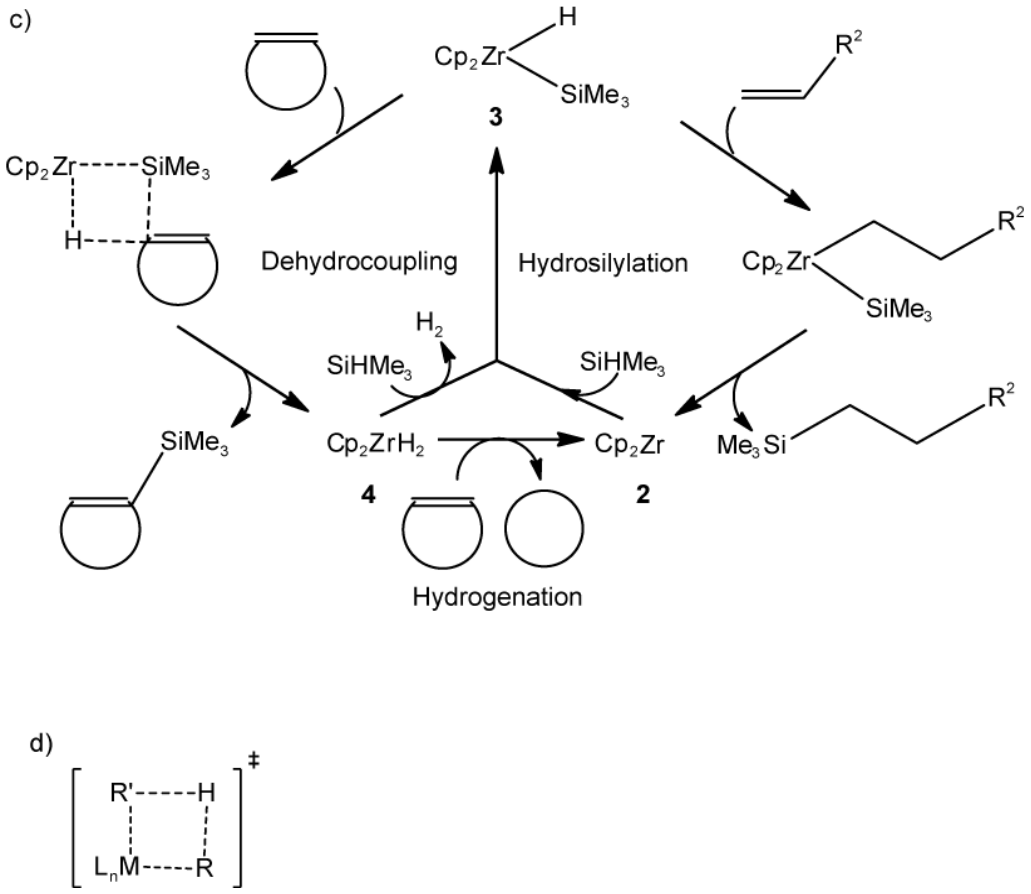

Figure 2.8 (continued). c) Catalyst regeneration in the SBM mechanism for the zinc metallocene catalyst. d) Crucial transition state suggested for the metal-alkyl SBM mechanism. Adapted from Refs. 46 and 101.

2.2.4 Glaser-Tilley Mechanism

The GT mechanism was proposed later than the other three mechanisms for a catalysis system based on a cationic Ru(I) complex: $[Cp^*(^iPr_3P)(H_2)Ru{=}Si(H)PhEt_2O][B(C_6F_5)_4]$.[21] The catalyzed reactions are the hydrosilylation of 1-hexene, ethylene, cyclohexene, styrene, and 1-methylcyclohexene, with mono-substituted silanes $PhSiH_3$ and $HexSiH_3$.[21] In most cases the catalysis was successful with respect to the yield of the desired product, between 70% and 94%, except for two cases $PhSiH_3$/ethylene and $HexSiH_3$/1-hexene, with yields of 54% and 50%, respectively.[21] Characteristic feature of this series of reactions is their insensitivity to the steric properties of alkenes, which cannot be explained with the so far well-established CH, mCH, or SBM mechanisms.[21] Experimentally, the addition of a deuterated reactant, ethylene, in excess led to the formation of the pure isotopomer $PhSi(H)_2CD_2CD_2H$, suggesting an irreversible olefin insertion – different from the reversible

type found in the deuteration experiments for the other mechanisms.[76,95,103,104] To rationalize this observation, a concerted addition of the C−C double bond across the Si−H bond was proposed, in a manner analogous to the step of B−C bond formation in the hydroboration of alkenes.[21] The hypothesis is theoretically comprehensible, as the 3-fold coordinated cationic silicon center is formally isoelectronic with the monomeric boranes (Figure 2.9a).[21] The full catalytic cycle is shown in Figure 2.9b. A theoretical work explored the barriers and energetics of this newly proposed mechanism in comparison with the CH and mCH mechanisms for a simplified reaction model.[37] That study revealed the energy profile of the GT mechanism, involving rate-determining activation barriers at the essential step, the C−C bond insertion into the Si−H bond in the initial phase, and the isomerization steps leading to the regeneration of the catalytic active silylene species in the end phase.[37] More detailed results of this work will be discussed in Chapter 4, where results of this earlier work will be compared to the present results obtained in this thesis.

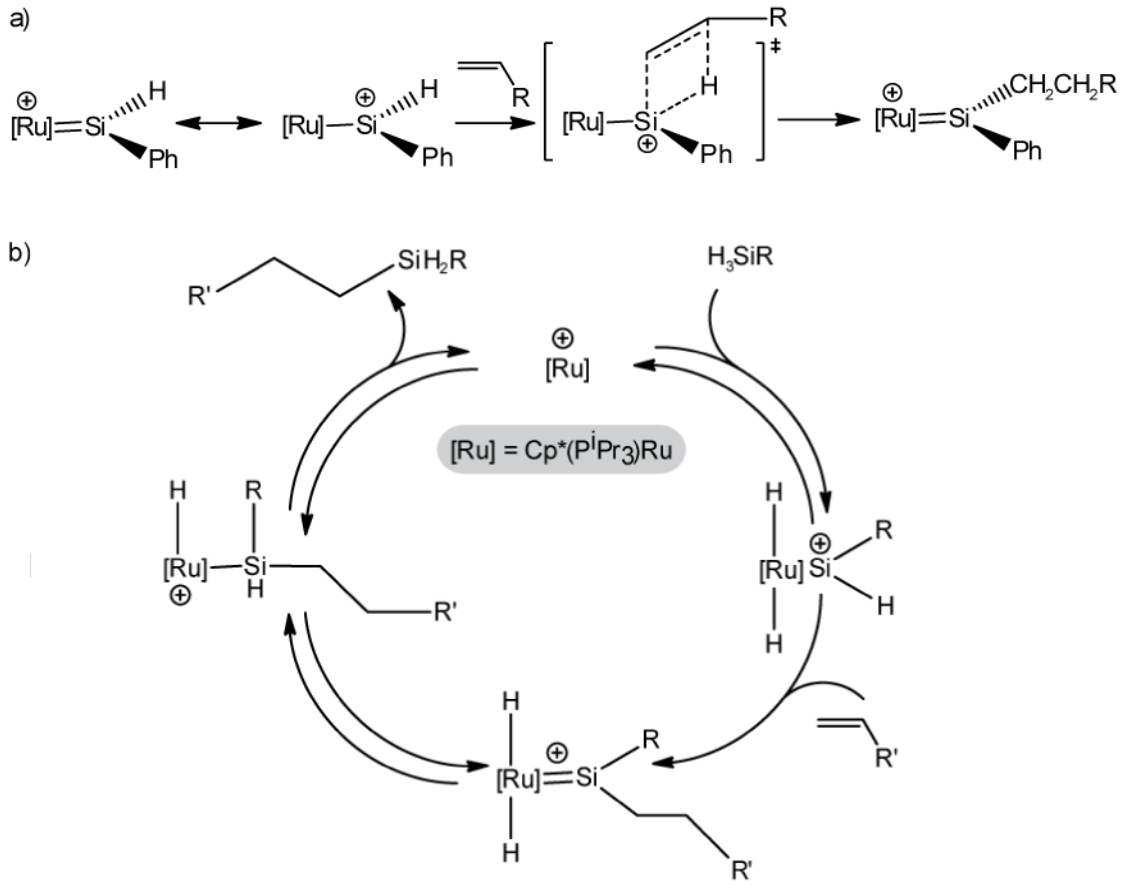

Figure 2.9. a) Insertion of the alkene into the Si−H bond of the three-coordinated cationic silicon center. b) Catalytic cycle of the Glaser−Tilley mechanism with a Ru(I) silylene complex. Adapted from Ref. 21.

2.2.5 Oxidative Addition of Silane

According to recent computational studies, the oxidative addition of silanes and the reductive elimination of the product are the two energy demanding steps in the catalyzed hydrosilylation of alkenes.[22-24,37] The latter process can be viewed as the reversed form of the first one. This reaction pair is not only important for the catalyzed hydrosilylation of alkenes, but also occurs in various other catalytic reactions, which are stoichiometric with regard to the silane.[94,105] For this reason, it is worthwhile to discuss this important step in a separate section.

Oxidative addition of silanes to transition metal complexes was normally studied on the example of stable transition metal silyl compounds.[105] Extensive experimental data and theoretical results, along with the conditions and challenges of the formation of transition metal silyl complexes was reviewed by Corey and Braddock-Wilking.[105] They introduced two terms to classify the main interactions between the metal complex and the silane moiety. The "classical" oxidative addition denotes the bonding nature of the transition metal silyl compounds in a two-center, two-electron fashion. The term "nonclassical" oxidative addition was assigned to a three-center, two-electron bonding situation (Figure 2.10a).[105] One feature of the more complicated nonclassical oxidative addition is the formation of a σ-complex involving an agostic bond.[105] The extent of such an agostic interaction, M−(η^2−HSi), depends on the orbital interactions between the metal center and the silyl moiety, being either a σ-bonding a π-back-bonding interaction; see Figure 2.10b.[105] The first interaction is between the metal d_σ-orbital and the σ-bonding orbital of Si−H; and the second interaction is between the metal d_π−orbital and the σ*−anti−bonding orbital of Si−H.[105] In most cases, the σ-bonding interaction dominates.[105] When other ligands are present, the Si−H bond is more basic than H−H or C−H bonds and a better σ-donor.[105] The Si−H bond is weakened when the fraction of π-back-bonding rises, and the oxidative addition proceeds further in a classical fashion, resulting in a fully separated Si−H bond.[105] Over sixty experimentally characterized complexes (by EPR, IR, NMR and XRD) were shown to contain a stable TM-Si moiety. These complexes were based on the triads of titanium, chromium, manganese, iron, cobalt, and nickel.[105] Various compositions include three types of silane (monosilane, secondary, and tertiary silanes) and two types of scaffold species (mono- and binuclear).[105] Bond dissociation energies of the M−Si bonds are comparable for Rh and Ir, 48−56 kcal·mol^{-1}. M−H bonds are of comparable strength (Rh), or slightly stronger, 57−61 kcal/mol (Ir).[105]

An improved description of the agostic bonds in a non-classical oxidative addition was given in a more recent review of Corey,[94] where the investigated bonding types were extended and the classification of the M−H−Si interactions refined into seven ranges according to the Si−H distance (Figure 2.10c). Among them there are two recently reported interactions: the IHI (interligand hypervalent interactions), and the SISHA (secondary interactions between a silicon and a hydrogen atom), which were sometimes referred to as M−H interactions with a silicon center.[106] Figure 2.10c shows a typical range of Si−H distances and their corresponding bond nature.[94] A free silane remote from the metal center has a Si−H bond length of 142−150 pm. The next span 170−180 pm is typical for a σ-complex which crosses over into an agostic bonding and on to an IHI complex during further bond elongation from 180 pm to 210 pm. Differences between a σ-complex, agostic bonding, and IHI were discussed more explicitly in another review by Nikonov.[107] The SISHA was identified mostly in polyhydride systems, featuring relatively long Si−H distances of 190−240 pm. Finally, complexes with a Si−H distance longer than 250 pm are referred to as silyl hydride.[94] The criteria for distinguishing these six stages of oxidative addition are mainly based on geometry factors such as bond distances and angles obtained by XRD, as well as hydride chemical shifts and coupling constants from NMR, and stretching frequencies from IR spectroscopies.[94] In the current theoretical study, gradual elongation of an originally nonactivated Si−H bond was observed, which passes through the state of an agostic bonding and hydride; see Section 4.2.1.

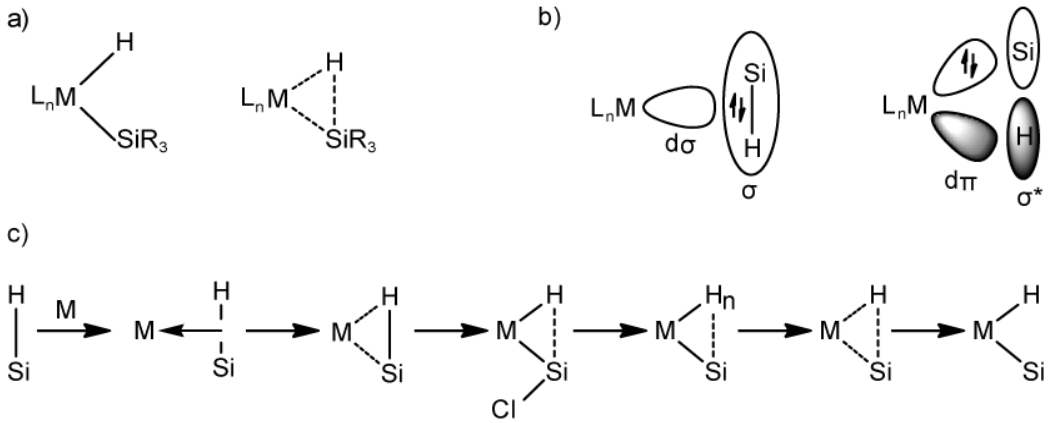

Figure 2.10. a) Classical and nonclassical oxidative addition of silane. b) M-(η^2-HSi) σ-bonding interaction and M-(η^2-HSi) π-back-bonding interaction. c) Typical range of the Si−H distances, from left to right: 142−150 pm, 170−180pm, 170−180pm, 180−210 pm, 190−240 pm, 240−250 pm, >250pm. Adapted from Refs. 94 and 105.

2.3 N-Heterocyclic Carbenes

This thesis explores rhodium complexes with N-heterocyclic carbenes. Ever since the 1960s, the carbene chemistry has gradually gained in versatility and depth.[108] Traditionally, this group of chemical compound was classified into two main categories, namely Fischer carbenes[109] and Schrock carbenes[110] (Figure 2.11).

Characteristics of the Fischer carbenes are: (*i*) metals are in a low oxidation state; (*ii*) middle and late transition metals, (*iii*) π-electron acceptor ligands, and (*iv*) π-donor substituents on the carbene atom (e.g., alkoxyl, alkylated amino groups). In contrast, Schrock carbenes exhibit opposite features: (*i*) metals are in a high oxidation state; (*ii*) early transition metals, (*iii*) π-electron donor ligands, and (*iv*) hydrogen and alkyl substituents at the carbene moiety. These two types of carbenes are remarkably different in the bonding nature of the M-carbene bond. Fischer carbenes have a σ-type electron donation from the lone-pair of the sp^2 hybridized orbital at the carbene carbon atom to an empty d-orbital of the metal, and a π-electron back bonding between a filled d-orbital of the metal and an unoccupied p-orbital of the carbene carbon atom, being electrophilic and in a singlet state. Schrock carbenes have a covalent bond between a triplet carbene and a triplet metal moiety, which is polarized towards the carbene carbon atom, turning it into a nucleophilic center (Figure 2.11).[108]

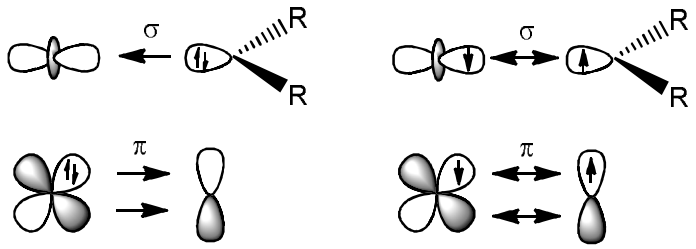

Figure 2.11. a) Fischer carbene and b) Schrock carbene. Adapted from Ref. 108.

Both Fisher carbenes and Schrock carbenes are widely applied in the organic synthetic chemistry, e.g., Fe(0), Mo(0), Cr(0), W(0), Mn(I), and Co(I) complexes (Fischer carbene), and the active complexes generated from the precursor Tebbe's reagent[111] (Schrock carbene), as well as Grubbs' catalyst (Schrock carbene); see Figure 2.12. Application areas of these carbenes are, e.g., the Wulff-Dötz reaction[112,113] for the generation of phenolic compounds (Fischer carbene), olefin metathesis[114,115] (Schrock carbene), and alcohol reduction to alkenes (Schrock carbene).[111]

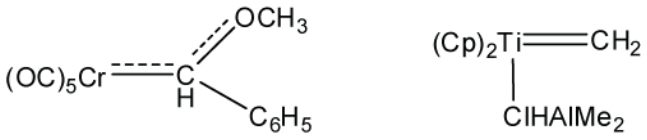

Figure 2.12. Examples for a Fischer carbene and a Schrock carbene: catalyst for the Wulff-Dötz reaction (left) and the *in-situ* generated catalytic species from Tebbe reagent (right). Adapted from Refs. 111 and 112.

2.3.1 Early Synthesis of NHC

The first N−heterocyclic carbenes were considered as a subclass of the Fischer carbene.[116] Yet in this case, the π-back donation from the metal to the carbene is negligibly small so that the carbene ligands are stable enough to be isolated and can be synthesized as free species,[116] though it was first discovered as ligand in transition metal carbene complexes.[116]

Wanzlick and Schönherr treated phenylimidazolium perchlorate with mercury acetate in dimethyl sulfoxide (DMSO) and obtained the complex bis(1,3-diphenylimidayolio)mercury diperchlorate, which is heat-resistant (m.p. ca. 370˚C) and stable with respect to acid (Figure 2.13a).[116] However, the back reaction was easily stimulated by traces of hydrogen sulfide involved in DMSO, and the original perchlorate salt and mercury sulfide were formed (Figure 2.13a).[116] The novel compound, a transition metal carbene, was identified by NMR.[116]

At the same time, Öfele intended to adapt an in situ synthetic strategy to generate the pyridinium alike NHC cation[117] (Figure 2.13b). Surprisingly, via simple heating in high vacuum a new transition metal carbene complex was synthesized instead, in good yield.[117] The chemical constitution thereof was confirmed by NMR spectroscopy, as it exhibited the same upfield shift on conversion from the imidazolium cation to a carbene ligand as reported before by Wanzlick and Schönherr[116] who furthermore characterized it by IR and UV spectroscopy.[117] The NHC-chromium-carbonyl compound was found to be chemical robust, air-stable, and decomposed only above 175˚C. It also features good solubility in common organic solvents such as ether, tetrachloromethane, alcohol, and benzene, but is insoluble in water. This preliminary communication soon stimulated great interest in a direct synthesis of transition metal NHC complexes as well as in further studies of their chemical properties and applications in catalysis.[118]

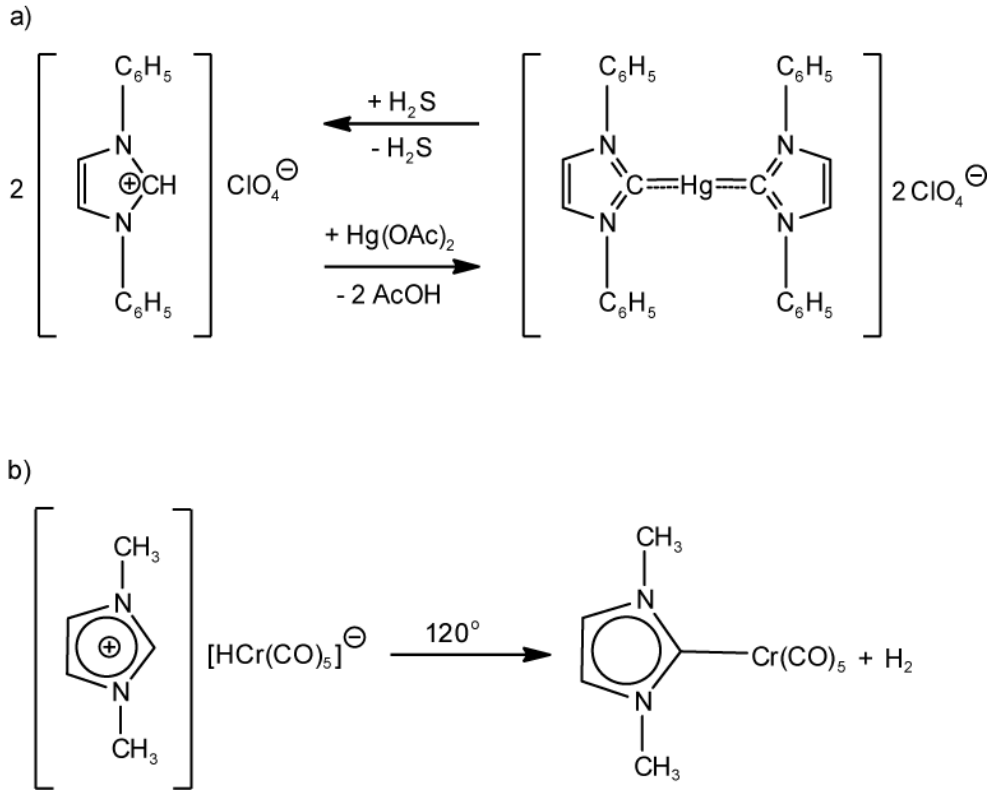

Figure 2.13. Pioneering studies on the metal-NHC compound: a) the discovery of Hg(II)-bis-NHC by Wanzlick and Schönherr and b) the isolation of a Cr(II)-NHC complex by Öfele. Adapted from Refs. 116 and 117.

One of the earliest reviews on transition metal-carbene complexes was published already in 1972.[118] Representatives of different kinds of carbene compounds were introduced (Figure 2.14).[118] The synthesis of modified carbene ligand was reported and the reactivity of such transition-metal complexes was found to depend on the metal center.[118] One of the most noticeable finding was the synthesis of the complexes bearing saturated NHCs – the dihydroimidazolinylidene.[118] As reported in the related experimental works, the electron-rich dimers of such carbenes are susceptible to electrophilic transition metal complexes, the so-called "carbene traps", and can facilely form the corresponding transition metal-carbene complexes.[119] Note this is a different strategy than the direct synthesis of complexes with unsaturated NHCs reported earlier, which proceeds via a deprotonation reaction.[117]

The next milestone in NHC chemistry was the breakthrough isolation of five free carbenes by Arduengo et al..[120] In 1991, Arduengo and co-worker reported the synthesis, structure and characterization of the first crystalline carbene.[120] The 1,3-di-l-adamantylimidazol-2-ylidene (the product complex in Figure 2.15) was synthesized via

deprotonation of 1.3-di-1-adamantylimidazolium chloride (the reactant complex in Figure 2.15) in THF (tetrahydrofuran) at room temperature.[120]

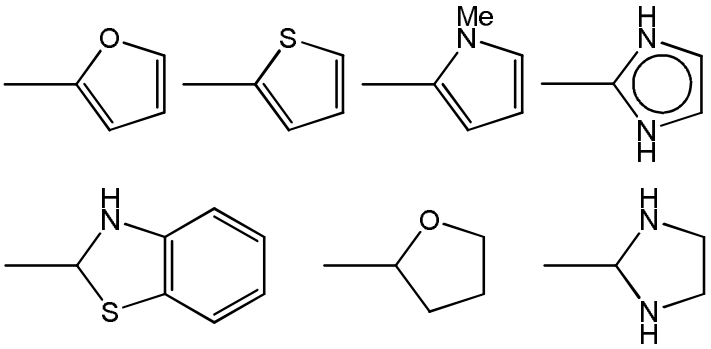

Figure 2.14. Different kinds of heterocyclic carbenes of the first generation. Adapted from Reference 118.

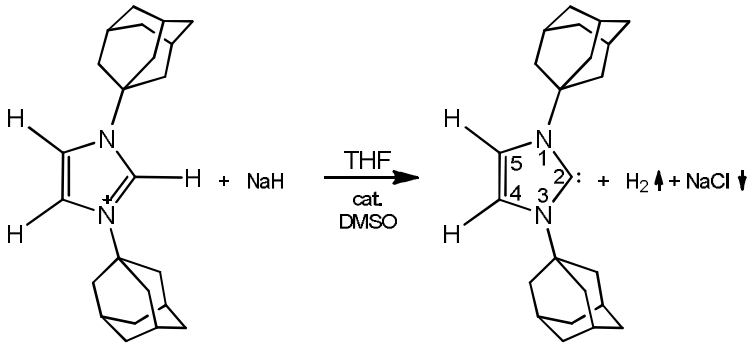

Figure 2.15. Synthesis of the first isolable NHC by Arduengo et al. Adapted from Ref. 120.

The product is oxygen- and moisture-sensitive and otherwise kinetically and thermodynamically stable, its melting point being 240−241˚C.[120] The stability of the carbene was speculated to be enhanced by π-donation of the electron rich π-system (N−C=C−N) into the p−orbital of the carbene carbon atom, as well as the lowering of the in-plane carbene orbital by the more electronegative nitrogen atoms.[120] The importance of π-donation was first highlighted by Wanzlick et al. in a series of publications directed towards the synthesis of nucleophilic carbenes.[121] They especially suggested enhancing the stability by varying the electronic features of the N atoms adjacent to the carbene atom.[121] In one study they emphasized this philosophy – "Wir müssen uns daran gewöhnen, dass sehr große Unterschiede in der chemischen Reaktivität auf *geringen lokalen* Überschussladungen beruhen." (Translated: "We should get used to the view that the great differences in the chemical reactivity are caused by small local excess charges.")[122] Besides such electronic factors, the steric point of view is also to be noted. Bulky substituents at the wingtip nitrogen atoms, e.g., adamantyl in Figure 2.15, also enhance the stability by hindering such species from participating in coupling reactions with available electrophilic moieties.[120]

2.3.2 Development of the TM-NHC Complexes

The isolation of the NHC compounds enabled the synthesis of versatile metal-NHC complexes. Research findings of the blooming period of the late 90s were extensively documented by Herrmann in the review "N-Heterocyclic carbenes as ligands for metal complexes – challenging phosphine ligands in homogeneous catalysis".[123] In this review, results of comparative studies between NHCs and phosphines (trialkylphosphanes and alkylphosphinates) were summarized, most of them being PhD works at Technische Universität München from 1992 to 2001.[123] The similarity in the electronic nature of the NHC and phosphine was revealed by spectroscopic studies.[74,123] From structural and thermochemical studies it was also concluded that NHC ligands bearing alkyl, aryl, amine, and ether N-substituents are in most cases better donors than the phosphine ligands.[123,124] To establish an easy access to NHC derivatives and their catalytic properties in versatile reactions, the so-called "ammonia method" was described for large-scale synthesis (Figure 2.16).[123]

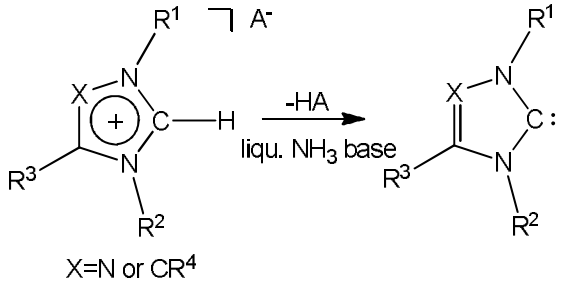

Figure 2.16. The ammonia method for large-scale synthesis of functionalized carbenes. Adapted from Ref. 123.

It was also noted that the oxidation reagent OsO_4 can be added across the C−C backbone of five-member NHCs (Figure 2.17), which revealed a rare reactivity of the NHC ligand.[123] According to Herrmann and co-workers, this reaction suggested little π-aromaticity of this class of NHC,[123] which is in accordance with a subsequently published charge-density study on free and metal-coordinated N-heterocyclic carbenes.[123,125] Regarding metal coordination chemistry, this review pointed out the unique bonding feature of the M-NHC bond, compared to the conventional Fischer and Schrock-type of carbenes, e.g., the rather long bond length (> 210 pm vs. < 200 pm).[123] Furthermore, the steric flexibility of the NHC ligand was speculated to be the result of substantially reduced "π-backbonding", which supposedly changes the nature of the bond from "double bond-like" in the Schrock and Fischer carbenes to "single bond-like" in the NHCs.[123] For example, the NHCs can rotate around the metal-carbon axis depending on the steric requirement, being much more adaptable than the

classical Fischer- and Schrock-carbenes.[123] That review[123] gives a comprehensive summary of the catalytic properties of metal-NHC complexes in versatile chemical transformations, including Heck and Suzuki coupling,[126,127] aryl amination,[128-130] amide α-arylation, hydrosilylation, olefin metathesis,[131-133] Sonogashira coupling,[134] ethylene/carbon monoxide copolymerization,[135] Kumada coupling,[136] Stille coupling,[137], hydrogenation,[138] hydroformylation,[139] alkyne coupling,[140] olefin cyclopropanation,[141] arylation and alkenylation of aldehydes,[142] reduction of aryl halides,[143] atom-transfer radical polymerization,[144] and asymmetric catalysis in hydrosilylation reactions.[145] In addition, further considerations such as the beneficial ionic liquid effects of the imidazolium salts, and strategies to avoid catalyst leaching were summarized.[87]

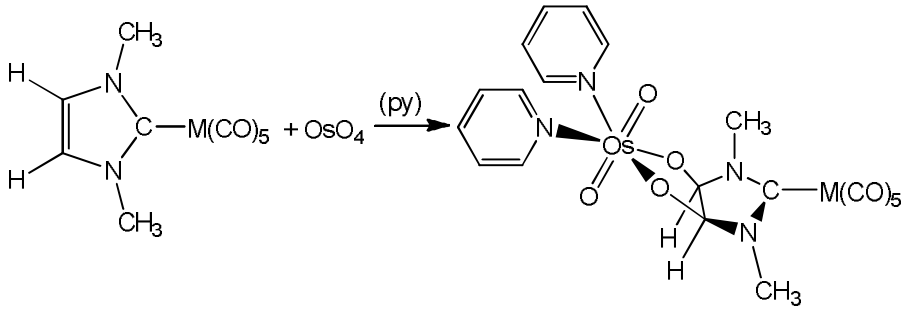

Figure 2.17. The first recorded reaction happening at the C−C backbone of NHC. Adapted from Ref. 123.

Another extensive review by Crabtree studied the application of NHCs in comparison to other well established ligands – "NHC ligands versus cyclopentadienyl and phosphine as spectator ligands in organometallic catalysis".[146] As already mentioned in Section 2.1, NHC, phosphine and cyclopentadienyl are the three main classes of ligands which are routinely applied in a wide range of metal complex catalysts. This more recent review compared them with respect to accessibility, synthesis, functionalization, degradation and cyclometallation.[146] It was pointed out that with respect to ligand substitution, the NHC maintains its advantages over phosphine, because the substituents are not directly attached to the donor atom – the carbene carbon atom, but to the adjacent nitrogen atoms or the carbon atoms on the backbone (Figure 2.18).[146] In other words, the immediate electronic environment of the carbene does not have to be changed along with the total steric demand, as suggested by computational results (DFT calculated frequencies).[146,147] As a result, steric and electronic factors can be treated independently in an approximate way.[146] In case a separate analysis of the electronic effect is required, the author suggested to vary the nature of the azole ring, to achieve a significant and analyzable change.[146]

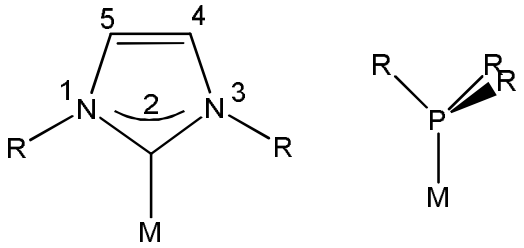

Figure 2.18. Comparison of substituted NHC and phosphine ligand. In an NHC ligand, substitution is at the N1/N3 or C4/C5 atoms, avoiding a direct influence on the metal-ligand bond; in a phosphine ligand, substitution is at the phosphor atom, which is directly bonded to the metal. Adapted from Ref. 146.

Turning to the chelate NHC ligands, Crabtree reported significant coherence between the length of the linker and the orientation of the azole rings.[146] In one metallation experiment, the factor of orientation turned out to be decisive for the selectivity of two competitive reaction pathways (Figure 2.19).[146] Whereas a methylene or ethylene linker favored the non-chelated product with coplanar NHCs, linkers consisting of more than three carbon atoms led to the formation of a chelate product with parallel orientated NHCs.[146] The author counted this effect as an analogy of the use of a linker group in the *ansa*-metallocene, which is applied to fix the indenyl ligands.[146] It was also speculated that the rotational orientation by varying the linkage length is more important for the fan-shaped NHC ligands than the cone-shaped Cp or phosphine ligands[146] (Figure 2.18).

Finally, Olaf Kühl in his review "The chemistry of functionalised N−heterocyclic carbenes", summarized the targeted synthesis of various NHC moieties.[148] He supplied rich background information about the synthesis of versatile NHCs carrying phosphine-, amino-, imino-, or oxygen functionalities.[148] Synthetic strategies were explained by considering the acidity/basicity of the source compound imidazole, the stability of the functional groups relative to base and temperature, as well as the chiral moieties carried by the NHC.[148] In a nutshell, the "gold rule" is to introduce the functional group first and generate the carbene last.[148] Exceptions were only found in cases where the carbene carbon atom was situated in a complicate surrounding, e.g., when the proton at the C2 atom and the protons from a secondary amine substituent compete during deprotonation, or when the C2 atom and the protons from an extended side chain at the N1/N3 atoms can interact. [148-150] In such cases, a bulky base for deprotonation or shielding the side-chain protons with protecting groups should be used. [148-150]

Turning to the catalysis, besides a group of cross-coupling reactions where the phosphines and carbenes were successfully employed,[123,148,151] the catalytic activity of achiral functionalized NHCs with established *bis*-carbene or *bis*-phosphino chelates were compared.[148] The catalytic performance due to functionalization was considered to be less efficient than that due to the chelate effect.[148] Nevertheless, chiral modifications of NHC by introducing a rigid scaffold at the nitrogen atoms are considered as a viable concept for asymmetric catalysis.[16,148,152]

The three abovementioned reviews complement each other regarding the research in the field of NHC. Pertinent research activities are growing at a rapid pace, and the topic has been thoroughly studied. Though an overview of all important research projects cannot be given within the scope of this dissertation, representative works regarding the main categories will be mentioned in the subsequent chapters.

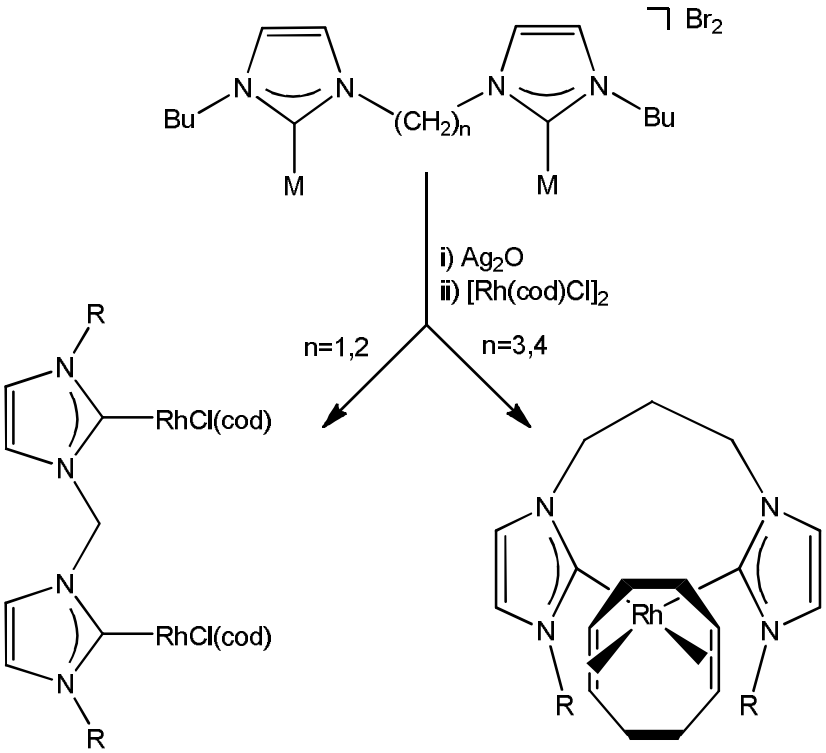

Figure 2.19. Illustration of the linkage effect. A non-chelated complex with NHC ligands placed in coplanar fashion (left) is compared to a chelated complex with NHC ligands arranged in parallel fashion. Adapted from Ref. 146.

2.3.3 Stability and Aromaticity of NHC

Before the discovery of NHC, carbenes were mostly transient and highly reactive species of short life time, such as Fischer[109] and Schrock[110] carbenes. The noticeable stability of a simple imidazol-2-ylidene carbene has attracted great interest in the investigation of the responsible electronic factors.[120,153] The first experimental study on the stability of carbenes can be traced back to 1991.[120] Supported by structural information from an X-ray analysis and ab initio calculations from the same group, Arduengo et al. drew the conclusion that the ylidic character of this compound is rather weak, and the cyclic p_π-p_π delocalization is not extensive either.[120] This was followed by a theoretical investigation by Cioslowski, done at the MP2 level.[153] He determined the localized natural orbitals[154] and covalent bond orders[155] to examine the electron distribution.[153] He compared the parent carbenium ion and an imidazolium cation.[153] According to his interpretation of electronic wavefunctions, he concluded that the stability of this carbene is mainly due to σ-backdonation from the carbenic carbon to the adjacent nitrogen atoms, while the π-donation from nitrogen to carbon plays only a minor role,[153] in accordance with the suggestions of Arduengo.[120] Furthermore, Cioslowski pointed out, that the π-electron stabilization has contributed to the unusually large proton affinity rather than the stability of the NHC.[153] As evidence, he listed the topological change of one of the occupied localized natural orbitals (orbital 17 in Figure 2.20a and Figure 2.20b) and the high exothermicity of the protonation reaction.[153] Comparing orbital 17 with other orbitals (Figure 2.20b), it can be seen that the C−H bond which is formed during protonation is of covalent nature, being similar to the other C−H bonds, e.g., orbital 14, 18, and 20, but less ionic than the orbitals 8, 10, and 12.[153]

Early comparative studies on the saturated and unsaturated NHCs considered above all their different stabilities.[74] Heinemann and Thiel concluded from optimizations at the closed- and open-shell restricted Hartree-Fock (RHF) level, followed by single-point calculations using Møller-Plesset perturbation theory MP2/MP3 and a TZ2P basis set that the prototype of the first isolated stable NHC has a substantially higher singlet-triplet splitting than its saturated analogue, ΔE_{S-T}(unsaturated) − ΔE_{S-T}(saturated) > 15 kcal·mol^{-1} (imidazol-2-ylidene vs. imidazolin-2-ylidene)[156] Kinetic stability of unsaturated NHCs was confirmed towards the 1,2-hydrogen shifts (ΔE_a > 45 kcal·mol^{-1}, E_a = activation energy).[157]

More criteria were established to learn about the role of π-electron delocalization, e.g., the magnetic susceptibility, the Laplacian charge distributions, and low-energy ionization processes such as removal of an electron from the lone-pair carbenic carbon.[156] An alternative charge analysis, following the “atoms in molecules” approach, was used to

evaluate the role of cyclic electron delocalization.[158] Accordingly, the electron delocalization in a unsaturated NHC is by far less pronounced comparing to benzene or the imidazolium cation.[156] A study of Frenking et al. revealed a dramatically reduced aromaticity of the substituted NHCs compared to those of benzene derivatives and traced it to the facilitated accommodation of the lone pair electrons by the endocyclic nitrogen atoms. That study relied on calculations carried out at the BP86/def2-TZVPP and MP2/def2-TZVPP levels of theory.[159]

In a review, Bourissou et al. discussed in detail the stability of various types of carbenes, including NHCs with different N-substituents.[160] Particularly, the important role of the π-donation from the amino group was demonstrated by a modified NHC, comprising two

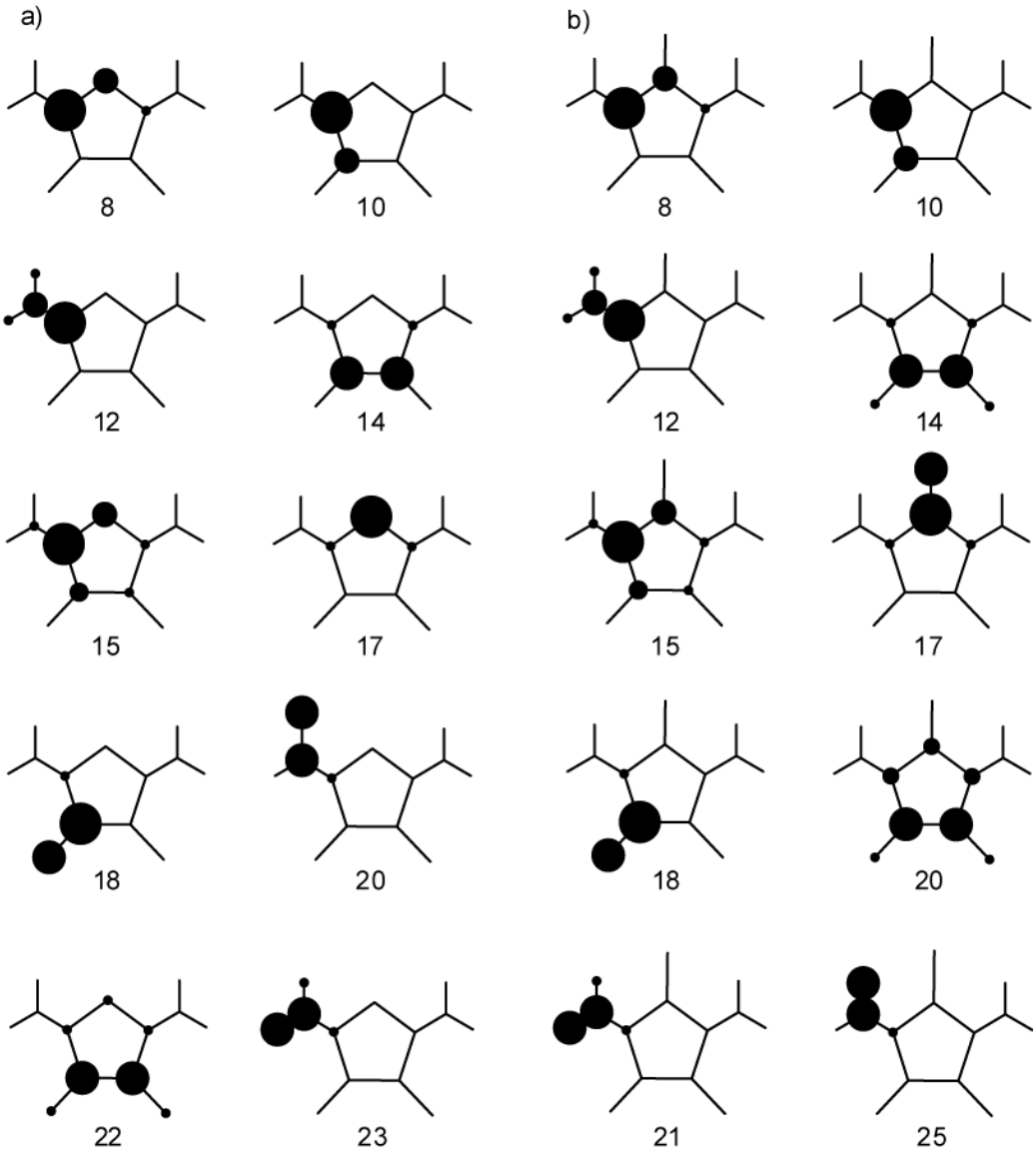

Figure 2.20. Occupied localized natural orbitals of a) the molecule $C_5H_8N_2$ (1,3-dimethylimidazole and b) $C_5H_9N_2^+$, the corresponding imidazolium cation. Orbital 17 in b) corresponds to the C−H bond. Adapted from Ref. 153.

bipyridine frameworks (Figure 2.21).[160] The additional electrons can delocalize into the bond between the carbenic carbon and the attached donor or acceptor fragment (Figure 2.21).[160] Hahn gave more examples of extensively substituted NHCs − both symmetrically and asymmetrically (Figure 2.22).[161] The stability of the NHCs also sparked interest in the synthesis of analogous heterocycles such as thiazol-2-ylidene, oxazol-2-ylidene, and PHC, see Figure 2.22.[161]

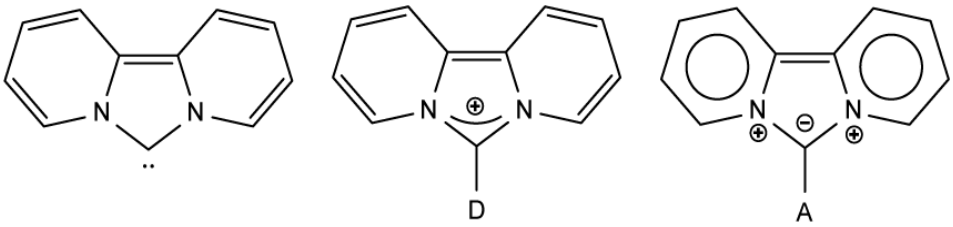

Figure 2.21. Modification of the electronic properties of carbenes by using a 2,2' -bipyridine framework. D: donor, A: acceptor. Adapted from Ref. 160.

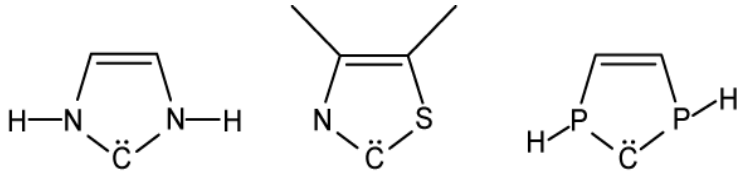

Figure 2.22. N-heterocyclic carbene vs. thiazol-2-ylidene, oxazol-2-ylidene, and P-heretocyclic carbene. Adapted from Ref. 161.

A rather exotic carbene compound is the divalent carbon(0) $C(NHC)_2$ (formally a fragment of NHC), inspired by analogue carbodiphosphoranes $C(PR_3)_2$.[162] This compound opens a new aspect in the application of NHC moieties. An NBO analysis suggested the Lewis structure to be C=C=C, in a bonding situation of the type NHC→C←NHC.[163] The NHC moieties were considered as closed-shell ligands, while the carbon atom has two lone pairs of σ- and π- symmetry respectively.[162] The calculations were carried out at the level of BP86/TZ2P.[162]

In the following I will briefly describe how one can assess the degree of aromaticity in a cyclic system. Hückel was the first who made a major contribution to the interpretation of the electronic configuration of benzene and relevant compounds.[164] He formulated the well-known rule bearing his name from his study on benzene and hydrobenezene for estimating the aromatic properties of a ring system.[164] The method was first proposed for planar, cyclic conjugated hydrocarbons, but later on extended to molecules involving heteroatoms, e.g., pyridine, pyrrole and furan.[164,165]

Noteworthy is a study by Sauers where he calculated a series of heterocyclic 6π-cyclic compounds using ab initio methods at the MP2/6-31G** level.[166] An important conclusion of that work was that among several carbene/ylide systems, the imidazolyl carbene is the most stable one which is comparable to furan and pyrrole.[166] To give an overview, the aromatic stabilization energy (ASE), the following (X,Y) systems (O,O), (O,NH), (NH,NH), (NH,S), and (S,S) (Figure 2.23) were calculated and compared to those of pyrrole and furan.[166] The resulting ASEs range from 7.65 to 21.2 kcal·mol^{-1} in the following order: (O,O) < (NH,O) ~ (S,S) < (NH,S) < furan < (NH,NH) < pyrrole, the ASE of the imidazolyl carbene being 21.2 kcal·mol^{-1}.[166]

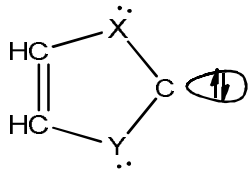

Figure 2.23. The general chemical structure of five-member ring systems involving heteroatoms X and Y. Adapted from Ref. 166

In general, Hückel's rule implies that a cyclic conjugated molecule with [4n+2] π-electrons (an odd number of electron pairs) is stable and aromatic, due to the stabilization caused by a resonance effect.[164] Later, the unstable counterpart with [4n] π-electrons or an even number of electron pairs was defined as anti–aromatic.[151] With the Hückel molecular orbital (HMO) method,[167] *a posteriori* or *a priori* criteria for aromaticity were proposed for more complicated conjugated systems, especially in the 1970s.[168-170] The most successful semi-empirical criterion was suggested by Hess and Schaad.[168] After classifying single and double bonds in hydrocarbons in eight types according to the number of attached hydrogen atoms, they discovered a linear dependency of the HMO π-energies on the number of each type of bond.[168] The resonance energy was then calculated as the energy difference between the HMO energy of the whole cyclic system and the additive energy from individual (double) bonds in the corresponding localized structure.[168] The defined resonance energy and the observed stability were confirmed to correlated in excellent fashion for an extensive data set.[168]

Alternatively, applying the graph theory from pure mathematics, Gutman et al. introduced the TRE concept (topological resonance energy) which depends solely on the topology of a conjugated system.[169] The TRE approach not only predicted the chemical behavior of a large number of neutral conjugated systems, but it was also used for studying conjugated radicals, ions, and even systems in excited states.[169] An essentially identical idea

was reported at the same time by Aihara,[170] although the reasoning was different. Thus, there are two different terminologies for the same criterion, TRE and the "A-II resonance energy".[170] From the 1980s to the first decade of this century, several new criteria or improvements of old criteria were suggested for quantifying the aromaticity, e.g., the absolute hardness by Zhou et al.,[171] the nucleus-independent chemical shift by Schleyer,[172] the theoretical bond and strain energies by Grimme,[173] the multicenter bond indices by Giambiagi et al.,[174] the anisotropy of the current-induced density by Herges et al., [175] the delocalization index by Poater et al.,[176] and the aromatic fluctuation index by Matito.[177]

2.3.4 Steric Properties of NHC

In organometallic chemistry, the NHC compounds were first introduced to replace phosphine ligands.[123] These two types of ligands differ in (local) symmetry. The monodendate phosphine ligand has at most a C_3 axis and NHC ligands at most a C_2 axis. In case of chelate complexes, the phosphor atom is not directly bonded to the metal but on other bidentate or polydentate ligands which are mostly rigid. In contrast, almost all *bis*- and polydentate NHCs are directly bonded to the metal via their carbene atom. With respect to these differences in steric properties, a new descriptor of steric demand (buried volume)[178,179] was introduced for the NHC ligands, in analogy to the "Tolman cone angle"[180] of the phosphine ligands.

The buried volume $\%V_{Bur}$ of the ligand is defined as the upper hemisphere of a spherical space centered on the metal atom, within a semi-empirically determined radius that depends on the M−C bond length between metal and NHC.[181] This method is mostly suitable for NHCs with flat ligands, e.g., aryl groups, which are perpendicular to the imidazole plane,[181] because such a spatial arrangement is space-demanding in two orthogonal directions (Figure 2.24) and can be best gauged by the sphere-model.[181] According to the authors, this concept is also appropriate for describing asymmetrically substituted NHC complexes, i.e., systems exhibiting uneven spatial distributions.[178,181] The buried volume was applied in a study of the interplay between electronic and steric factors of saturated and unsaturated NHC complexes,[181] as will be described below in Section 2.3.5 "Stability and Reactivity of the TM-NHC Bond".

It should be noted that the buried volume was originally proposed for monodentate NHC ligands.[161] In the current work, I studied catalysts bearing a bidentate NHC ligand. This class of *bis*-NHC ligands differs from the monodentate NHC or phosphine ligands in their basic scaffold so that in most cases there is no local symmetry axis. In this respect, either the buried volume[161] or the Tolman cone angle[180] is adequate for describing the steric demand. Instead of occupying the whole semisphere, the present *bis*-NHC ligand separates the space in

proximity to the metal center in two variable proportions, depending on the ligand conformation. A dihedral angle γ between the two imidazole rings is introduced to describe this specific flexibility of the bidentate NHC ligand (Figure 2.25).[93] Rotational isomerization of the ethylene bridge leads to conformational changes for which two main spatial forms can be discerned, "bent" and "open", according to the size of the dihedral angle γ between the planes of the two imidazole rings (Figure 2.25). A ligand conformation is referred to as "open" if $\gamma > 140°$, otherwise as "bent". Accordingly, the side, to which the *bis*-NHC ligand is bent, is defined as the "front" side of the catalyst complex (Figure 2.25).[93]

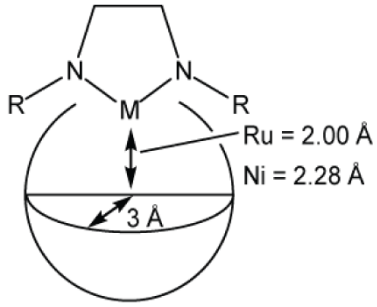

Figure 2.24. Illustration of the concept "buried volume", adapted from Ref. 181.

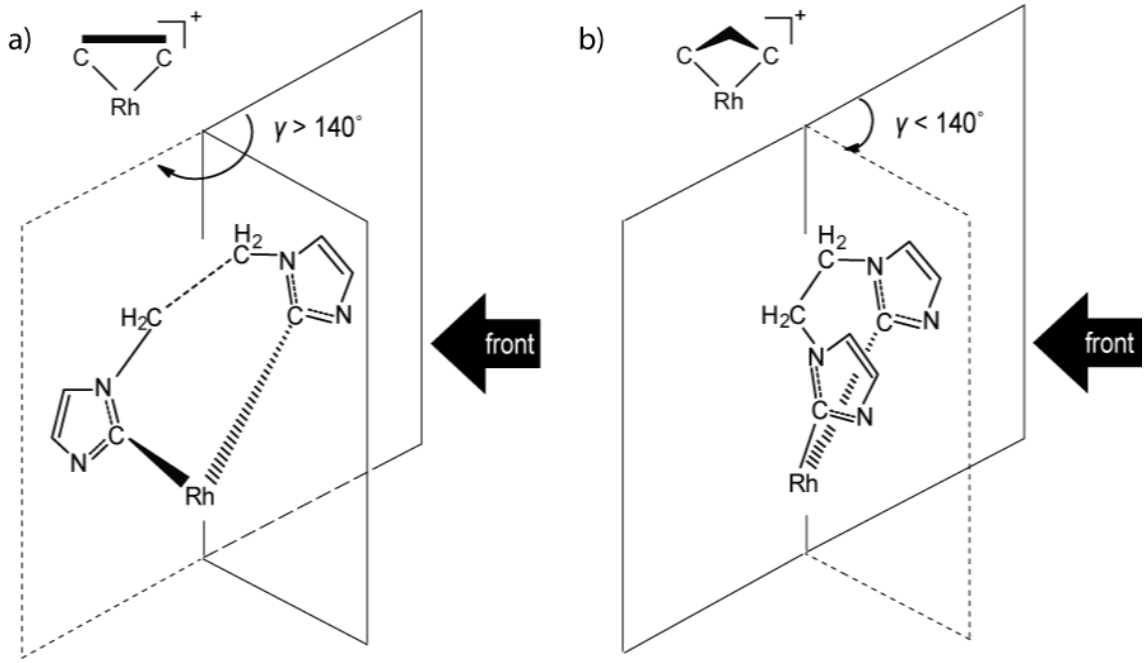

Figure 2.25. Classification of "open" and "bent" conformations of the ethylene bridged bis–NHC ligand. Simplified symbols depict complexes in front view. Adapted from Ref. 93

2.3.5 Stability and Reactivity of the TM-NHC Bond

By virtue of the growing numbers of pertinent publications, key questions like the stability and reactivity of the M-NHC bond arose. Crudden and Allen comprehensively reviewed the potential decomposition pathways and the key reactions catalyzed by NHC-metal complexes.[182] In the first part of that review, they distinguished between two pathways, the associative reductive elimination and the displacement of NHC ligands by competing ligands. Examples were arranged according to the chelation situation of the complexes and the ancillary ligands, as well as the central metal atoms. The second part of the review presented findings in the range of C−H/C−C activations, the generation of the NHC-metal complexes, as well as the reactivity of the π-bond of the unsaturated NHC ligands.[182] Based on the material presented, the authors summarized that the factors that facilitate the reductive elimination of monodentate NHC ligands: above all the presence of positive charges on the metal, but also the appropriate auxiliary ligands, alkyl- or aryl-groups *trans* or *cis* to the σ-donor ligand NHC,[182] as well as the steric bulkiness of the NHC ligands.[182]

It is noteworthy that the migratory insertion reactions of the free carbene are reminiscent of the chemistry known for the isoelectronic carbon monoxide and isonitriles, but more complex (Figure 2.26a).[182,183] In the case of chelated NHCs, this process does not necessarily lead to the de-complexation but can also form complexes bearing NHC ligands with an oxidized carbene atom (Figure 2.26b).[182,183] The reaction is favored both kinetically (E_a = 7.8 kcal·mol^{-1}, activation energy) and thermodynamically (H_R = −32.2 kcal·mol^{-1}, reaction enthalpy).[182]

As the denticity increases from bidentate to tridentate, the flexibility of the NHC ligand decreases and its steric hindrance increases.[182] Some tridentate NHC-metal complexes can decompose at high temperatures.[182,184,185] Further information of the NHC-metal-bond stability was revealed in a series of displacement reactions. NMR spectroscopic evidence suggested the displacement of carbene in small, unobservable concentration, resulting from the presence of the competing ligands,[182,186,187] or even replacement of the NHC ligands by phosphine ligands, which are generally considered more labile.[188] Exchange between NHC ligands and free NHCs in the environment was also observed.[188] The relation between the stability and reactivity of the TM-NHC bond was illustrated by 15 Pd-NHC complexes in two Mizoroki−Heck reactions.[182] The mechanism assigned to these reactions is known for involving many key intermediates which are prone to decomposition.[187]

Jacobsen et al. introduced quantified basic factors for clarifying the NHC-metal bonding properties.[189] Motivated by experimental observations such as different catalytic activities between saturated and unsaturated NHC ligands, and the completely different stabilization types between the 16-electron complex $IrCl(ItBu)_2$ and 14-electron complex $[Ir(ItBu)_2]^+[PF_6]^-$, steric and electronic contributions were separated.[189] The authors concluded from their datasets of monodentate NHC-metal complexes[189] that, generally, the NHC ligands bind more tightly than phosphines to the transition metal, and the bond dissociation energies of saturated and unsaturated NHC ligands differ hardly, being around 1 kcal·mol^{-1}.[189] Additionally, the authors analyzed the frontier molecular orbitals of the saturated NHC ligand.[181] The choice of this simplified model type was aimed at facilitating the analysis, so that only three π atomic orbitals are needed for describing the interactions between the NHC and the metal center (Figure 2.27).[189] Two interactions were suggested explicitly for group 11 and group 9 metals – d→π* back-donation and π→d donation (d→MO4 and MO1→d), respectively (Figure 2.27).[189] Furthermore, they proposed that the electronic nature of the metals could influence the π partition in the σ-dominated NHC-metal bonds. As a result of an enhancement of the π fraction, late transition metal-NHC compounds can be more stable than their phosphine counterparts.[189]

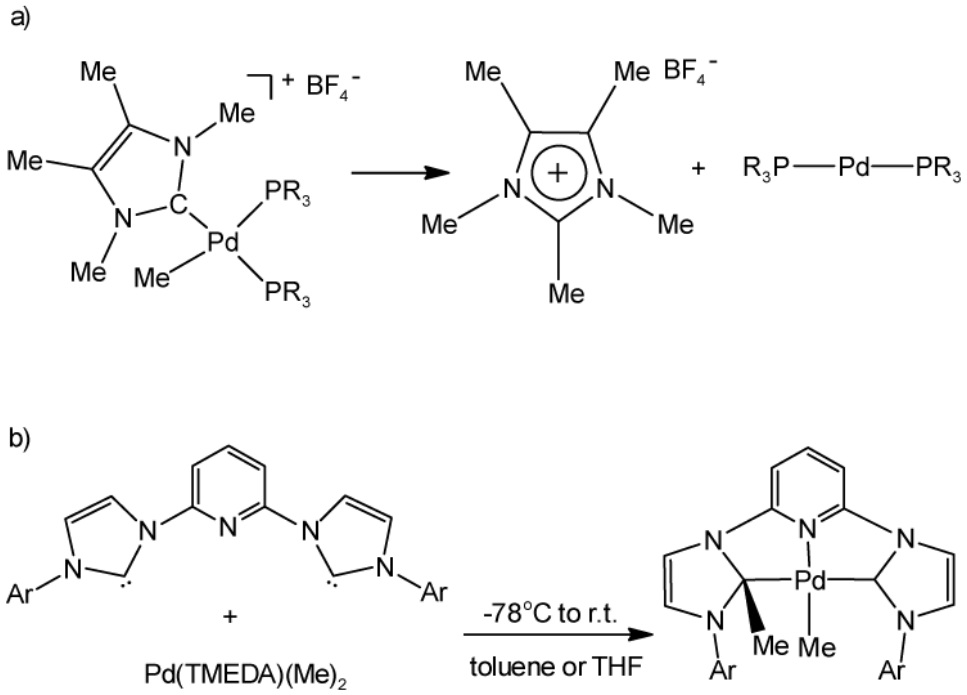

Figure 2.26. Alternative pathways induced by migratory insertion of a methyl group: a) de-complexation of monodentate NHC ligand and b) oxidation of the carbenic carbon atom in a chelate NHC ligand. Adapted from Ref. 182.

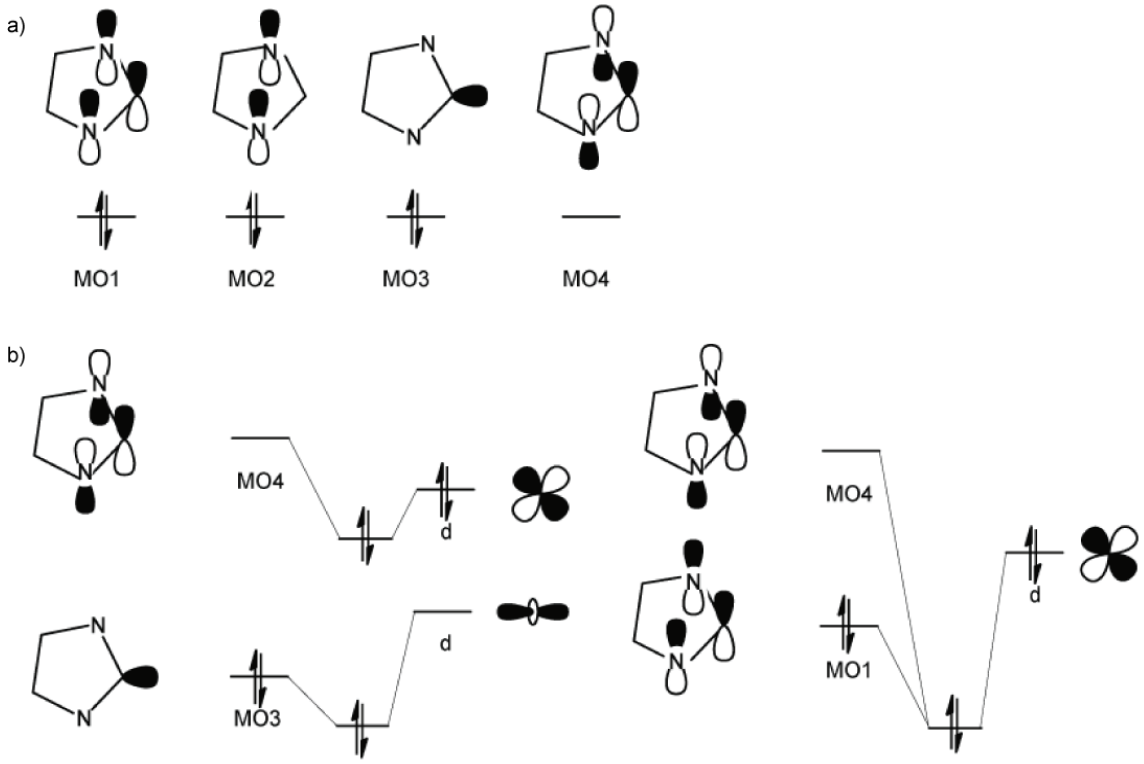

Figure 2.27. a) The frontier orbitals of a saturated NHC involved in the NHC-metal bonding and b) the NHC ligand as σ-donor, π*-acceptor, and π-donor, adapted from Ref. 189.

The steric effect of chosen saturated and unsaturated Ru-NHC complexes was analyzed regarding the dependence of the M−C bond dissociation energy on the buried volume.[190] Note that the combined QM/MM method chosen by the authors overestimate the bond strength for NHC ligands with small N-substituents and exclude the feasibility of NHC-metal complexes bearing bulky N-substituents.[190] Moreover, though the saturated NHC ligands generally feature slightly larger buried volumes than their unsaturated counterparts, experimental data give evidence for stronger NHC-metal bonds in saturated than in saturated Ru-NHC complexes. [190] Thus, the steric effect may not be readily understood in this way.

In addition to the different stabilities, distinct catalytic activities of saturated and unsaturated M-NHC complexes were also reported and discussed.[190-192] Theoretical studies focused on the comparative analysis of the metal-NHC bond properties.[190,191] The main findings are as follows. (*i*) The difference in the catalytic activities originates from very small changes in the donor partition of the M-NHC bond.[190] (*ii*) π-donation from NHC to metal, instead of the biased π-back donation, may contribute to the catalytic process as well.[191] (*iii*) Systematical variation of the N-substituents affects the reaction kinetic more clearly in the unsaturated NHC, most likely due to a larger electron delocalization in the five-member

ring.[191] An experimental study traced the solution dynamics by NMR spectroscopy.[192] On the example of the α-arylation of ketones and Buchwald-Hartwig amination catalyzed by palladium complexes bearing unsaturated and saturated NHCs, it was determined that the catalytic activity can be induced by the steric demand as well.[192] The superior catalytic activity of the saturated NHC complexes was nicely illustrated in a study based on a series of palladium *bis*-NHC catalysts for Suzuki-Miyaura coupling,[193] where the catalytic activity of the complexes bearing different ligands decrease in the order (sat-NHC)$_2$PdCl$_2$ > (sat-NHC)(unsat-NHC)PdCl$_2$ > (unsat-NHC)$_2$PdCl$_2$.[193]

Crabtree pointed out that the NHC-metal bond is inert as the reactivity of NHC carbenes is much smaller than that of Schrock and Fischer carbenes.[146] The main argument is that the NHCs are not involved as intermediates in many reactions, unlike the latter two classical metal carbenes.[146] Especially, he investigated the advantages of the NHCs such as the electronic and steric adjustability by analyzing the frontier orbitals.[146] The stability of the NHC-M bond was rationalized as follows. While the carbene carbon atom prefers to remain in sp^2 hybridization in order to accept π-donation from the adjacent nitrogen p-orbitals and to maintain the aromaticity of the ring, cleavage of the M-NHC bond requires intermediates with an sp^3 carbon; therefore, it is less likely.[146] Furthermore, the orientation of the NHC ligand with respect to other co-ligands may be related to the degree of back-donation.[146] As shown in Figure 2.28, the orientation of the p_z orbital (left), and the two N−C σ^*-orbitals (middle) of NHC, as well as the three X−P σ^*-orbitals (right, only one orbital depicted) of phosphine are all fixed in space relative to the ligand orientation. Hence the acceptor ability of the ligand depends not only on substituents on the ligand, electronic features of co-ligands, and metal, but also on the relative orientation of the ligand (Figure 2.28).[146] It is conceivable that the NHC ligand tends to behave as π-acceptor or even π-donor (left) – depending on the occupancy of the carbene p_π-orbital – and whether the metal d orbital is perpendicular to the azole ring. The σ-interactions requires the σ* orbital of the NHC carbene (middle) and the metal d orbital to be aligned in the same plane.

The electronic influence of the NHC ligands on the transition metal complexes can be evaluated directly by calculating the M-NHC bond dissociation energies.[194,195] Frenking et al. carried out theoretical studies on metal-NHC complexes by varying either the metal center,[194,195] or using carbene analogues, e.g., silylene and germylene.[194] Different types of carbenes were also compared, e.g., aNHC − abnormal NHC vs. the most stable isomer form of NHC[195] (Figure 2.29).

The most important findings of their work can be summarized as follows. First, no clear trends were found for metals of the same group or the same period.[194,195] Second, to describe the bonding situation in a more precise way, it is necessary to consider concurrently various charge partitioning methods such as natural bond orbital analysis (NBO), charge decomposition analysis, atoms in molecules theory and energy decomposition analysis.[196-198] Third, the metal-NHC bonds are more stable than the metal-silylene and metal-germylene bonds.[194] Finally, the stabilities of nHNC (normal NHC, see Figure 2.29), aNHC and IMID follow the trend: IMID > nNHC > aNHC.[195] Nevertheless, the less stable aNHC is also widely applied in organometallic chemistry besides the relatively more stable nNHC.[178] A comprehensive analysis of the prevalence of aNHC comparing to the nNHC was given by Arnold and Pearson.[199]

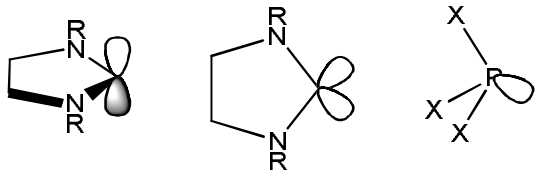

Figure 2.28. Frontier orbitals which can be involved in π-backdonation. From left to right are: the p_z orbital of the carbenic carbon atom, the N−C σ^*−orbitals and the P−X (X=aryl, alkoxyl, or halides) σ^*-orbitals. Adapted from Ref. 146.

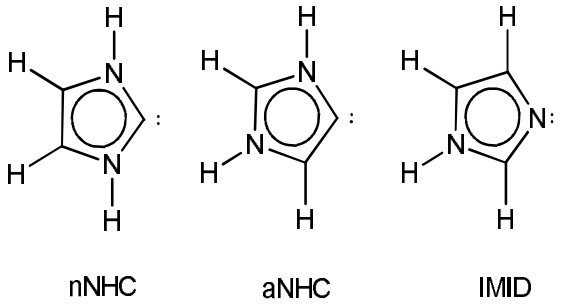

Figure 2.29. Three types of NHC: normal NHC (nNHC), abnormal NHC (aNHC), and the most stable isomer form of NHC (IMID) according to Tonner's definition. Adapted from Ref. 195.

An indirect way of evaluating the electronic influence of the NHC ligands on the transition metal is, for instance, the analysis of binding energies of co-ligands.[198,200] There are many other interesting experimental observations which have revealed the properties of metal-NHC bonds from various aspects, e.g., the exchange of NHC and iodo ligands between two different Pd(II)-complexes.[201]

This thesis aims to study the applicability of *bis*-NHC-Rh(I) complexes in the hydrosilylation of olefins. Rhodium complexes of similar constitution were determined as

active catalysts for related chemical transformations such as hydrogenation,[200,202-204] hydrosilylation of ketones,[27,205-208] hydroformylation,[200] and hydroamination.[209] Many of these complexes are applied in asymmetric catalysis.

2.3.6 Free NHCs

NHC compounds are more than promising ligands in the transition metal catalysts. Several free NHCs are also found to be catalytic active. For instance, as summarized in a mini-review by Fuchter from 2010, NHCs can mediate the addition of silyl pro-nucleophiles (utilized for safety reason, e.g., trimethylsilyl cyanide), to a variety of electrophiles, promote organic and inorganic polymerization, and the reduction of carbon dioxide by hydrosilanes.[71] Grasa et al. also reported that the bare NHCs can act as excellent nucleophilic catalysts for transesterification and acylation reactions.[210]

3 Computational Methods

In Chapter 4,[93] all calculations were carried out with the software package Gaussian 03,[211] using the hybrid B3LYP DFT approach.[212-214] For main group elements, the standard 6-31G(d,p) basis set was applied to all atoms except Rh. For Rh, the Stuttgart-Dresden effective core potential MWB28 was employed.[215] TSs were located with the synchronous transit-guided quasi-Newton method.[216,217] For each stationary state, a normal mode analysis was carried out to confirm a local minimum with no imaginary frequency, or a TS with exactly one imaginary frequency, checking also the direction of the reaction coordinate at the TS. Discussions are based on relative enthalpy barriers (RB) H_a, i.e., the enthalpy difference (see below) between the transition state and the immediately preceding intermediate as initial state. As convergence criterion, the elements of the density matrix were required to change at most by 10^{-6} au and on average at most by 10^{-8} au.

All calculations were applied to models in the gas phase to keep the present results comparable to those of previous computational studies.[22-24,37] Thus, the thermochemical analysis was done at room temperature, i.e. 298.15 K, for systems in vacuum. Experimentally, olefin hydrosilylation by primary silanes is explored in organic solutions of rather low dielectric constants. As standard methods are insufficient for accurately determining Gibbs free energies for reactions in solution,[21] the reaction profiles are shown on the basis of calculated enthalpies. However, at the end of this chapter, (formal) entropy contributions $-T\Delta S$ are also provided for steps where external molecules enter or depart the metal coordination sphere, i.e., oxidative addition and concerted elimination. Furthermore, free energy contributions ΔG_{solv} of solvation (at room temperature) were estimated by carrying out single-point calculations with dichloromethane as solvent (dielectric constant = 8.93) at key intermediates and TS structures using a polarizable continuum model;[218,219] atomic radii for determining the molecular cavity were specified using the united-atom model.[220]

In Chapter 5,[221] applied DFT functionals involve four types of exchange functionals, namely the generalized-gradient approximations Becke88 (B88),[212,213] Perdew-Burke-Ernzerhof (PBE),[222-224] modified Perdew-Wang (mPW), [225,226,227-229] and Tao-Perdew-Staroverov-Scuseria (TPSS),[230] as well as four types of correlation functionals, namely Lee-Yang-Parr (LYP),[214] Perdew86,[231] PBE,[222,223] and Perdew-Wang 91 (PW91).[225,226,232,233] Two additional functionals, M06-L[234] (GGA) and M06[235] (hybrid GGA − HGGA) were chosen as they were recommended for energies of TM systems.[235] The M06-

L functional, although being "semi-local", was reported to perform, in general, better than the hybrid functional B3LYP.[234] Table 3.1 provides details on the exchange-correlation functionals employed; for hybrid functionals, the percentage of the exact exchange is also given.

Table 3.1. Components of each density functional applied in the present study, including percentage of EEX, (exact exchange), and references for X (exchange) and C (correlation) functionals. Adapted from Ref. 225.

Functional	EEX, %	Refs. for X	Refs. for C
B3LYP	20	212,213	214
BP86	-	212	231
PBE0	25	222-224	222, 223
PBE	-	222, 223	222, 223
mPWPW	-	225, 226, 227, 232, 233	225, 226, 232, 233
MPW1K	42.8	225, 226, 227, 228, 232, 233	225, 226, 232, 233
MPW3LYP	21.8	225, 226, 227, 229, 232, 233	214
BLYP	-	212	214
B3PW91	20	212,213	225, 226, 232, 233
M06−L	-	234	234
M06	27	235	235
TPSS	-	230	230

All calculations were carried out using the Gaussian suite of programs, Gaussian 09[236] for M06-L and M06; Gaussian 03[211] for the other functionals. Geometries for molecules in the gas phase were optimized with the functionals B3LYP, BP86, BLYP, B3PW91, PBE, PBE0, mPWPW, MPW1K, M06-L, M06, MPW3LYP, and TPSS, starting from the reported B3LYP structures.[93]

The basis set, effective core potential, and the procedure for evaluating the thermochemistry data are the same as used in Chapter 4. The discussion of results is based on the relative enthalpy barriers H_a. Corresponding relative Gibbs free energy barriers G_a and zero-point energy barriers E_a (in kcal·mol^{-1}) are given for comparison (Table 5.2 in Chapter 5) For species consisting of two weakly interacting moieties, the basis set superposition error, estimated by the counterpoise method,[237] was found to increase activation barriers E_a by at most ~1 kcal·mol^{-1} (Table 5.2 in Chapter 5). For complexes discussed in Section 5.3.2, a natural bond orbital (NBO) analysis was carried out invoking the program NBO 3.1 included with Gaussian 09.[238-240] Geometry results including crucial bonding and nonbonding distances are given in the Appendix .

In Chapter 6, all calculations were carried out with the generalized gradient approximation BP86 using Gaussian 03[211] or Gaussian 09.[236] Except for the choice of functional, the computational details are as same as for Chapter 4 and 5. The semi-local functional was confirmed to be an adequate method for calculating the chosen catalysis system, as will be discussed in Chapter 5.[221] The energetics of the calculated species will be discussed on the basis of calculated Gibbs free energies, which is directly related to the reaction kinetics via the Eyring-Polanyi equation.[241] Relative enthalpies and energies are also given for comparison with the previous studies.[93,221] For the discussion of the electronic structures in Section 6.2.2, an NBO analysis was carried out with the same package given in the last paragraph.

To assess the regioselectivity, the difference (ΔH_a) between the two crucial relative activation barriers (RB) along the anti-Markovnikov (aM) and Markovnikov (M) pathways, H_a(aM) and H_a(M) were calculated and compared to a criterion for the selective formation of the aM product. As shown in Eq. (1),

$$\begin{aligned}\frac{k(M)}{k(aM)} &= \frac{\exp(-G_a(M)/RT)}{\exp(-G_a(aM)/RT)} \\ &= \exp\{[H_a(aM)-H_a(M)]/RT\}\cdot\exp\{[S_a(M)-S_a(aM)]/R\}, \\ &\approx \exp\{[H_a(aM)-H_a(M)]/RT\}\end{aligned} \qquad (1)$$

this criterion can be derived from the Eyring-Polanyi equation[241] and is based on the rate constants k(M) and k(aM), which describe the velocities of the two competitive steps leading to the formation of M and aM intermediates. The entropy term can be neglected in this case, because its contribution to the two compared activation barriers is similar, being less than 1 kcal·mol^{-1}. Besides, the analysis based on relative enthalpies allows one to compare the results in Chapter 6 to those in Chapter 4 and 5.

In general, the program NBO 3.1[238-240] implemented in Gaussian provides supporting information about the electronic features of the analyzed transition metal complexes. Besides its charge analysis, the program also performs an analysis of the natural atomic orbitals (NAO type, occupancy, and energy), the general quality of the determined natural Lewis structure (number of the valence and non-valence electrons), the analysis of the natural bond orbitals, including the occupancy of the orbital, type of bonding, coefficients of the two participating natural hybrid orbitals and details of their composition (percentage of participating NAOs). Finally, the donor-acceptor interactions between the NBOs are estimated, giving additional information of the electron delocalization in the analyzed system.

4 Full Pathways of the Mechanisms

The catalyst models studied in this thesis are a series of *bis*-NHC Rh(I) complexes. In this chapter, the full catalytic cycles of the GT, CH, mCH, and SBM mechanisms are studied on an example of this family, a Rh(I) complex involving an ethylene bridged, N-methyl-substituted *bis*-NHC ligand, denoted as **1** (Figure 4.1).

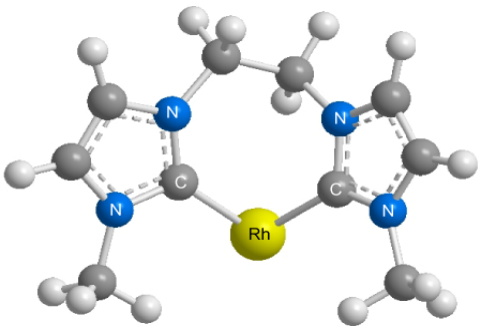

Figure 4.1. Optimized structure of the bare catalyst complex *bis*-NHC-Rh (I) **1**. Adapted from Ref. 93.

In Chapter 2, the stability of the N-heterocyclic carbenes and the TM-NHC bonds, as well as the reactivity and catalytic activity of this group of compounds were discussed based on results of various experimental and theoretical studies. Comparing to the monodentate NHC ligand, bi-chelating NHC ligands recently received increasing attention for their higher thermal and chemical stability.[242] Connecting two NHC rings via a "bridge" also opens a new aspect of catalyst design whereby the spatial requirement of the ligand can be tuned by its flexible conformation. Additional complex modifications are possible if stereo-centers are introduced by the bridge.

Recently, various Pt(II) catalysts with *bis*-NHC ligands were found to be comparable with the Karstedt catalyst[34,35] regarding the catalytic activity and the regioselectivity in olefin hydrosilylation.[73] Related *bis*-NHC Rh(I) catalysts showed good catalytic activity in the hydrosilylation of ketones.[243] These findings motivated the present computational exploration of a Rh complex of this type in olefin hydrosilylation (Figure 4.1). In the following the full catalytic cycles of all four types of mechanism – GT, CH, mCH, and SBM – including variants where appropriate will be addressed in detail.

Before entering the catalytic cycle, the two rings of the *bis*-NHC ligand form a bent structure, which during the course of CH, mCH, and SBM mechanisms changes to an almost co-planar, open conformation, $\gamma \approx 160°$; see Figure 2.25 in Section 2.3.4. An experimental

study of *bis*-NHC rhodium catalysts with different bridge lengths concluded that $(CH_2)_n$ bridges generally favor an essentially square-planar Rh(I) conformation,[243] as also calculated in this thesis. Recall that a square-planar motif is common to transition metal complexes with d^8 configuration.[244,245]

As model reaction hydrosilylation of ethylene CH_2CH_2 by monosilane SiH_4 was chosen. In this way, the model system was kept elementary as a comprehensive study of the overall enthalpy profiles can be carried out for all pathways of the four mechanisms. This choice of model avoids side reactions such as β-hydrogen elimination or double-bond isomerization; focusing rather on the essential steps of the actual catalytic cycles.

In general, the (formally) bare active reaction center of the *bis*-NHC-Rh complex is generated by removing ligands, e.g., cyclooctadiene[242] or norbornadiene,[65,66] during an induction period. On the current model catalyst, two ethylene moieties were considered as ligands which can be removed at the expense of 23.7 kcal·mol^{-1} for the first, and of 30.8 kcal·mol^{-1} for the second ethylene ligand. These energies are almost compensated by consecutive (GT) or synchronous (CH, mCH, and SBM) coordination of the reactants. Silane coordination at the bare catalyst entails an enthalpy gain of 23.6 kcal·mol^{-1}; coordination of both reactants, silane and ethylene, induces a total enthalpy gain of 40.1 kcal·mol^{-1}.

Hydrogen transfer from the silane (SiH_4) to the olefin (CH_2CH_2), formation of a C−Si bond, as well as the displacement of the product with the help of additional reactants, SiH_4 and CH_2CH_2, are the crucial steps of hydrosilylation. Detailed catalytic cycles of the most favored reaction pathways of each mechanism, along with alternative pathways and side reactions are presented in Sections 4.2 and 4.3.

Intermediates are denoted with labels that indicate the mechanism and enumerate a structure along the path, e.g. **GT2** (Figure 4.2). TSs are designated in analogous fashion, by the two structures they connect, e.g. **GT2−3** (Figure 4.2). The model reaction is overall exothermic, with a total change in enthalpy of −27.3 kcal·mol^{-1}.

4.1 GT Pathway

For the GT mechanism complex **GT1**, a Rh-silylene complex that formally consists of the bare catalyst **1** and a coordinated SiH_4 molecule, **2** (Figure 4.2), was chosen as reference for calculating enthalpies in the catalytic cycle (Figures 4.2 and 4.3). Crucial geometry parameters of all optimized structures of the GT mechanism are collected in Table 4.1.

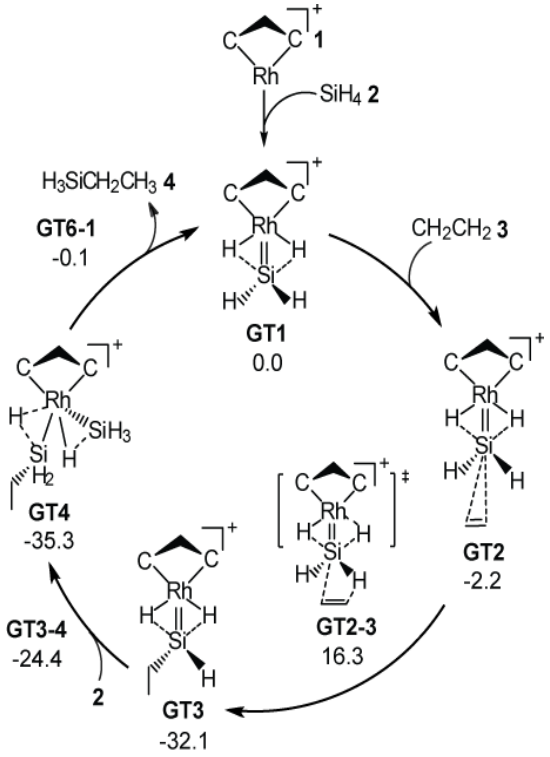

Figure 4.2. Catalytic cycle of the GT mechanism showing all crucial steps. Enthalpies of intermediates and transition states, relative to GT1, in kcal·mol^{-1}. The isomerization steps **GT4** → **GT5** → **GT6**, with the highest (relative) enthalpy barrier at 7.2 kcal·mol^{-1}, are omitted for clarity; see Figure 4.3. Adapted from Ref. 93.

The initial Rh-silylene structure **GT1** is especially stabilized by two H−Rh interactions. In the next reaction step, the reactant ethylene **3** coordinates to the silyl group in a position remote from the metal center, to yield structure **GT2** (Figure 4.2), followed by the insertion of **3** into a Si−H bond via TS **GT2–3**. This last transformation **GT2** → **GT3**, the actual hydrosilylation, is the decisive step of the GT mechanism (Figure 4.3) where the C−Si bond is formed and one hydrogen atom is transferred from **2** to **3** to form the alkyl ligand at the Si center in the intermediate **GT3** (Figure 4.2). The corresponding (relative) activation barrier is calculated at H_a = 18.5 kcal·mol^{-1} (Figure 4.3); it is the second highest of this mechanism. The coordination environment of the metal center in the initial structure **GT1** (Figure 4.2; Rh−Si = 2.31 Å, see Table 4.1) is locally similar to that in **GT3** where the product is bound

via a stable Rh−Si bond, 2.32 Å. Therefore, the displacement of product **4** is expected to be challenging. Indeed two isomerization steps are required, **GT4** → **GT5** → **GT6** (Figure 4.3) which will be discussed in a moment.

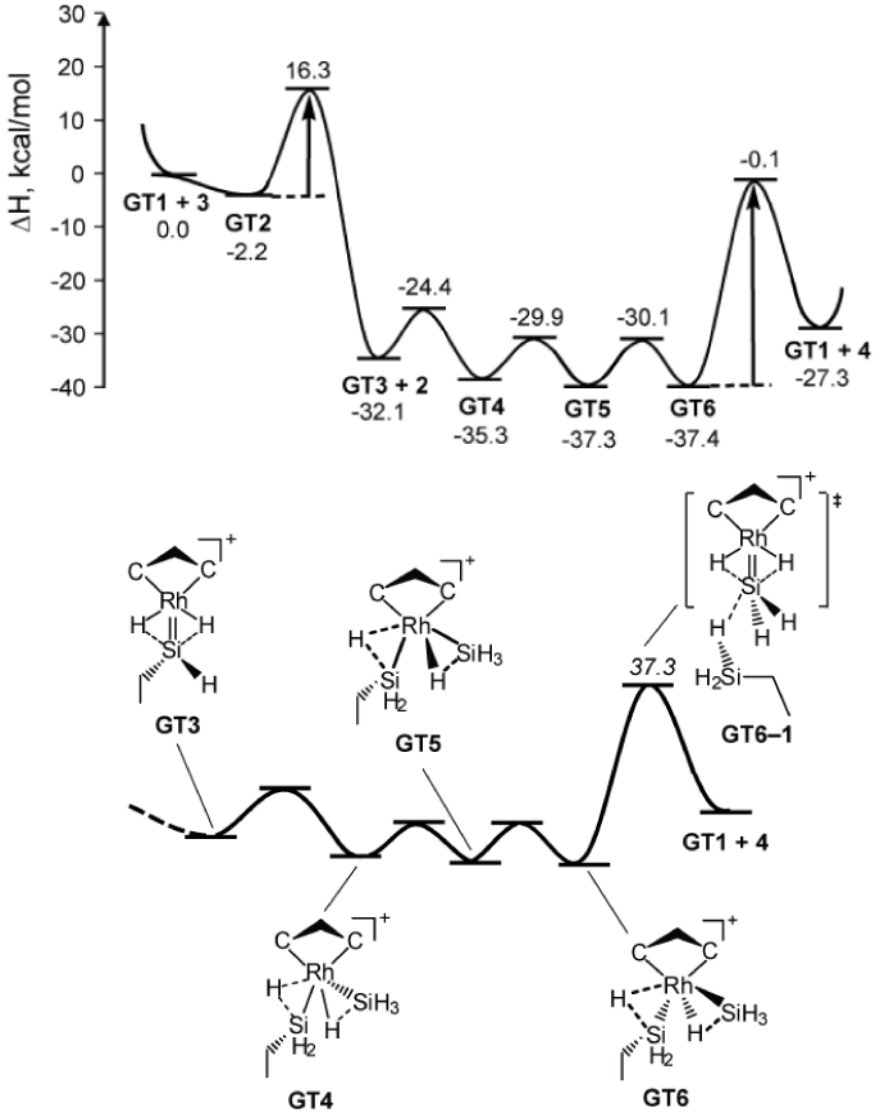

Figure 4.3. Upper panel: enthalpy profiles of the most favored pathway in the **GT** mechanism. The catalytic active species **GT1** is used as enthalpy reference. Crucial steps with highest relative activation barriers are marked by arrows. Relative enthalpies of each intermediate and TS are given in kcal·mol^{-1}. Lower panel: Product elimination for the **GT** mechanism. Relative activation barrier H_a is given in kcal·mol^{-1}. Adapted from Ref. 93.

From **GT3** to **GT4**, the Rh−Si bond between **1** and **4** is elongated to 2.41 Å as a second SiH_4 molecule coordinates at the metal center, with Rh−Si = 2.82 Å (Table 4.1). This new coordination takes place on the less substituted back side of the catalyst; hence the system has to overcome only a low (relative) activation barrier, 7.7 kcal·mol^{-1} (Figure 4.3). Finally, in the step **GT6** → **GT1**, the original Rh–Si bond is cleaved via the highest (relative) activation

barrier **GT6-1** of the GT mechanism, H_a = 37.3 (!) kcal·mol^{-1} (Figure 4.3). The catalytic cycle closes with structure **GT1** of the rhodium complex.

Table 4.1. Crucial distances indicating the formation of silylene complex and the product, as well as the dihedral angle γ in all optimized structures of the GT mechanism. Distances are given in Å and angles in degree. In case of Rh−Si distances, values in the first and second columns are given for the first and second silane, respectively. Adapted from Ref. 93.

	Rh−Si		C−Si	C−H	γ
GT1	2.31	-	-	-	106.5
GT2	2.31	-	3.47	3.09	107.8
GT2−3	2.19	-	2.06	1.70	106.8
GT3	2.32	-	1.88	1.09	108.1
GT3−4	2.47	-	1.88	1.10	103.6
GT4	2.41	2.82	1.88	1.09	98.6
GT4−5	2.45	2.75	1.88	1.09	96.4
GT5	2.46	2.67	1.90	1.09	99.0
GT5−6	2.68	2.50	1.89	1.09	96.5
GT6	2.52	2.48	1.89	1.09	99.2
GT6−1	3.02	2.28	1.89	1.09	101.1

It was not possible to describe the elimination of product **4** without the isomerization steps **GT4** → **GT5** → **GT6** where the silane **2**, just introduced, and product **4** change places relative to the metal center (Figure 4.3). In step **GT4** → **GT5**, with a relative activation enthalpy of 5.4 kcal·mol^{-1}, **4** rotates from the front to the back side, followed by a shift of **2** from the back to the front side, **GT5** → **GT6**, with a relative activation barrier of 7.2 kcal·mol^{-1}. During these isomerization steps, the Rh–Si distances of the two silane moieties change in opposite directions (Table 4.1): the first one, of the eventual product, elongates to 2.52 Å in **GT6** while the corresponding bond of the second silane shortens to 2.48 Å.

Because the GT pathway involves an undercoordinated metal center, it is not competitive for the present Rh catalyst, as will become clear from Sections 4.2 and 4.3.

4.1.1 GT: the Silylene Complex

One characteristic of the GT mechanism is the formation of a catalytic active silylene complex.[21] Compared to the other three mechanisms in the following sections, the GT mechanism is the only one starting from a rhodium-silane adduct instead of a rhodium-silane-olefin adduct. In the current study, **GT1** (the rhodium-silylene complex) was calculated to be thermodynamically less favored than **CH1** (−23.6 kcal·mol^{-1} vs. −40.1 kcal·mol^{-1}, relative

enthalpies with respect to separate bare catalyst and reactants, see Figure 4.14 at the end of this chapter. However, it was reported that rhodium silane adducts can be stable enough to be isolated.[246] At this point, it is worthwhile to recall one pioneering study on the Rh catalyzed hydrosilylation of alkenes, to gain insight into an alternative mechanism based on rhodium silane adduct.[247]

In the year 1987, Ruiz et al. applied the pentamethylcyclopentadienyl rhodium complex to the hydrosilylation of ethylene and observed the formation of a mixture mainly composed of the dehydrogenated product alkenylsilanes.[247] The desired product alkylsilane was a minor component.[247] Though the catalysis was unsuccessful, the experimental results were actually very interesting, indicating the concurrent decomposition of the crucial intermediate in the CH mechanism and the formation of the main side-product of in the mCH mechanism – a "composite" of the experiment[38] of Chalk and Harrod and the experiment[44] by Seitz and Wrighton. Note that the mCH (Seitz-Wrighton) mechanism was published a few months after the work of Ruiz et al. The only reference regarding the catalysis mechanism for Ruiz et al. was the work of Chalk and Harrod,[38] while the mechanism proposed by Seitz and Wrighton was being developed at the same time. Whereas Seitz and Wrighton tried to improve the CH mechanism by closer examination of the elementary steps starting from the metal-alkene adduct (olefin first), see Section 2.2.2.[44] Ruiz et al. estimated that the first step – the oxidative addition of silane (silane first) – is rate-limiting along the reaction pathway.[247] They reported the intermediate after this step to be a novel and a surprisingly inert species $[(Cp^*)Rh(H)_2(SiEt_3)_2]$ (Figure 4.4). The structure of the same complex has been studied by Fernandez et al. in 1984.[246]

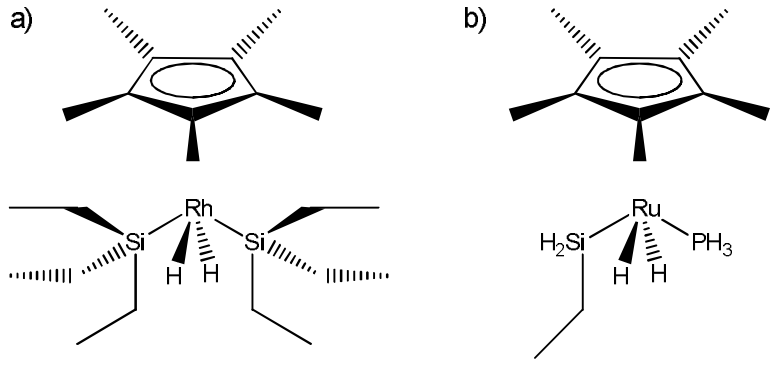

Figure 4.4. Comparative stereo view of the species $[(Cp^*)Rh(H)_2(SiEt_3)_2]$ (a) and $[(Cp^*)(PH_3)Ru(H)_2(SiH_2R)]$ (b); R=ethylene. Adapted from References 246 (a) and 21 (b).

Being described as the "four-legged piano stool",[246] this complex involves two Rh−Si distances of 2.38 Å, being close to the Ru−Si distance (2.30 Å, computed) reported in the

DFT study on the GT mechanism.[37] The close resemblance between these two catalytic active species, [(Cp*)Rh(H)$_2$(SiEt$_3$)$_2$] and [(Cp*) (P^{i}Pr$_3$)Ru(H)$_2$(SiHR)] can be clearly seen (Figure 4.4). They only differ in the central metal (Rh vs. Ru) and one ligand (silane vs. phosphine). The stable intermediate discovered by Ruiz et al. seems to be closely related to the family of the GT -silylene complex. Besides, NHC stabilized transition metal (V(I), Co(I), and Fe(I)) silylene compounds were recently successfully synthesized.[248] It would be of great interest to investigate whether such a compound is catalytically active in the hydrosilylation of alkenes, and whether the GT pathway would be preferred in that case.

4.2 CH and mCH Pathways

Unlike the GT mechanism where the catalytic cycle starts from a Rh(I) silylene complex, in the two types of the Chalk-Harrod mechanism, CH and mCH, both reactants **2** and **3** initially bind to catalyst **1**, forming complex **CH1** which serves as reference for reaction and activation enthalpies of the subsequent steps (Figure 4.5). Both variants of the Chalk-Harrod mechanism comprise three phases: (*i*) oxidative addition of **2** together with addition of **3**, (*ii*) formation of the product, and finally (*iii*) elimination of the product, concerted with a regeneration of the catalytic species **CH1**. Figure 4.5 shows crucial intermediates of the energetically most favored pathways. For both types of mechanisms, CH and mCH, three variants each were studied (Figure 4.6). For intermediates of the two less favorable alternative pathways of CH and mCH the nomenclature is extended, invoking extra labels "**a**" and "**b**" where appropriate (Figure 4.6). The complete enthalpy profiles of the CH and mCH pathways, including the details of the product elimination, are given in Figure 4.7.

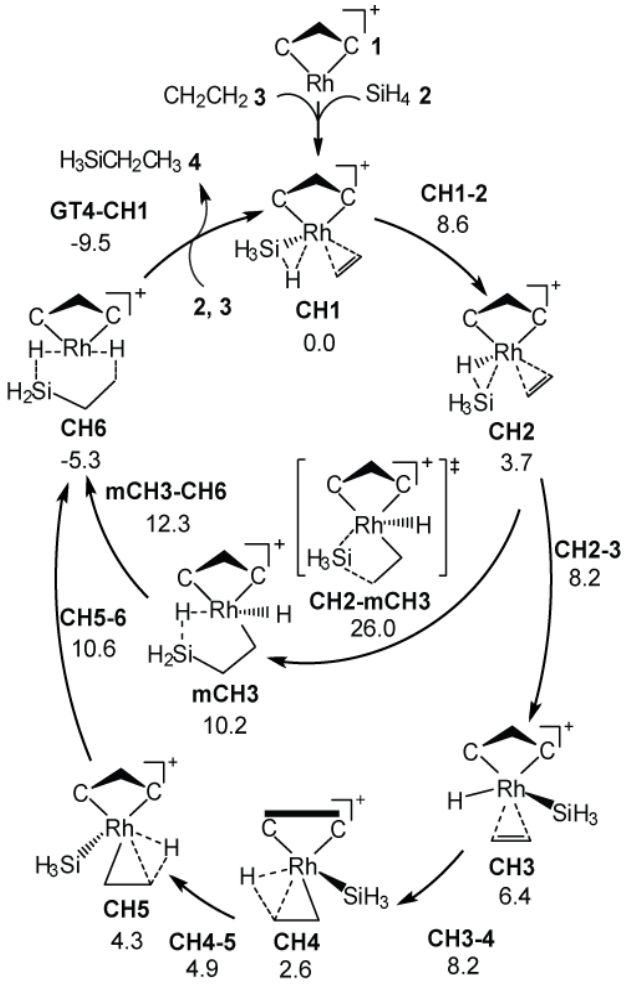

Figure 4.5. Catalytic cycles of the **CH** mechanism (outer cycle) and the **mCH** mechanism (inner cycle). Enthalpies of intermediates and transition states, relative to **CH1**, in kcal·mol^{-1}. The isomerization steps **CH6** → **CH7** → **GT3** → **CH1** and the insertion of a second silane **GT3** → **GT4** are given in Figure 4.7. Adapted from Ref. 93.

4.2.1 Variants of the Initial Phase

Experimental results suggest oxidative addition of silanes on transition metals to be exothermic, with a small activation barrier, because the driving force of this step is the formation of a strong M−Si bond, associated with the cleavage of a weaker sp^3 Si−H bond.[94] Three variants of the first phase of the CH mechanism were considered, namely indirect oxidative addition (*IOA*) [a silyl hydride complex forms via an η^2(Si-H) intermediate], direct oxidative addition (*DOA*), and coupled oxidative addition (*COA*) (a silyl hydride complex forms synchronously with a hydrogenation or silylation of the olefin) (Figure 4.6). The first two variations of the oxidative addition may easily be discriminated by the Si−H distance. An uncoordinated Si−H bond is 1.42−1.50 Å; in an η^2 intermediate, the Si−H distance is elongated to 1.70−1.80 Å, and in a hydride complex this distance is larger than 2.5 Å.[94] In the following, only the kinetically preferred variant *IOA* of the Chalk-Harrod mechanism will be discussed and major differences of the alternative variants *DOA* and *COA* will be briefly described. For each of the three variants of oxidative addition, the first activation barrier was calculated to be the highest during this first stage of olefin hydrosilylation.

The *IOA* pathway starts with a two-step oxidative addition of **2**. The Si−H distance at first increases from 1.50 Å to 1.60 Å (**CH1** → **CH2**), and then to 2.63 Å (**CH2** → **CH3**) (Table 4.2), with the silyl moiety and the hydride ligand to be transferred, arranged in *cis* coordination (Figure 4.6). If one starts the oxidative addition with the hydrogen, which in **CH1** is part of an activated Si−H bond (Si−H = 1.70 Å), one obtains an alternative structure, **CH2b**, and thus the *COA* pathway. Returning to *IOA*, in the first step, **CH1** → **CH2**, the SiH_4 moiety rotates such that the SiH_3 moiety is pointing to the front of the complex (Figure 4.6), passing its highest enthalpy barrier, 8.6 kcal·mol^{-1} (Figure 4.6). **CH2** is slightly less stable, by 3.7 kcal·mol^{-1}, than **CH1**, a consequence of the higher spatial demand of the *bis*-NHC ligand toward the front of the catalyst. Therefore even higher energy differences between **CH1** and **CH2** are expected for bulkier N-substituents or larger silanes which are often used in experiment.[73] Subsequently the hydrogen separates from the silyl group while proceeding over a relatively small barrier, H_a(**CH2** → **CH3**) = 4.5 kcal·mol^{-1}.

Along the alternative pathway *DOA*, oxidative addition encounters a relatively high barrier, H_a(**CH1** → **CH2a**) = 26.7 kcal·mol^{-1} (Figure 4.6). The barrier of *COA*, H_a(**CH1** → **CH2b**) = 12.0 kcal·mol^{-1}, is by 3.4 kcal·mol^{-1} higher than that of the preferred pathway *IOA*. The main difference in the final states of these three variants is the relative positioning of the three ligands H, SiH_3, and C_2H_4 (Figure 4.6).

The modified Chalk-Harrod mechanism (Figure 4.6) starts at structure **CH2** where **2** and **3** are advantageously positioned for silyl transfer. The preferred pathway was explored, namely the *COA* (which leads to the final structure **CH6** via intermediate **mCH3**) as well as the two *IOA* variants, *IOA*1 and *IOA*2. A *DOA* variant, similar to that of the CH mechanism, was also considered but turned out to be very unfavorable because of the *trans*-coordination of silyl and ethylene moieties (Figure 4.6).

Along the *COA* variant, the Si−H distance increases to 3.14 Å (**CH2** → **mCH3**). Simultaneously, the C−Si distance shortens by 1.33 Å to 1.90 Å, which represents a normal C−Si bond (Table 4.2). However, this variant is more complicated than the *COA* variant of the **CH** mechanism because several bonds are simultaneously cleaved or formed (Figure 4.6). The coupled C=C bond activation and Si−Rh bond cleavage (**CH2** → **mCH3**) features a higher barrier (H_a = 22.3 kcal·mol^{-1}, Figure 4.6) than the step to **CH3** of the **CH** mechanism because the ligand sphere of the metal center has to rearrange notably.

Both *IOA* variants of the mCH mechanism start with the oxidative addition **CH2** → **CH3** of the CH mechanism and continue with the isomerization **CH3** → **CH3a** which facilitates forming the C−Si bond.

All variants of CH and mCH reunite at **CH6** (Figure 4.6). The indirect oxidative addition *IOA* is kinetically preferred at the start (!) of both mechanisms. However, in total the *IOA* variant is favored only for the CH mechanism, whereas for the mCH mechanism the compact chemical transformations of the *COA* variant are kinetically preferred.

In the following, earlier results on the oxidative addition, obtained with essentially the same computational methodology as used here will be discussed. For hydrosilylation by a Ru-silylene complex with phosphine and cyclopentadienyl ligands,[37] the *IOA* pathway, shared by both the CH and the mCH mechanism, was determined favorable, with a barrier G_a = 24 kcal·mol^{-1}. For a Ru(II) complex with phosphine and chlorine ligands,[22] the highest enthalpy barrier, H_a = 9.0 kcal·mol^{-1}, of the *DOA* variant of the CH mechanism was calculated similar to that of the *IOA* pathway presented here. A Ru(II) complex with aryl and chlorine ligands was determined to exhibit a very facile oxidative addition, H_a = 0.6 kcal·mol^{-1}, again for both mechanisms, CH and mCH.[24] However, the Si−H distance remains so short, 1.73 Å, that the "oxidative addition" is not finished yet according to the definition in the first paragraph of this section.[94] For Rh(I) phosphine complexes,[82] higher activation energies E_a, 17.3 kcal·mol^{-1} on the CH pathway and 15.7 kcal·mol^{-1} on the mCH pathway, were calculated for the *DOA* variant. In short, for the oxidative addition of the CH and mCH

mechanisms, the current *bis*-NHC Rh(I) catalyst model is competitive to or better than the catalysts previously studied.[22,24,37,82]

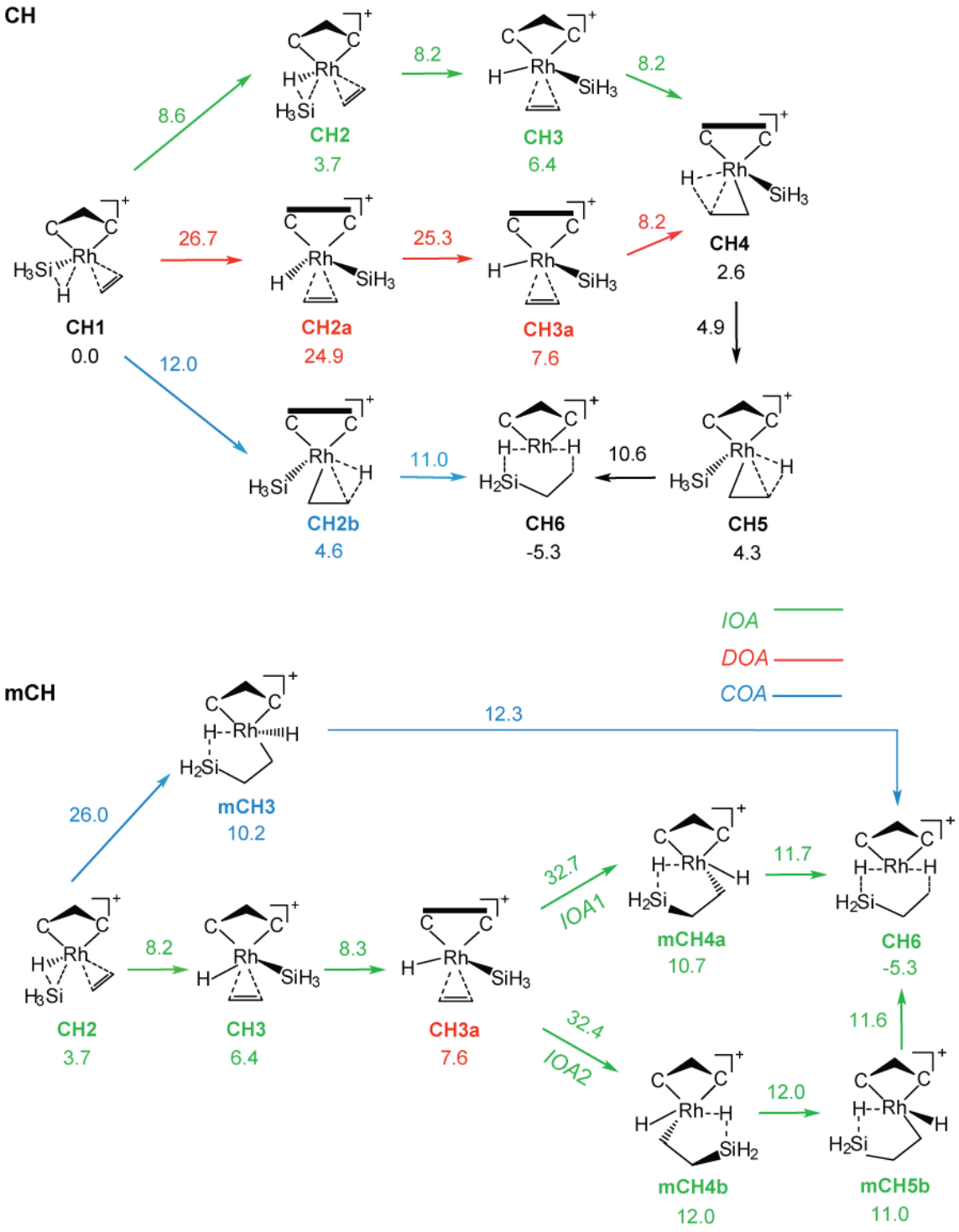

Figure 4.6. Alternative pathways of the oxidative addition during the CH (upper panel) and the mCH (lower panel) mechanism. Enthalpy values of intermediates (sketched) and transition states (arrows) in kcal·mol^{-1}, with reference to **CH1**. Adapted from Ref. 93.

4.2.2 Formation of the Product

After the oxidative addition the CH mechanism continues with the hydrogenation of the olefin. Passing over a very low barrier, H_a(**CH3** → **CH4**) = 1.8 kcal·mol^{-1}, the C−H distance

Table 4.2. Crucial distances indicating the oxidative addition and product formation, as well as γ in all optimized structures in the CH and mCH mechanism. Distances are given in Å and angles are given in degree. Two Si−H distances are given to demonstrate the isomerization of silane during the oxidative addition. Adapted from Ref. 93.

	Si−H		C−Si	C−H	γ
CH1	1.70	1.50	3.29	2.60	97.8
CH1−2	1.51	1.52	3.57	2.86	92.0
CH2	1.48	1.60	3.23	2.74	92.2
CH2−3	1.50	2.14	3.18	2.43	89.3
CH3	1.49	2.63	3.18	2.28	107.4
CH3−4		-	3.49	1.41	146.8
CH4		-	3.39	1.17	150.6
CH4−5		-	2.80	1.16	134.7
CH5		-	2.63	1.15	102.3
CH5−6		-	2.03	1.12	105.3
CH6		-	1.90	1.12	101.6
CH6−7		-	1.90	1.10	108.8
CH7		-	1.90	1.10	108.8
CH7−GT3		-	1.90	1.10	100.9
GT4−CH1		-	1.90	1.10	102.4
CH1-2a	4.03	1.49	2.91	2.30	150.1
CH2a	4.12	1.50	3.15	2.41	150.3
CH2a-3a		-	3.35	2.18	142.7
CH3a		-	3.59	2.13	142.0
CH3a−4		-	3.52	1.66	146.8
CH1−2b	2.33	1.50	3.78	1.44	94.9
CH2b	3.09	1.49	2.87	1.16	134.8
CH2b−6		-	2.04	1.13	108.2
CH2−mCH3	2.88	1.48	2.09	2.43	99.8
mCH3	3.14	1.56	1.90	2.43	115.7
mCH3−CH6		-	1.88	1.77	105.2
CH3−3a		-	3.50	2.15	140.6
CH3a−mCHa		-	2.10	2.75	111.1
mCH4a		-	1.90	2.44	127.2
mCH4a−CH6		-	1.89	2.12	109.2
CH3a−mCH4b		-	2.11	2.74	106.5
mCH4b		-	1.90	2.45	132.9
mCH4b−5b		-	1.89	2.32	119.9
mCH5b		-	1.88	2.50	107.2
mCH5b−CH6		-	1.89	1.76	104.1

of **CH3** shortens by 1.11 Å, to 1.17 Å in **CH4** (Table 4.2). Two further steps, **CH4 → CH5 → CH6**, complete the silylation of the alkyl species. The first step, **CH4 → CH5**, combines ligand isomerization and reorientation of the pertinent moieties. The C−Si bond actually forms in the second step, **CH5 → CH6**. Overall, the C−Si distance shortens in two steps, by 0.76 Å (**CH4 → CH5**) and subsequently by 0.73 Å (**CH5 → CH6**), to reach the final value, 1.90 Å, in **CH6** (Table 4.2). The reorientation step **CH4 → CH5** proceeds over a small barrier of 2.3 kcal·mol^{-1}; the silylation step **CH5 → CH6** exhibits an activation enthalpy of 6.3 kcal·mol^{-1} (Figure 4.6).

The *DOA* variant of the CH mechanism joins the lowest pathway at **CH4**, after two very facile isomerization steps, **CH2a → CH3a → CH4**, the highest barrier being 0.6 kcal·mol^{-1} (Figure 4.6). Complex **CH2b** of the *COA* variant transforms in one step to the product **CH6**, via a barrier of 6.4 kcal·mol^{-1}. Along all routes of the CH mechanism, the formation of the product, hydrogenation and silylation of the olefin, requires less activation enthalpy than the oxidative addition; see Section 4.2.1.

Because in the overall preferred *COA* variant of the mCH pathway the silylation has already occurred, the hydrogenation step which is relatively facile can subsequently be accomplished, H_a(**mCH3 → CH6**) = 2.1 kcal·mol^{-1}, because the initial state is relatively high in energy (Figure 4.6). The C−H distance shortens by 1.31 Å (Table 4.2). In the *IOA* variants of mCH the silylation of the olefin is unfavorable; both barriers are quite high: H_a(**CH3a → mCH4a**) = 25.1 kcal·mol^{-1}, H_a(**CH3a → mCH4b**) = 24.8 kcal·mol^{-1}. Afterwards both mCH variants merge with the CH pathway, via very low hydrogenation barriers, $H_a \leq 1$ kcal·mol^{-1} to reach intermediate **CH6**. Unlike on the CH pathways, product formation, especially silylation, is the crucial step of the mCH mechanism for all three variants (Figure 4.6).

The CH and mCH mechanisms share the enthalpy reference **CH1**; therefore, one can directly compare their energetics. Oxidative addition on the CH pathway, has the highest relative activation barrier calculated at 8.6 kcal·mol^{-1} (Figure 4.6). In contrast, on the preferred mCH pathway, coupled oxidative addition and hydrosilylation have the highest relative activation barrier at 22.3 kcal·mol^{-1} (Figure 4.6). In view of these relative enthalpy barriers, the CH mechanism is favored over the mCH mechanism.

4.2.3 Elimination of the Product

During the final stage of the catalytic cycle, starting from structure **CH6**, the mechanisms CH and mCH share the same route for product elimination (Figure 4.7). After two C−C bond rotation steps, **CH6** → **CH7** → **GT3**, where Rh−H bonds are cleaved and re-formed, one obtains the silylene complex **GT3**, an intermediate of the GT mechanism.

To reconstitute the initial state **CH1**, the product has to be eliminated and new reactants, a silane and an olefin moiety, have to be added at the metal center. First a silane is added, **GT3** → **GT4**, before addition of ethylene extrudes the product via a low barrier, H_a(**GT4** → **CH1**) = 9.3 kcal·mol^{-1} This barrier is by 27.9 kcal·mol^{-1} (!) lower than that of the final step of the GT mechanism (Figure 4.7 vs. Figure 4.3).

The present results, namely that both CH and mCH mechanisms pass through one step of the GT mechanism, **GT3** → **GT4**, match the findings of a previous study[37] on Ru(I) complexes. In that earlier work, the product is subsequently eliminated, forming an analogue of **GT1**, before ethylene is inserted to form the analogue of **CH1**. Here a notably more favorable ending of the catalytic cycle is presented, which is closed by ethylene assisted product elimination, forming **CH1**.

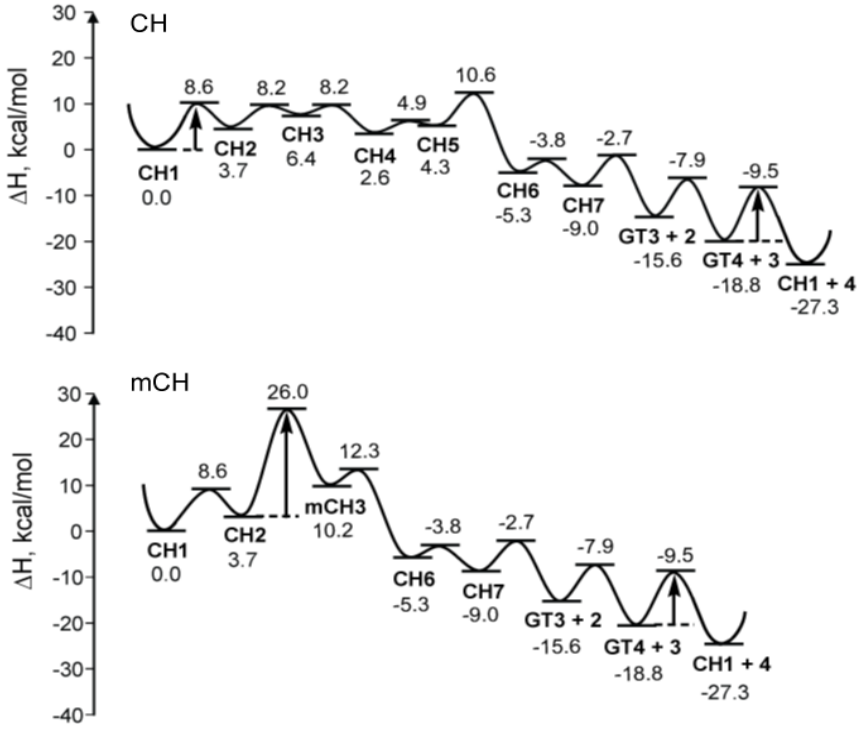

Figure 4.7. Enthalpy profiles of the most favored pathways of the CH and mCH mechanisms. **CH1** is used as enthalpy reference. Crucial steps with highest relative activation barriers are marked by arrows. Relative enthalpies of each intermediate and TS are given in kcal·mol^{-1}. Adapted from Ref. 93.

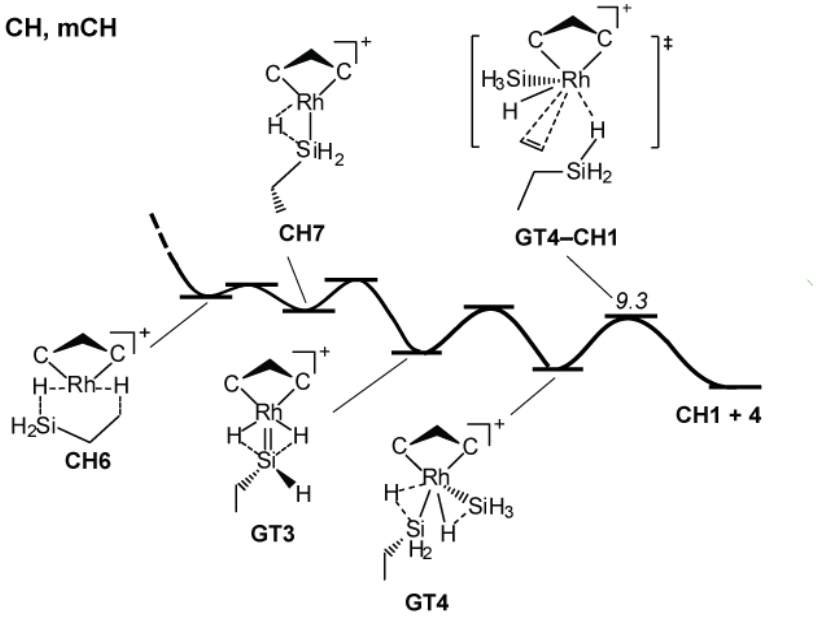

Figure 4.7 (continued). Enthalpy profiles of the product elimination for the CH and mCH mechanisms. Relative activation barrier H_a is given in kcal·mol^{-1}. Adapted from Ref. 93.

4.2.4 CH: *bis*-NHC and *trans*-Effect

The coupled C=C bond activation and Si−Rh bond cleavage (**CH2** → **mCH3**, *COA* in mCH) features a higher barrier (H_a = 22.3 kcal·mol^{-1}, Figure 4.6) than the step **CH1** → **CH2b** (*COA* in CH, Figure 4.6) possibly because of a *trans*-effect; see the optimized structures of the two transition states in Figure 4.8.

In the TS **CH1**−**2b**, the bonds Rh−C (Rh-NHC) and Rh−C (Rh-olefin) in *trans* position are 2.05 Å and 2.16 Å, respectively. Possibly the relatively strong *σ*-donation from the NHC carbene to the Rh atom strengthens the Rh-NHC bond and causes the Rh-olefin bond to loosen (Rh−C = 2.16 Å, left-hand side of Figure 4.8), facilitating the reorganization of the olefin moiety and enabling it to approach more easily the hydrogen atom. In contrast, in the TS **CH2**−**mCH3**, the olefin binds more strongly to the Rh center (Rh−C = 2.05 Å, right-hand side of Figure 4.8), as a consequence of the loosened Rh-NHC bond in trans position (Rh−C = 2.16 Å, right-hand side of Figure 4.8), thus being more difficult to migrate. The weakening of one of the Rh-NHC bonds may be due to the increased coordination number of the Rh center (one more Rh−H bond in **CH2**−**mCH3** compared to the TS **CH1**−**2b**, Figure 4.8). In the TS **CH2**−**mCH3**, the mobilization of the silyl group is correlated with the shortening of

the Rh-NHC bond *trans* to it (Rh−Si = 2.76 Å, Rh−C = 2.01 Å, right-hand side of Figure 4.8).

Apparently, the strength of the two Rh-NHC bonds can remarkably affect the bonding situation in their respective *trans* positions. If both moieties, coordinated at the metal center, to form a bond, can be mobilized due to a trans effect, e.g., the hydrogen atom and the ethylene moiety in the TS **CH1**−**2b**, then this reaction occurs easily (left-hand side of Figure 4.8). If due to two simultaneous, but opposite trans effects one moiety is loosened from the metal center, but the other one is held back, e.g., the silyl and the ethylene moieties in the TS **CH2**−**mCH3**), then the reaction may exhibit a higher activation energy.

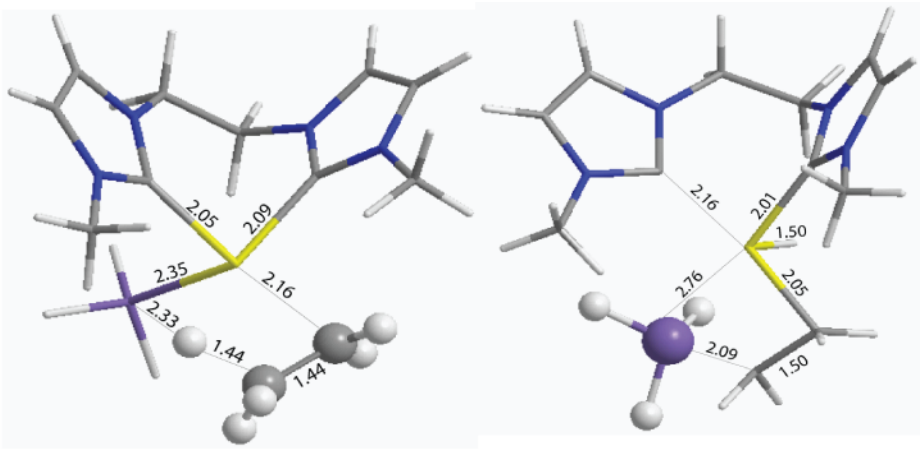

Figure 4.8. Optimized structures of the transition states **CH1**−**2b** and **CH2**−**mCH3**. Distances are given in Å. Adapted from Ref. 93.

4.3 SBM Pathway

The catalytic cycle of the SBM mechanism shares the oxidative addition (*IOA*) with the CH pathway, the two-step process **CH1** → **CH2** → **CH3** (see Figure 4.6 in Section 4.2). The SBM mechanism proceeds with the insertion of a second silane **2**, as also found previously.[37] This insertion requires an activation enthalpy of 6.5 kcal·mol^{-1}. In consequence, the agostic bond between the Rh and *β*-C−H bond in **CH4** breaks upon going from **CH4** to **SBM5** (Figure 4.9). The hydrosilylation product forms immediately, **SBM5** → **SBM6** (Figure 4.9). The corresponding TS **SBM5−6** features a four-member ring Rh−C−Si−H, characteristic for the SBM mechanism. During this step, the two bonds Si−C and Rh−H form, and two others break, Rh−C and Si−H. Crucial geometry parameters of all optimized structures of the SBM mechanism are given in Table 4.3.

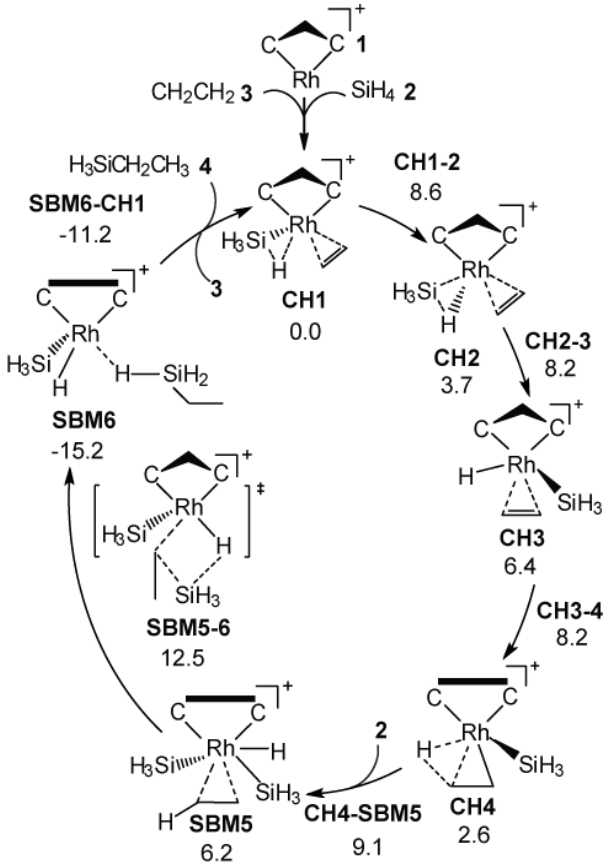

Figure 4.9. Catalytic cycles of the **SBM** mechanism. Enthalpies of intermediates and transition states, relative to CH1, in kcal·mol^{-1}. Adapted from Ref. 93.

In addition to the hydrosilylation of ethylene, this transformation simultaneously accomplishes a hydrogen transfer from silane to rhodium (Figure 4.9). The highest relative barrier of the mechanism SBM, 8.6 kcal·mol^{-1} (*IOA*), is slightly lower than the highest

barrier of the CH mechanism, 9.3 kcal·mol^{-1} (product elimination); Figure 4.10 vs. Figure 4.7. However, considering the highest absolute barriers in the overall catalytic cycles, **CH** is favored over SBM (10.6 kcal·mol^{-1} of **CH5−6** vs. 12.5 kcal·mol^{-1} of **SBM5−6**, (Figure 4.10) In the SBM mechanism, the elimination of the product starts by inserting a second ethylene. This induces a rotational isomerization of the silyl group and cleavage of the Rh−H bond to the product. The enthalpy barrier of this final step, 4.0 kcal·mol^{-1}, is notably lower than that of the product elimination step of the CH mechanism (Figure 4.10 vs. Figure 4.7).

Experimentally, the SBM mechanism is known to promote also olefin hydrogenation.[22,46] Hence this potential side reaction was also examined. In this side reaction, the system undergoes two hydrogen transfer steps instead of passing via the four-member ring structure. One hydrogen atom is transferred from Rh to C, **CH4 → SBM5**. A second hydrogen atom migrates from Si via Rh to the C center, thus avoiding a temporary under-coordination at the metal center, **SBM5 → SBM6S** (Figure 4.10). Consequently, the silane remains partially unsaturated, with only three covalent bonds formed at the Si center (Si−Rh, 2×Si−H); the third Si−H is elongated by 0.16 Å to coordinate also to the metal center. With 20.9 kcal·mol^{-1}, the activation enthalpy of this step is much larger than the competing highest barrier along the desired hydrosilylation pathway, 6.3 kcal·mol^{-1} (Figure 4.10). Thus, with the *bis*-NHC-Rh catalyst studied, ethane is highly unlikely as side product of the **SBM** mechanism. This finding is an important advantage of the present Rh catalyst over the Ru catalysts studied experimentally where this side reaction was observed.[22]

Table 4.3. Crucial distances, as well as the dihedral angle γ in all optimized structures in the SBM mechanism. Distances are given in Å and angles are given in degree. Adapted from Ref. 93.

	C−Si	C−H	γ
CH4−SBM5	3.77	1.13	153.6
SBM5	2.72	1.13	152.7
SBM5−6	2.09	1.11	152.7
SBM6	1.90	1.10	151.8
SBM6−CH1	1.88	1.09	155.6

In summary, for the *bis*-NHC Ru(I) *model* catalyst examined here, the **SBM** and **CH** mechanisms were calculated kinetically very similar. Oxidative addition at the beginning of the catalytic cycle is rate-limiting in the SBM mechanism whereas the highest enthalpy barrier of the CH mechanism was calculated for the final step, product elimination (Figure 4.10). In both mechanisms the backward reaction is notably more difficult, with barriers of

17.8 kcal·mol^{-1} for **CH1** → **GT4** and 16.1 kcal·mol^{-1} for **CH1** → **SBM6**. A potential shortcoming of the SBM mechanism may be the relatively crowded arrangement at the metal center in its key intermediate, **SBM5**–**6**. This aspect may be problematic for larger reactants, silanes and olefins (see Section 4.3.1), and for steric more demanding N-substituents on the *bis*-NHC ligand.

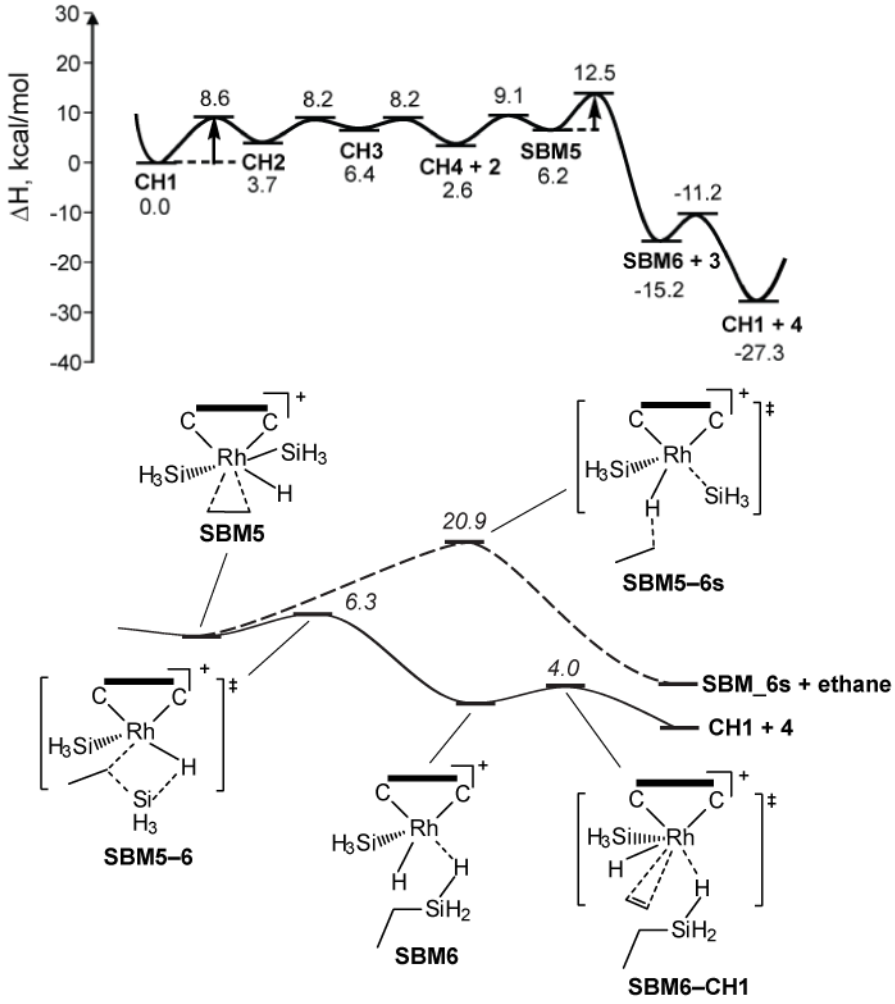

Figure 4.10. Enthalpy profiles of the most favored pathway in the SBM mechanism (upper panel), and product elimination as well as potential side reaction (lower panel). **CH1** is used as enthalpy reference. Crucial steps with highest relative activation barriers, are marked by arrows. Relative enthalpies of each intermediate and TS are given in kcal·mol^{-1}. In the lower panel, H_a is given in kcal·mol^{-1}. Adapted from Ref. 93.

4.3.1 SBM: Change in the Coordination Sphere

The cleavage of the Rh−H−C agostic bond in **CH4** (Figure 4.11) occurs with assistance of the addition of a second silane (TS **CH4−SBM5**). The coordination sphere around the metal center changes notably during this process. In the final state **SBM5**, the Rh center is relatively crowded. The weakening of the interaction between the metal and the NHC-ligand or other coordinated moieties can be observed in the change of the bond length. Besides the cleaved agostic bond, three additional bonds are weakened, i.e., one Rh−C (Rh-NHC) bond (from 2.01 Å in **CH4** to 2.12 Å in **SBM5**), one Rh−Si bond (from 2.31 Å in **CH4** to 2.37 Å in **SBM5**), and one Rh−C bond (from 2.08 Å in **CH4** to 2.14 Å in **SBM5**).

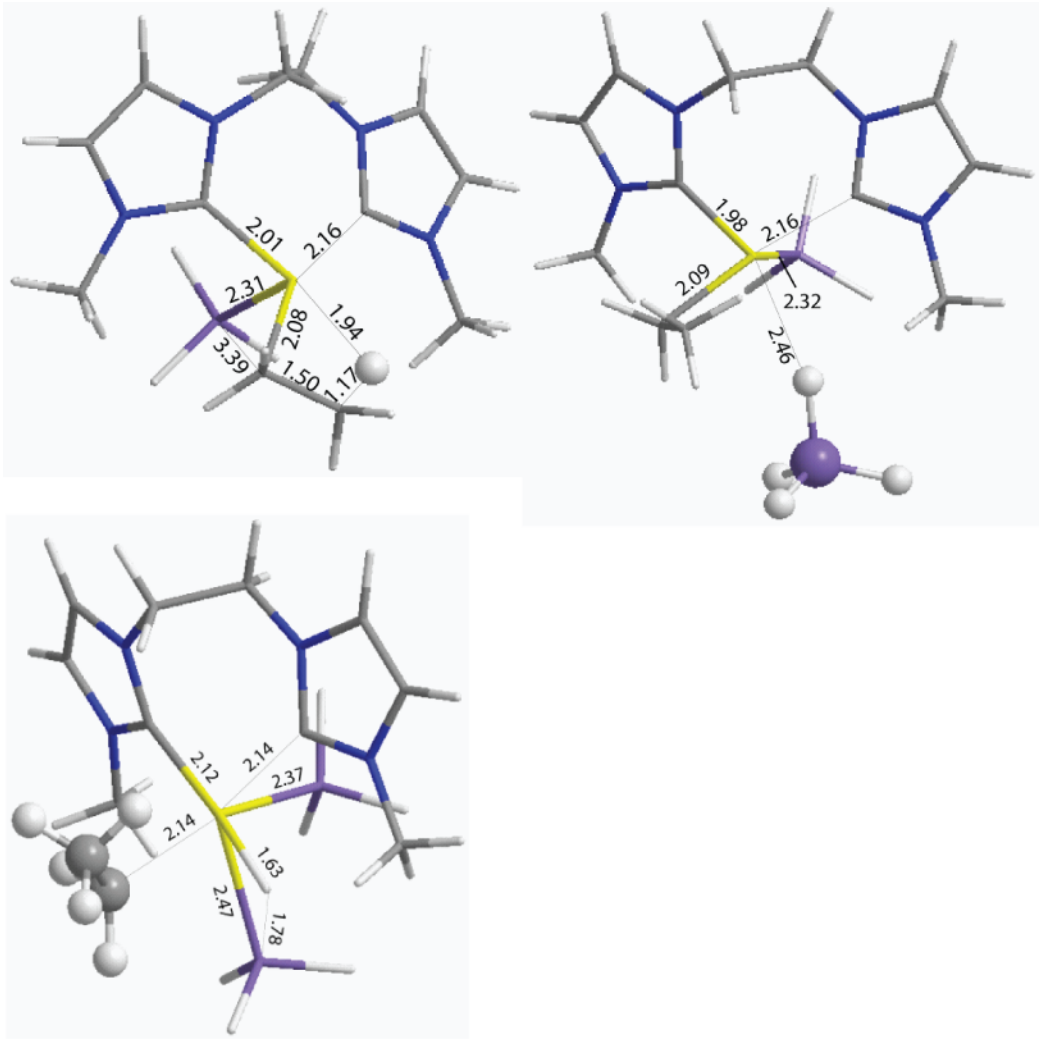

Figure 4.11. Optimized structure of intermediate **CH4**, TS **CH4−SBM5** (upper panel) and **SBM5** (lower panel). Distances are given in Å. Adapted from Ref. 93.

4.4 Performance of the *bis*-NHC Ligand

Catalysts with the same metal center but different ligands do not necessarily share the same mechanistic features.[22-24] In the following the electronic and spatial characteristics of the present *bis*-NHC ligand will be discussed and its influence on the hydrosilylation reaction catalyzed will be analyzed.

NHC ligands are strong σ-donors and weak π-acceptors,[123] and thus facilitate the formation of stable catalyst complexes with strong ligand-metal bonds, which in the present case are strengthened even more by the two binding sites of the bidentate ligand. Along the various pathways, the Rh-NHC bonds vary in the range 1.93−2.23 Å; the average value over all calculated stationary states is 2.06 Å. When one NHC ligand is moving away from the metal center, the other one draws closer.

A noteworthy feature of the Rh(I) catalyst studied is the flexible conformation of the *bis*-NHC ligand system. The present bridged bidentate *bis*-NHC ligand does not occupy a full hemisphere of the metal center, but mainly divides space into two parts in a flexible fashion. The spatial requirement varies as the ethylene-bridge changes its conformation, altering the dihedral angle between the two imidazole rings. To delineate these conformational changes in a quantitative way, the dihedral angle γ between the imidazole rings was determined by fitting a plane to the five atoms of each ring.

Figure 4.12 presents pertinent results for the structures along the various reaction pathways, delineating the values of γ together with crucial distances C−Si and C−H of intermediates and TSs along the most favorable pathways of each of the four mechanisms. One notes some obvious correlations between changes in the dihedral angle γ and crucial transition states, e.g., of the oxidative addition in the CH pathway.

The dihedral angle γ hardly changes in the GT mechanism; this reflects the fact that in this mechanism the actual reaction does not take place at the catalyst center, but occurs remotely on the silylene ligand. In contrast, the correlation between angle γ and the formation of the various bonds can clearly be seen for the other mechanisms CH, mCH, and SBM. During the indirect oxidative addition, **CH1** → **CH2** → **CH3**, of the CH and the SBM mechanisms, angle γ first decreases by 6° and then increases by 10° (Table 4.1 − Table 4.3). In this way, space is cleared as needed for the spatial requirement of the reactants and their migration. One observes an analogous effect in the mCH mechanism, where angle γ changes up to 20° at about the same stage of the mechanism. In contrast, during the SBM mechanism, angle γ changes even up to 60°, not in a single peak, but rather in a plateau-like phase during which the catalytic transformation occurs (Figure 4.12).

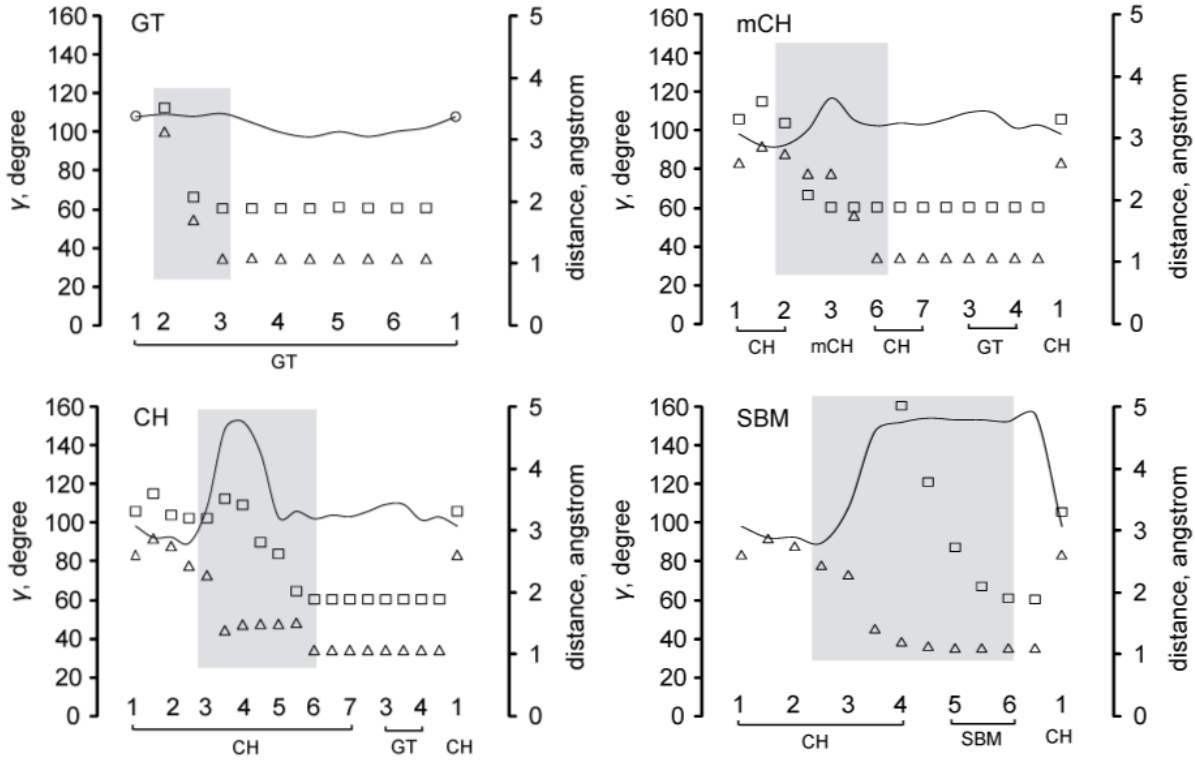

Figure 4.12. Dihedral angle γ (in degree) between the two imidazole rings (solid line), C−Si (squares) and C−H (triangles) distances (in Å) along the most favored pathways of the GT, CH, mCH, and SBM mechanisms, starting with the catalytically active species **GT1** and **CH1**, respectively. No distances are given for **GT1** as the reactants are separated. For SBM, C−Si distances are measured between ethylene and the second SiH_4 moiety. Shading indicates the crucial steps of product formation. Adapted from Ref. 93.

The phases with larger values of the dihedral angle γ occur at crucial steps of the various mechanisms. In fact, they are decisive for obtaining low barriers with the *bis*-NHC ligand. A test calculation where the dihedral angle γ was constrained at the value of **CH4,** 150°, during the formation of the C−Si bond, **CH4 → CH5 → CH6,** results in the (more direct) activation barrier **CH4 → CH6** (Figure 4.13) which, however, is by 16.7 kcal·mol^{-1} higher than that calculated with the flexible *bis*-NHC ligand.

In Table 4.4 the energetics and the ligand geometry of the crucial reaction steps of the various mechanisms pathways are compared along the most favored pathways. The CH and SBM mechanisms are equally preferred with highest barriers of ~9 kcal·mol^{-1}, while the mCH and GT mechanisms, with highest barriers of 22 kcal·mol^{-1} and 37 kcal·mol^{-1}, respectively, are not competitive. Rh−Si bond cleavage is difficult in the latter two mechanisms, whereas this process is facilitated by an incoming additional reactant in the SBM and CH mechanisms. The hydrogenation of the olefin is never rate-limiting in any of the four mechanisms. Only in the mCH mechanism, formation of the C−Si bond is notably

more difficult than C−H formation, with H_a(**CH2 → mCH3**) = 22 kcal·mol^{-1} compared with H_a(**mCH3 → CH6**) = 2 kcal·mol^{-1}. Only for the CH and SBM mechanism does one find drastic changes in the dihedral angle γ, by more than 40°, between the two imidazole rings, to enable C−H bond formation.

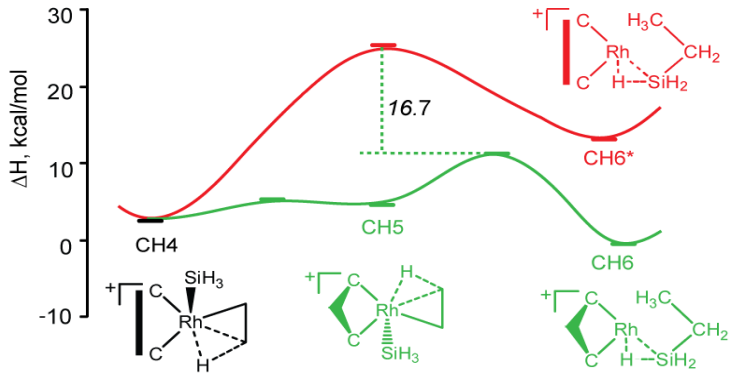

Figure 4.13. Enthalpy profile CH4 → CH5 → CH6 explored with a flexible bis−NHC ligand (green) and with the *bis*-NHC dihedral angle fixed at its value for CH4, 150° (red). This alternative pathway CH4 → CH6 has an activation barrier relative to CH5 → CH6 that is by 16.7 kcal·mol^{-1} higher. Adapted from Ref. 93.

Table 4.4. Pertinent activation barriers H_a in kcal·mol^{-1} of various mechanisms and geometric characteristics of the corresponding transition structures: dihedral angle γ between the two NHC moieties, distances of C–Si or C–H bonds formed. Adapted from Ref. 93.

	GT	CH	mCH	SBM
TS	**GT6–1**	**GT4–CH1**	**CH2–mCH3**	**CH1–2**
H_a(max)	37	9	22	9
γ	101	106	100	92
TS	**GT3–4**	**CH5–6**	**CH2–mCH3**	**SBM5–6**
H_a(C–Si)	19	6	22	6
γ	104	105	100	153
d(C–Si)	1.88	2.03	2.09	2.09
TS	**GT3–4**	**CH3–4**	**mCH3–CH6**	**CH3–4**
H_a(C–H)	19	2	2	2
γ	104	147	105	147
d(C–H)	1.10	1.66	1.77	1.66

Finally it is worthwhile to compare the present results for the *bis*-NHC Rh(I) complex as catalyst to results of previous DFT studies on Rh and Ru complexes, mainly involving phosphine and chlorine ligands. The highest relative barriers of the favored mechanisms in previous studies vary substantially. Sakaki et al. determined for a phosphine-based Rh

catalyst, using $SiHMe_3$, the mCH pathway to be preferred over CH for the hydrosilylation of ethylene, with E_a = 15.7 kcal·mol^{-1}.[85] Beddie and Hall calculated the GT mechanism as preferred over CH and mCH, with G_a = 18.9 kcal·mol^{-1}, when adding SiH_4 across ethylene, using a Ru complex with phosphine and cyclopentadienyl ligands.[2] In three studies on Ru complexes with varying ligands, Tuttle et al. examined adding diethoxymethylsilane to diethoxymethylvinylsilane.[22-24] Using phosphines and chloride as ligands of a Ru complex, studying the CH, mCH, and SBM mechanisms, Tuttle et al. found SBM as lowest energy pathway, with H_a = 21.8 kcal·mol^{-1}.[89] A Ru complex with chloride and acetonitrile was identified to proceed also to favor the SBM mechanism (over GT and CH), with H_a = 13.1 kcal·mol^{-1}.[23] For a Ru complex, with a cymene ligand instead of acetonitrile, the preferred mechanism changed to CH out of the CH, mCH, and SBM mechanisms studied, with H_a = 15.5 kcal·mol^{-1}.[91]

Earlier works suggested the catalysis to start with stepwise addition of the reactants, beginning with silane to yield a metal-silylene[37] or a metal hydride complex[43] as catalytic active species. In contrast, it was determined that the common active species of the CH, mCH and SBM mechanisms involves not only silane but also the olefin (**CH1**); this species is energetically favored over the Rh-silylene complex (**GT1**) which was also studied for the GT mechanism (Figure 4.14). This provides a further hint that the GT mechanism is unlikely in the current system, as its intermediate is so much less stable. For the oxidative addition (separation of Si and H by more than 2.50 Å) at the present Rh complex, a lower activation barrier was calculated than determined previously for Ru complexes.[22-24,37]

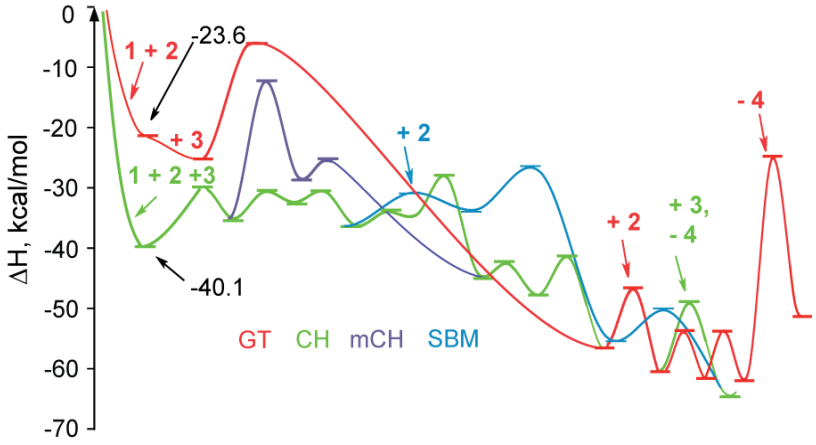

Figure 4.14. Profiles of the most favored pathways of the mechanisms GT, CH, mCH, and SBM, relative to the bare catalyst and separate substrates. Reaction enthalpies for the formation of the catalytically active species **GT1** and **CH1** in kcal·mol^{-1}. Steps where reactants are added or the product is eliminated are marked by arrows. Adapted from Ref. 93.

Entropy contributions, thus far not included in the discussion, affect most activation barriers only in a marginal way, by less than 5.4 kcal·mol^{-1}. Exceptions occur when an extra reactant is added (Table 4.5). These latter barriers increase by up to ~10 kcal·mol^{-1} (**GT3 → GT4**) if one includes the term $-T\Delta S$ in full; however, these entropy corrections are certainly an upper bound.[249,250] This correction renders the ethylene-assisted product elimination, presented here for the first time, more difficult, but should not invalidate the preferred reaction pathways discussed here in view of the calculated very low barriers.

Table 4.5. Enthalpy ΔH and entropy contributions $-T\Delta S$ as well as solvation effects ΔG_{solv} of crucial activation energies, relative to the preceding intermediates. ΔG_{solv} values determined in single-point fashion at structures optimized in the gas phase (kcal·mol^{-1}), see Chapter 3. Adapted from Ref. 93.

	ΔH	$-T\Delta S$	ΔG_{solv}		ΔH	$-T\Delta S$	ΔG_{solv}
GT2−3	18.5	5.4	−3.2	**CH5−6**	6.3	0.1	−2.1
GT6−1	37.5	1.8	−1.3	**CH2−mCH3**	22.3	0.8	−4.1
CH1−2	8.6	0.7	−1.8	**SBM5−6S**	20.9	−2.2	−0.3
GT4−CH1	9.3	6.8	−0.8	**SBM6−CH1**	4.0	6.2	−1.5

4.5 Conclusion

In this chapter, a computational study of olefin hydrosilylation by a *bis*-NHC Rh(I) *model* catalyst was presented, for the *model* reactants ethylene and monosilane. All four popular mechanisms were addressed: Glaser-Tilley GT, Chalk-Harrod CH, and its modified variant mCH, as well as σ-bond metathesis SBM.

Along the various pathways, the ethylene bridged *bis*-NHC catalyst ligand is able to change between "bent" and "open" conformations, enabling a total of three variants each of the oxidative addition for the CH as well as the mCH mechanism. The indirect oxidative addition turned out to be the most favorable variant of the CH mechanism, with the final step, displacement of product, to be rate-determining. In this last step, insertion of an additional reactant (ethylene) facilitates cleavage of the Rh−Si bond. The other variants, coupled oxidative addition and direct oxidative addition, the latter involving a separation of Si and H to *trans*-coordinated sites, were calculated to exhibit notably higher activation barriers. The silylation steps of all variants of the mCH mechanism have high barriers of which the variant starting with coupled oxidative addition turned out to be most favorable. Overall the SBM mechanism was calculated to have the lowest relative barriers, slightly lower than that of the CH mechanism. Formation of ethane as side reaction of the SBM mechanism is much less favorable than hydrosilylation. The GT mechanism was also ruled out as the relative barrier of the cleavage of the Rh−Si bond and displacement of the product was calculated very high. Absolute rate-determining barriers with respect to the full catalytic cycles are 16.3, 10.6, 26.0 and 12.5 kcal·mol^{-1} for GT, CH, mCH and SBM mechanisms, respectively. In summary, the CH and SBM mechanisms feature the most favorable enthalpy profiles for hydrosilylation by the *bis*-NHC Rh(I) catalyst.

A crucial aspect of hydrosilylation by metal complexes is the release of the product where a metal-Si bond needs to be cleaved. Indeed, elimination of the product involves the highest barriers of the mechanisms studied (the second highest in the case of SBM).

The ethyl-bridged *bis*-NHC model ligand used in this study makes the resulting metal complex a very attractive catalyst for the hydrosilylation of olefins. The Rh-NHC bonds are rather stable. Yet, the bidentate character of the ligand allows notable elongations in one of these two metal-ligand bonds, while the other one remains tight and thus prevents a loss of the ligand which might occur without the ethyl bridge. On the other hand, this bridge is flexible enough to permit the required arrangement of the two imidazole rings relative to each other.

5 Method Dependence of Competing Mechanisms

In the preceding chapter, all four mechanisms for the hydrosilylation of ethylene by monosilane were computationally examined.[93] The four mechanisms were explored with the hybrid functional method B3LYP, as to date it is most commonly used in computational studies.[251] It was concluded that the two preferred mechanisms are SBM and CH, while their highest relative barriers (HRB) differ by only 0.7 kcal·mol^{-1}.[93] This chapter addresses the question, important to computational and experimental chemists alike, whether the results obtained by a DFT based method are sensitive to the functional chosen. The importance of this question can be illustrated by reference to the catalysis model, where small changes in the energy results might evoke a change in mechanistic preference.

Beddie and Hall also studied the method-dependent mechanistic preference of olefin hydrosilylation.[252] They examined two key reaction steps (including 4 intermediates and 2 transition states), comparing a series of DFT and "ab initio" methods, in conjunction with basis sets of various degrees of flexibility along the pathways of the GT and CH mechanisms.[252] They based their discussion on single-point calculations of structures optimized at the B3LYP level in a preceding mechanistic study.[37] With the "ab initio" methods MP2 and MP4SDQ they determined the CH mechanism as preferred. In contrast, the MP3 method, all DFT methods and the CISD method confirmed the preference of the GT mechanism. Their CCSD and CCSD(T) calculations predicted a change in the preferred mechanism from CH to GT when the basis sets were increased.[252]

This chapter, addressing hydrosilylation by the Rh(I)-*bis*-NHC complex, extends the mechanistic study of the last chapter, where two characteristics of this system were revealed that render the present case more complicated than the case just described.[252] For the example addressed in the last chapter, firstly, the pathways of the four mechanisms are interrelated at several junctures. Secondly, the potential energy profiles of the SBM and CH mechanisms are overall flat.[93] Therefore, it is worthwhile to extend the scope of the study beyond single-point calculations employing other functionals. Rather, in this methodological study considerably more crucial structures were included and each of them was optimized for the chosen functionals. Also, it seemed interesting to use an extended set of DFT methods because the performance of the most popular functionals has been widely reviewed against experimental and ab initio data.[253] Especially, the accuracy of functionals in calculating geometries of TM complexes[254-256] and reaction energetics of catalytic systems based on TM complexes[257] have been assessed.

By analyzing the energies calculated with several functionals for competing mechanisms, this chapter aims at exploring a potential method dependence of DFT studies in homogenous TM catalysis on the example of a somewhat intricate case.

The following discussion will focus on the energetics, RBs in particular. The overall strategy of the comparison is as follows. First it is shown that for each of the four mechanisms a complete set of all stationary points along the most favored pathways, determined with the functional BP86, results in an energy profile that is rather parallel to that previously calculated with the B3LYP approach.[93] Then, two crucial barriers of the GT mechanism, and three crucial barriers each for the CH, mCH, and SBM mechanisms will be optimized with three additional functionals, mPWPW, PBE, and PBE0, and the influence of these five functionals on the ranking of the barriers will be analyzed. Next, the comparison will be extended to seven additional density functionals, BLYP, B3PW91, MPW1K, MPW3LYP, M06-L, M06, and TPSS, for the four most important barriers, obtained by full optimization of the intermediate and TS structures with all chosen functionals. It will be examined in particular how the preferred mechanism may change depending on the functional used. Finally a case of a strong change in barrier height and how this barrier is described by an extended set of functionals will be discussed in detail.

In addition, changes in geometries evoked by the various functionals were examined. To assess the quality of the structures calculated for the inspected catalyst system with the 12 functionals, the bonding distances of the optimized bare catalyst to X-ray diffraction data were compared (Figure 5.1, Table 5.1).

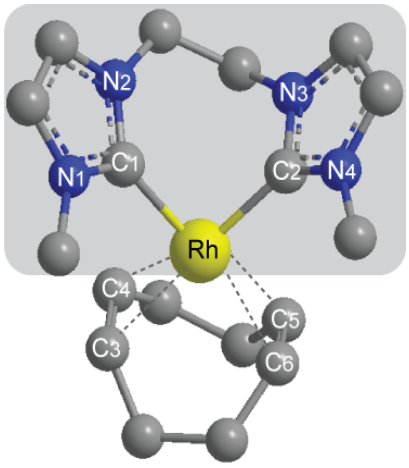

Figure 5.1. Sketch of the structure of the catalyst precursor, the Rh(I) bis−NHC cyclooctadiene (COD) complex. The active species is the shaded upper part, the Rh(I) bis−NHC complex. The lower part shows the spectator ligand COD. Hydrogen atoms on the ligands are omitted for clarity. Adapted from Ref. 221.

Table 5.1. Characteristic distances (Å) of the experimentally determined and calculated structures of the catalyst precursor, the Rh(I) *bis*-NHC COD complex. See Figure 5.1 for the numbering of the atoms. [a] Adapted from Ref. 221.

	Rh−NHC		Within NHC				Rh−COD			
	$Rh–C_1$	$Rh–C_2$	$C_1–N_1$	$C_1–N_2$	$C_2–N_3$	$C_2–N_4$	$Rh–C_3$	$Rh–C_4$	$Rh–C_5$	$Rh–C_6$
XRD	2.05	2.04	1.37	1.38	1.37	1.36	2.26	2.22	2.25	2.22
B3LYP	2.07	2.05	1.37	1.36	1.37	1.36	2.29	2.25	2.27	2.24
BP86	2.05	2.04	1.37	1.38	1.38	1.37	2.26	2.22	2.25	2.22
mPWPW	2.05	2.04	1.37	1.38	1.38	1.37	2.26	2.22	2.24	2.22
PBE	2.05	2.04	1.37	1.38	1.38	1.37	2.25	2.21	2.24	2.21
PBE0	2.05	2.05	1.36	1.36	1.36	1.35	2.24	2.20	2.22	2.20
BLYP	2.08	2.06	1.38	1.39	1.38	1.37	2.31	2.26	2.29	2.26
B3PW91	2.05	2.04	1.36	1.37	1.36	1.35	2.25	2.21	2.23	2.21
MPW1K	2.05	2.04	1.35	1.35	1.35	1.34	2.24	2.20	2.23	2.20
MPW3LYP	2.07	2.05	1.36	1.37	1.36	1.36	2.29	2.25	2.27	2.24
M06–L	2.07	2.05	1.36	1.37	1.36	1.36	2.24	2.20	2.23	2.20
M06	2.06	2.04	1.36	1.36	1.36	1.35	2.26	2.23	2.25	2.22
TPSS	2.07	2.05	1.37	1.38	1.37	1.37	2.25	2.21	2.23	2.21

[a]Distances calculated with the 12 functionals used in this study differ at most by 0.05 Å from the corresponding X-ray data, thus confirming that the selected functionals are appropriate for modeling the Rh(I) bis-NHC catalyst.

5.1 Differences between B3LYP and BP86 for the Four Mechanisms

Figure 5.2 shows the complete reaction profiles, obtained with the B3LYP and BP86 functionals, of the most favored pathways of the four mechanisms under study, with intermediates and transition states (TSs) completely optimized. Apparently, the two functionals B3LYP and BP86 result in rather parallel energy profiles, such that it is possible to evaluate analogous crucial RBs of each mechanism; see below the detailed discussion.

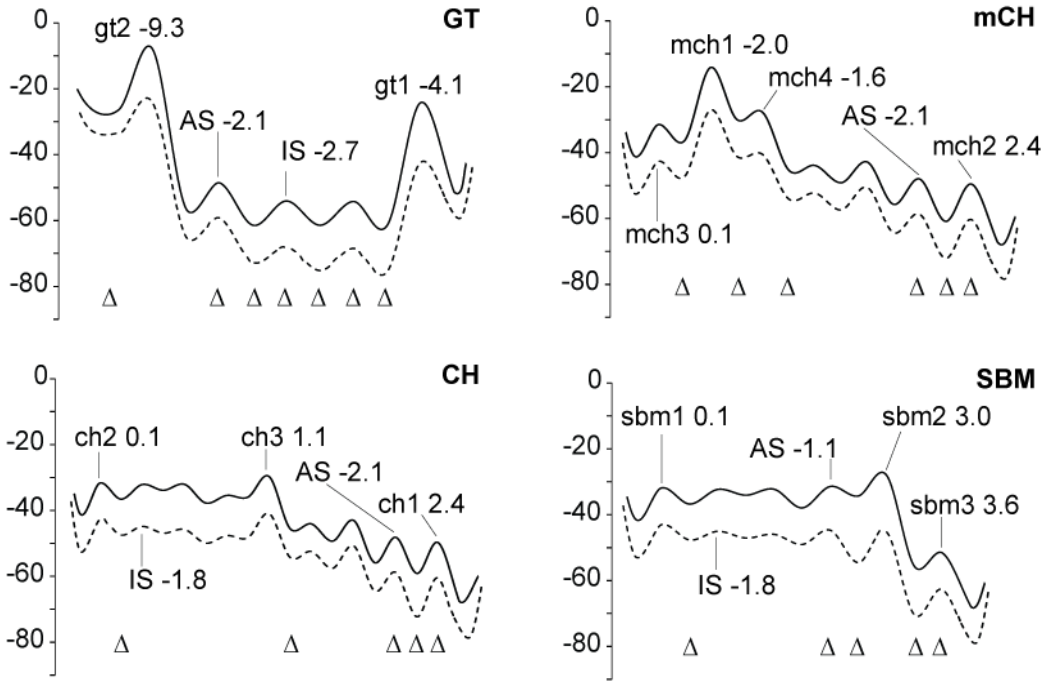

Figure 5.2. Enthalpy profiles (kcal·mol^{-1}) of the four mechanisms calculated by the B3LYP (solid lines) and the BP86 method (dashed lines). Note that ch1 = mch2, ch2 = mch3 = sbm1. The largest changes in activation enthalpies ΔH_a (more than 1.5 kcal·mol^{-1} in absolute terms) are explicitly given. Triangles indicate notable geometric differences $|\Delta d| > 0.1$ Å in the intermediate or the transition state structures. Adapted from Ref. 221. For the numerical values of the relative enthalpies and crucial distances, see Tables A1 and A2 of the Appendix.

First labels will be introduced for easy reference of the RBs to be discussed. Labels in lower-case are used to identify the mechanism, followed by a number that indicates the ranking according to the barrier height in the same mechanism, starting with the highest, as obtained with the B3LYP method.[93] For example, the label "gt2" denotes the second-highest RB along the GT pathway. The same label also identifies the corresponding TS, while the prefix "i", as in "igt2", marks the intermediate, immediately preceding that TS, in the present example TS gt2. This ranking focuses on the highest RBs, but does not account for smaller

(or less important) barriers, such as those of the isomerization steps (IS) or the addition of a second silane (AS). Often, these less important barriers are shared by several mechanisms. Unless otherwise noted, IS or AS barriers are lower than the crucial HRBs selected for the more detailed comparison in Section 5.2. First the energy data and then the geometry results will be discussed.

Going from B3LYP to BP86, four of the overall five RBs along the GT pathway decrease, barrier gt1 by 4.1 kcal·mol^{-1}, gt2 by 9.3 kcal·mol^{-1}, one AS by 2.1 kcal·mol^{-1}, and one IS by 2.7 kcal·mol^{-1}. The two HRBs gt1 and gt2 also feature the largest absolute changes. These changes reflect the well-established fact that GGA functionals tend to yield lower RBs, as a rule underestimating experimental values.[258,259] Barrier gt2 remains higher than the AS, by 10.9 kcal·mol^{-1} (B3LYP) and 3.7 kcal·mol^{-1} (BP86). Hence the energy profiles calculated with these two functionals run sufficiently well in parallel (Figure 5.2) to justify restricting further calculations to gt1 and gt2 when additional functionals will be evaluated (Section 5.2).

Passing altogether via nine TSs (Figure 5.2), the CH pathway is more complicated than the GT pathway. Changing from the B3LYP to the BP86 functional, one IS and one AS (of GT) barriers decrease by 1.8 kcal·mol^{-1} and 2.1 kcal·mol^{-1}, respectively, while the HRB ch1 *increases* by 2.4 kcal·mol^{-1}. In this way, ch1 is the HRB of both profiles. The second-highest RB ch2 also keeps its rank at the BP86 level, with its value essentially unchanged, by 0.1 kcal·mol^{-1}. Because the energy profile along the CH pathway is relative flat, ch2 is only by 2.3 (B3LYP) and 1.4 kcal·mol^{-1} (BP86) higher than ch3 (Table A1 of the Appendix). Thus it seemed advisable to include also ch3 in the next step of the evaluation strategy. Note that the RB ch3 is lower than AS by 1.4 kcal·mol^{-1} at the B3LYP level, but higher than it by 1.8 kcal·mol^{-1} at the BP86 level. Based on the consideration that ch3 represents one crucial step, the C−Si bond formation ch3 was chosen instead of AS.

The mCH pathway involves in total seven activation barriers. Four RBs changed by about 2 kcal·mol^{-1} at the BP86 level, compared to the B3LYP results: mch1, mch4, one AS (= AS in GT and CH) and mch2 (= ch1). While the RBs mch1, mch4, and AS decreased by 2.0 kcal·mol^{-1}, 1.6 kcal·mol^{-1}, and 2.1 kcal·mol^{-1}, respectively, barrier mch2 (= ch1) *increased* by 2.4 kcal·mol^{-1}. Both mch1 and mch2 (= ch1) remain the HRBs at the BP86 level. The third HRB mch3 (= ch2) is also ranked the same in both profiles. Hence mch1, mch2 (= ch1), and mch3 (= ch2) were selected for further evaluation in Section 5.2.

Finally, three of the six activation barriers along the SBM pathway changed remarkably: one IS (= IS of CH), sbm2, and sbm3. While the first barrier is reduced by 1.8 kcal·mol^{-1} at

the BP86 level, the other two barriers *increase* by 3.0 kcal·mol^{-1} (sbm2) and 3.6 kcal·mol^{-1} (sbm3). Note that the highest barrier of the SBM mechanism is identical to the second highest one of the CH mechanism, sbm1 = ch2. The two highest B3LYP barriers sbm1 and sbm2 exchange their ranks at the BP86 level, while RB sbm3, 7.6 kcal·mol^{-1}, comes close to RB sbm1, 8.7 kcal·mol^{-1} at this level of theory. Therefore also for the SBM mechanism, three HRBs were included for further evaluation. Due to the smooth potential energy surface at the B3LYP level, sbm2 is of the same height as the AS (6.4 vs. 6.5 kcal·mol^{-1}), while RB sbm3 is only by 0.4 kcal·mol^{-1} lower than one IS RB. At the BP86 level, sbm2 is by 4.0 kcal·mol^{-1} higher than the AS, and sbm3 is by 5.0 kcal·mol^{-1} higher than the IS.

Regarding the locations of the eight barriers chosen above, it can be summarized that in total, one barrier is selected from the shared initial phase (ch2 = mch3 = sbm1), four are chosen from the crucial C−Si or C−H bond formations (gt2, ch3, mch1, and sbm2), and three are related to the elimination of product (gt1, ch1 = mch2, and sbm3). Hence the current set of RBs includes all key steps along the most favored pathways of the four mechanisms, see Figure 5.3.

Aside from the changes in enthalpy differences just discussed, the functional BP86 in some cases also entailed noteworthy structure changes. In view of the complexity of the system under study, only interatomic distances pertinent to the reaction were examined. These are either bonding distances of specific structures, e.g., the distances Rh−Si and Rh−H in the silylene complexes igt1 and igt2, or distances describing bond formation or cleavage, e.g., the distances Si−C and Si−H in igt2 and gt2 (Table A2 of the Appendix). In Figure 5.2, triangles point out where the variation in crucial non-bonding distances is above 0.1 Å. Altogether there are seven structures along the GT pathway, five along the CH and SBM pathways, and six along the mCH pathway which revealed at least one noticeably changed non-bonding distance when the functional was altered from B3LYP to BP86 (Figure 5.2, Table A1 of the Appendix). Two conclusions can be drawn from Figure 5.2. First, all activation barriers which are sensitive to an alteration of the functional contain an intermediate or/and a transition state, where some (non-) bonding distances were described differently by BP86 and B3LYP. Second, it is apparent that especially in the GT structures many changes over 0.1 Å occur, most frequently for the interactions between the rhodium and the silane subunits; see Table A2 of the Appendix. These differences involve either the formation or cleavage of the Rh−Si bond, or a hydrogen transfer reaction between the two units. In general, B3LYP predicts the non-bonding Rh−Si and Rh−H distances longer, and the Si−H distances shorter than BP86, except for one case in the transition state mch1 (Table

A2 of the Appendix). Further deviations were found in the non-bonding distances between rhodium and the ethylene subunits, and the ethylene and the silane subunits. In these latter cases, BP86 predicts the two units to be much closer to each other than B3LYP. Except for a few distances of these three types (Rh-silane, Rh-ethylene, silane-ethylene), all crucial distances were calculated rather consistently by B3LYP and BP86 (Table A2 of the Appendix).

In summary, the current analysis shows that geometries determined by the B3LYP approach and the more economical BP86 functional are quite comparable. The energy profiles run almost parallel, and the crucial barriers along each pathway were in the majority

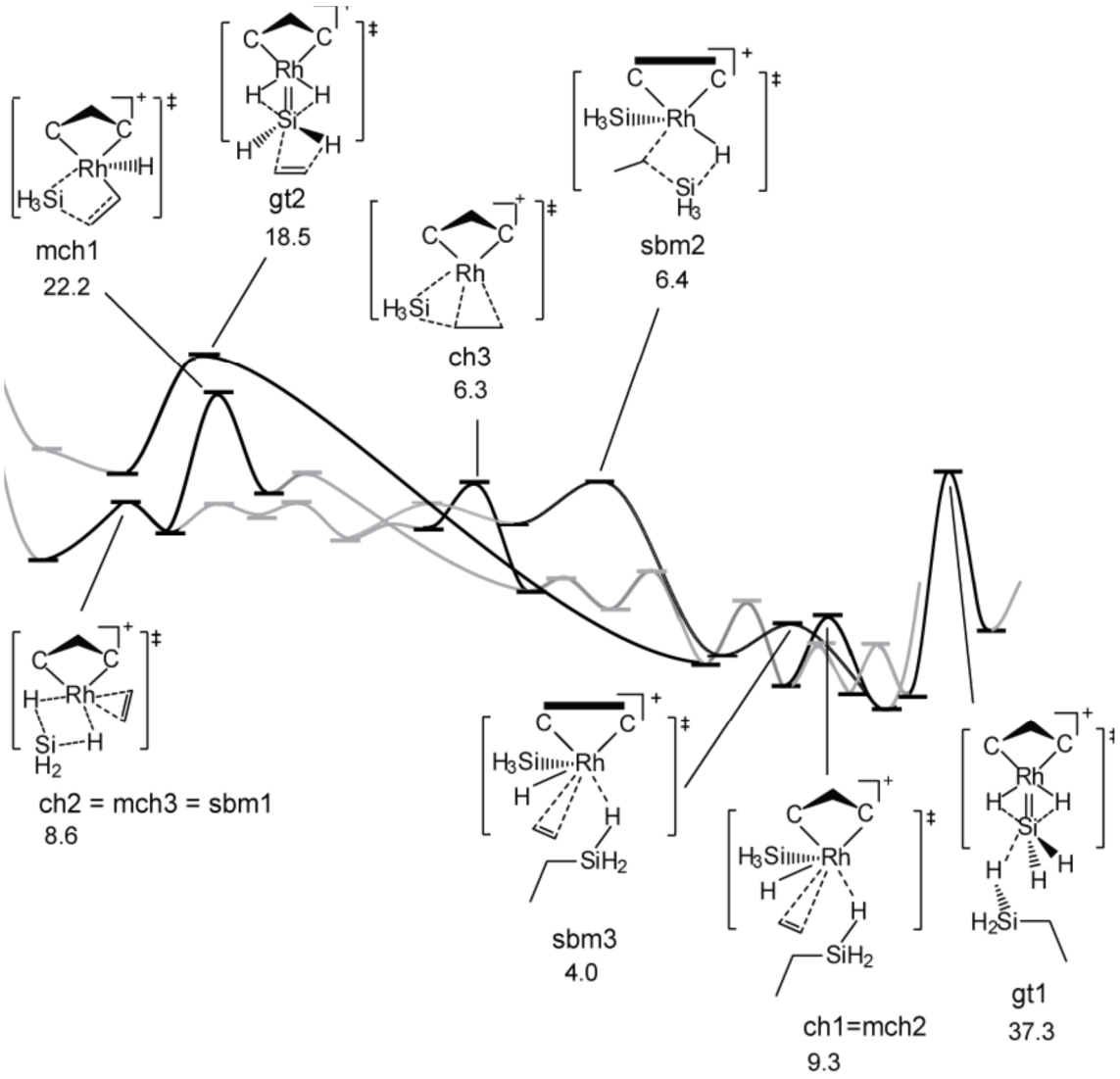

Figure 5.3. Overview of the interrelated pathways of the four mechanisms and location of the eight selected relative barriers. Less important steps shown in light gray. Relative enthalpy barriers (kcal·mol^{-1}) were calculated with the B3LYP method in Chapter 4. Sketches of the transition state structures are depicted to illustrate the chemical transformation occurring in the various steps. Adapted from Ref. 221.

of cases also the most sensitive to this functional change. The relative energies obtained by single-point calculations BP86//B3LYP vary by -3.4 kcal·mol^{-1} to 2.2 kcal·mol^{-1} with respect to the relative energies determined in full optimizations at the BP86 level (Table A1 of Appendix). The most significant changes were found in the structures involved in the barriers gt1, gt2, ch1, ch2, sbm2, and sbm3, showing that geometry changes have a larger impact on the energetics of these structures (Table A1 of Appendix).

5.2 Optimization of Eight Selected Barriers by Five Functionals

Next, using a total of five functionals, all pertinent structures for the set of eight barriers, selected in the preceding section, were optimized. In addition to BP86, two other semi-local functionals, mPWPW and PBE, were chosen. Besides B3LYP, the hybrid counterpart of PBE, PBE0 was also employed. Depending on how the rankings of the selected crucial barriers are affected by the various functionals, potential changes in the preferred mechanism can be monitored. Secondly, the barrier heights of four functionals will be compared to those of the corresponding B3LYP results.

5.2.1 Ranking of Barriers

In Figure 5.4, for each of the five functionals, the calculated relative enthalpy barriers H_a are arranged in descending order. The ranking spectra have qualitatively similar profiles. The first two HRBs (three in the case of B3LYP) stand out for their remarkable heights. The remaining sequence is rather flat, while barriers in a certain position vary typically no more than 1 kcal·mol^{-1} among the five functionals

All chosen functionals predict the barriers gt1 and mch1 to be the two highest ones, amounting to 33 kcal·mol^{-1} and 20 kcal·mol^{-1}, respectively, for the semi-local functionals. These same barriers are up to 4 kcal·mol^{-1} higher for the two hybrid functionals. Depending on the functional, the second highest barrier, mch1, is by 3.6–9.5 kcal·mol^{-1} higher than the next lower one (Figure 5.4). Therefore, also for this extended set of functionals, the GT and the mCH mechanisms are not competitive with the CH and the SBM mechanisms. The remaining six barriers decrease rather smoothly and largely independently of the functional, with relatively small successive decrements, 0.1–2.3 kcal·mol^{-1}. Yet, there is one exception: with B3LYP, H_a(gt2) is 9.2 kcal·mol^{-1} higher than the subsequent barrier H_a(ch1), Figure 5.4. This finding reflects the fact that only B3LYP yields barrier gt2 rather high, whereas the other four functionals all predict gt2 to be comparable with the barriers of the preferred mechanisms CH and SBM (Figure 5.4).

The hybrid functionals B3LYP and PBE0 produce two rather similar rankings: gt2 > ch1 (= mch2) > ch2 (= mch3 = sbm1) > sbm2 with only ch3 and sbm3, of almost the same height, exchanged at the end of the series. The ranking changes when the semi-local functionals BP86 and mPWPW were applied: ch1 (= mch2) > sbm2 > gt2 > ch2 (= mch3 = sbm1). These four functionals all predict barriers ch3 and sbm3 to be the two lowest barriers of the inspected series. Only for PBE, ch3 ranks higher: sbm2 > ch1 (= mch2) > ch3 > ch2 (= mch3 = sbm1), but ch3 is still not the highest relative barrier along the CH pathway.

Focusing on the preferred mechanisms, the crucial barriers are ch1, ch2 = sbm1, and sbm2 (Table 5.2). With the semi-local functionals BP86, mPWPW, and PBE, the barriers of ch1 and sbm2 are higher than determined with the hybrid functionals. With B3LYP, sbm1 (= ch2) is the highest relative barrier along the SBM pathway, whereas PBE0 predicts the barriers sbm1 and sbm2 to be essentially equal (Figure 5.4). All three semi-local functionals yield sbm2 as highest barrier on the SBM pathway (Table 5.2). The three barriers ch1, ch2,

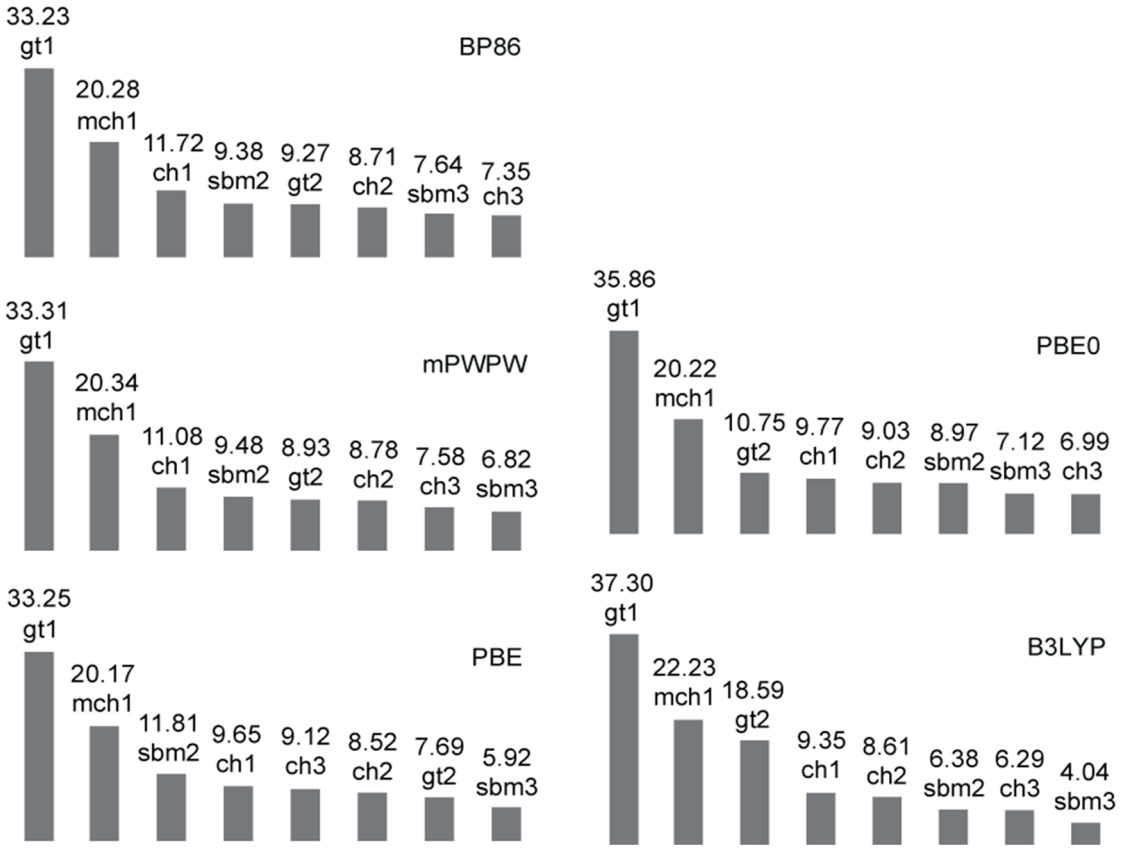

Figure 5.4. Eight crucial enthalpies of activation H_a (kcal·mol^{-1}) calculated with the density functionals BP86, mPWPW, PBE, PBE0, and B3LYP. For each functional, the barriers are arranged according to descending heights. Adapted from Ref. 221.

and sbm2, crucial for the overall preferred mechanism, as well as barrier gt2 (see above), will be studied further in Section 5.3, using a larger set of functionals.

Table 5.2 gives a brief overview over the mechanisms CH and SBM which are preferred as their highest relative barriers (HRB) are calculated lower than the HRBs of the GT and mCH mechanisms. Only BP86 and PBE yield substantial differences $\Delta H_a = H_a(ch1) - H_a(smb2)$ for these crucial barriers, $\Delta H_a(BP86) = 2.3$ kcal·mol^{-1} and $\Delta H_a(PBE) = -2.2$ kcal·mol^{-1} (Table 5.2). BP86 predicts the largest CH barrier ch1, 11.7 kcal·mol^{-1}, to be higher than the largest SBM barrier smb2, 9.4 kcal·mol^{-1}; the corresponding PBE results appear in reverse order, $H_a(ch1) = 9.6$ kcal·mol^{-1} and $H_a(sbm2) = 11.8$ kcal·mol^{-1}. Thus far in this study, PBE is the only functional to prefer the CH mechanism over SBM. The semi-local functional mPWPW yields similar results as BP86: $H_a(ch1) = 11.1$ kcal·mol^{-1}, $H_a(sbm2) = 9.5$ kcal·mol^{-1}; only the difference of these enthalpy values is reduced, $\Delta H_a(mPWPW) = 1.6$ kcal·mol^{-1}.

For the two hybrid functionals, not only the differences in barriers were reduced, ΔH_a (B3LYP) = ΔH_a (PEB0) = 0.7 kcal·mol^{-1}, but also the most dominant barrier along the SBM pathway is changed from sbm2 to sbm1 (Table 5.2). The oxidative addition of the first silane, sbm1 = ch2 (Figure 5.4), is predicted as HRB of the SBM mechanism by both B3LYP and PBE0: $H_a(sbm1) = 9.0$ kcal·mol^{-1} and $H_a(sbm1) = 8.6$ kcal·mol^{-1}, respectively. In contrast, for the semi-local functionals BP86, mPWPW, and PBE, the actual metathesis step sbm2 is the HRB of the SBM mechanism (Figure 5.4). At variance with the SBM mechanism, all five functionals considered here yield the ethylene-assisted product elimination ch1 as the HRB of the CH pathway.

Table 5.2. Selected relative barriers (kcal·mol^{-1}) calculated with five density functionals. Adapted from Ref. 221.

		H_a	G_a	E_a	$E_{a,corr}$
BP86	gt1	33.23	33.46	33.58	–
	gt2	9.27	13.55	10.57	11.23
	ch1	11.72	22.53	11.94	–
	ch2	8.71	9.77	8.98	–
	ch3	7.35	5.65	7.11	–
	mch1	20.28	20.33	20.57	–
	sbm2	9.38	9.11	9.45	–
	sbm3	7.64	16.31	7.39	–
mPWPW	gt1	33.31	34.01	33.74	–
	gt2	8.93	13.43	10.27	10.89
	ch1	11.08	22.21	11.35	–
	ch2	8.78	9.89	9.05	–
	ch3	7.58	5.73	7.30	–
	mch1	20.34	20.83	20.72	–
	sbm2	9.48	9.14	9.52	–
	sbm3	6.82	12.65	6.23	–
PBE	gt1	33.25	34.04	33.71	–
	gt2	7.69	11.78	8.98	9.59
	ch1	9.65	20.69	9.97	–
	ch2	8.52	10.03	8.86	–
	ch3	9.12	7.08	8.78	–
	mch1	20.17	20.20	20.46	–
	sbm2	11.81	7.73	10.79	–
	sbm3	5.92	15.24	5.75	–
PBE0	gt1	35.86	37.00	36.40	–
	gt2	10.75	15.45	12.15	12.64
	ch1	9.77	19.61	9.96	–
	ch2	9.03	10.24	9.33	–
	ch3	6.99	6.33	6.96	–
	mch1	20.22	20.54	20.60	–
	sbm2	8.97	8.70	9.00	–
	sbm3	7.12	13.75	6.31	–
B3LYP	gt1	37.30	39.07	37.95	–
	gt2	18.59	24.03	20.07	21.10
	ch1	9.35	16.16	8.88	–
	ch2	8.61	9.30	8.79	–
	ch3	6.29	6.42	6.42	–
	mch1	22.23	23.32	22.85	–
	sbm2	6.38	7.01	6.70	–
	sbm3	4.04	10.28	3.50	–

5.2.2 Performances of Density Functionals

Next the relative barrier heights of the four functionals X = BP86, mPWPW, PBE and PBE0 are compared to those of the corresponding B3LYP results (Figure 5.5). For only one barrier,

ch2 = mch3 = sbm1, the same result was obtained by all five functionals. In all other cases, the functionals X yield three reduced barriers (gt1, gt2, mch1; Figure 5.5), and four increased barriers (ch1 = mch2, ch3, sbm2, sbm3; Figure 5.3). For most functionals the variations of gt2, mch1, sbm2, and sbm3 are larger than 2 kcal·mol^{-1}. From this point of view, GT and SBM are the two mechanisms for which hybrid and semi-local functionals most likely furnish large variations. Barriers of the CH mechanism are less sensitive to the choice of the functional. Among the set X, the GT barriers are reduced, the SBM barriers are increased relative to the B3LYP results.

Comparing the semi-local functionals to each other, one notes rather similar RBs for BP86 and mPWPW, with deviations of at most 0.8 kcal·mol^{-1} (Figure 5.5; Table 5.3). PBE results differ from those of BP86 and mPWPW, predicting barriers ch3 and sbm2 higher, and barriers gt2 and ch1 lower, by up to 2 kcal·mol^{-1} (Figure 5.5; Table 5.3). For the RBs gt1, mch1 and ch2, all three semi-local functionals yield the same height (Figure 5.5). The structures determined by the semi-local functionals BP86, mPWPW, and PBE are quite similar, with exceptions only for the non-bonding distances C−Si of igt2, two distances Rh−Si of ich1 and sbm3, and the distance Rh−C of ich3 (Table A3 of the Appendix).

PBE predicts ch3 by 2.1 kcal·mol^{-1} and sbm2 by 2.8 kcal·mol^{-1} higher than PBE0 (Figure 5.5). In contrast, the RBs gt1 and gt2 are obtained lower, compared to PBE0, by 2.6 kcal·mol^{-1} and 3.2 kcal·mol^{-1}, respectively. The functionals PBE and PBE0 yield very similar values, within 1.2 kcal·mol^{-1}, for the RBs ch1, ch2, mch1, and sbm3 (Figure 5.5). Also the underlying geometries agree quite well, except for two non-bonding distances Rh–Si and Rh−H of sbm3 (Table A3 of the Appendix).

For the RBs gt2, mch1, sbm2, and sbm3, the results of the hybrid functional PBE0 differ notably from those of the analogous B3LYP results (Figure 5.5) although both hybrid functionals contain comparable fractions of exact exchange; see Table 3.1 in Chapter 3.

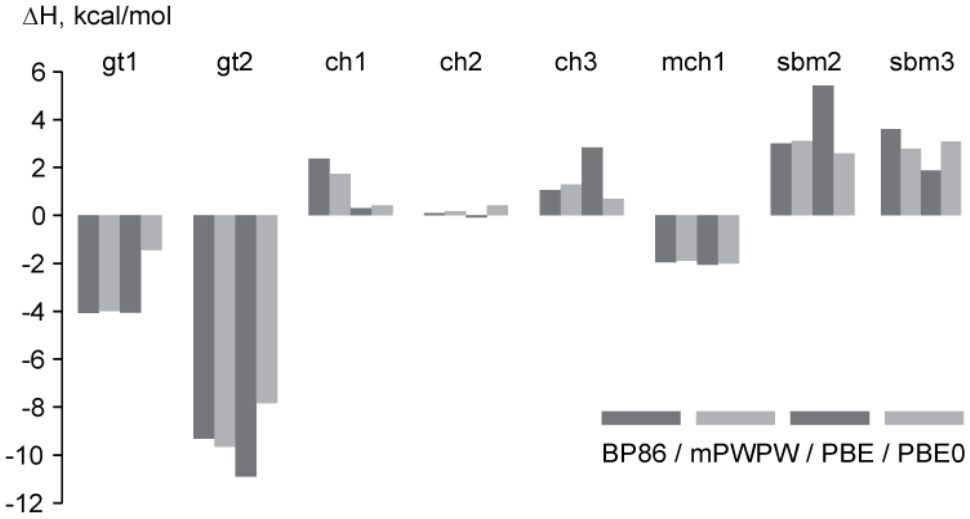

Figure 5.5. Changes ΔH_a (kcal·mol^{-1}) of eight selected barriers calculated with the functionals BP86, mPWPW, PBE, and PBE0, relative to the corresponding B3LYP results. Adapted from Ref. 221.

Table 5.3. Change $\Delta H_X = H_X - H(B3LYP)$ (kcal·mol^{-1}) in the formation enthalpies of selected intermediates (IM) and the corresponding transition states (TS), relative to the B3LYP results, calculated with 4 functionals. Adapted from Ref. 221.

	BP86	mPWPW	PBE	PBE0
igt1	−13.64	−15.33	−21.62	−21.28
gt1	−17.71	−19.31	−25.67	−22.71
igt2	−6.48	−6.70	−9.97	−8.84
gt2	−15.80	−16.36	−20.87	−16.67
ich1	−12.76	−14.35	−21.50	−20.74
ch1	−10.39	−12.61	−21.20	−20.32
ich2	−10.80	−11.57	−15.77	−13.82
ch2	−10.71	−11.40	−15.87	−13.40
ich3	−11.89	−12.86	−17.67	−16.56
ch3	−10.83	−11.58	−14.84	−15.86
imch1	−10.49	−11.24	−15.53	−13.59
mch1	−12.45	−13.14	−17.59	−15.61
isbm2	−19.82	−21.73	−29.51	−26.56
sbm2	−16.81	−18.63	−24.08	−23.97
isbm3	−14.31	−15.82	−22.38	−20.74
sbm3	−10.70	−13.03	−20.49	−17.66

5.3 Optimization of Four Selected Barriers by 12 Density Functionals

From the test set discussed in Section 5.2 four barriers were selected for re-examination with an even larger set of functionals. For this purpose, four barriers were chosen, including the

three HRBs ch1, ch2 (= sbm1) and sbm2 of the dominant mechanisms CH and SBM (Figure 5.6) as well as RB gt2 (Figure 5.7). The latter barrier was chosen for further evaluation of the large variation in activation enthalpy noted for the set of five functionals (Section 5.3.2).

5.3.1 Mechanism Preference between CH and SBM

Figure 5.6 shows how the activation enthalpies of the barriers ch1, ch2 (= sbm1) and sbm2 vary for the 11 functionals relative to the results calculated for B3LYP. The corresponding values are given in the Table A4 of the Appendix.

The following findings are particularly noteworthy: (*i*) the semi-local and hybrid functionals of the same composition behave remarkably similar for ch1 and ch2 (see

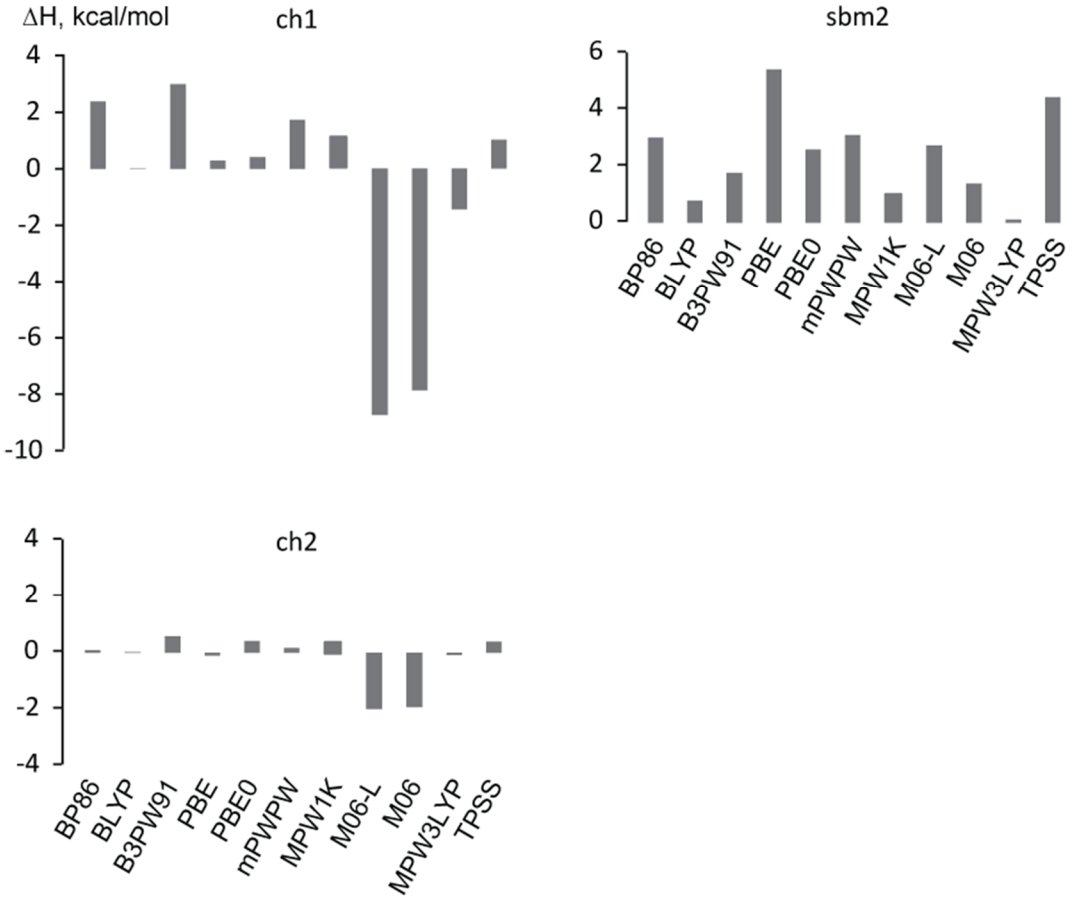

Figure 5.6. Changes ΔH_a (kcal·mol^{-1}) of the enthalpy barriers ch1, ch2 (= sbm1), and sbm2 calculated by 11 functionals, relative to the corresponding B3LYP results. Adapted from Ref. 221.

PBE/PBE0, mPWPW/MPW1K, and M06-L/M06); (*ii*) results with the functionals M06-L and M06 predict the two CH barriers quite differently than the other functionals; (*iii*) for sbm2, all 11 functionals yield higher activation enthalpies than B3LYP with the smallest

differences obtained for functionals that contain the LYP correlation part. Considering these results, the HRBs of the CH and SBM mechanisms may be changed from what has been reported in Section 5.2.1. Thus the analysis of activation enthalpies H_a of the HRBs was extended to seven additional functionals (Table 5.4).

First the HRBs of each of the two mechanisms CH and SBM will be analyzed. The highest relative barrier calculated with most functionals for the CH mechanism is ch1, the reductive elimination, see Figure 5.6. Exceptions are obtained for M06-L, M06, and MPW3LYP (Table 5.4); the first two of these exceptional functionals actually predict the ch1 step to occur without effort, H_a(M06-L) = 0.6 kcal·mol^{-1} and H_a(M06) = 1.5 kcal·mol^{-1} (Table 5.5).

Table 5.4. Highest relative (enthalpy) barriers H_a (HRB) of the CH and the SBM mechanisms as calculated by 12 functionals in kcal·mol^{-1}. For each functional, the difference $H_a = H_a(CH) - H_a(SBM)$ between the HRBs of the CH and the SBM pathways is also shown. Note that sbm1 = ch2. Adapted from Ref. 221.

	CH		SBM		ΔH_a
	HRB	H_a	HRB	H_a	
BP86	ch1	11.7	sbm2	9.4	2.3
mPWPW	ch1	11.1	sbm2	9.5	1.6
PBE	ch1	9.6	sbm2	11.8	−2.2
PBE0	ch1	9.8	sbm1	9.0	0.8
B3LYP	ch1	9.3	sbm1	8.6	0.7
BLYP	ch1	9.3	sbm1	8.6	0.7
B3PW91	ch1	12.3	sbm1	9.2	3.1
MPW1K	ch1	10.4	sbm1	9.0	1.4
M06−L	ch2	6.6	sbm2	9.1	−2.5
M06	ch2	6.7	sbm2	7.8	−1.1
MPW3LYP	ch2	8.5	sbm1	8.5	0.0
TPSS	ch1	10.4	sbm2	10.8	−0.5

The dispersion energy, which is included in these two functionals but missing in the other functionals, has a notable influence on the height of the barrier ch1. For instance, by

Table 5.5. Selected relative barriers (kcal·mol^{-1}) calculated with 12 density functionals. Note that ch2 = sbm1. E_{dis} was calculated with Grimme's script DFT-D3. Adapted from Ref. 221.

		H_a	G_a	E_a	$E_a + E_{disp}$
B3LYP	ch1	9.35	16.16	8.88	4.35
	ch2	8.61	9.30	8.79	9.34
	sbm2	6.38	7.01	6.70	8.38
BP86	ch1	11.72	22.53	11.94	1.79
	ch2	8.71	9.77	8.98	9.14
	sbm2	9.38	9.11	9.45	11.75
BLYP	ch1	9.34	16.54	9.93	–
	ch2	8.63	9.38	8.81	–
	sbm2	7.16	7.85	7.16	–
B3PW91	ch1	12.33	21.13	12.93	–
	ch2	9.19	10.38	9.19	–
	sbm2	8.14	8.00	8.14	–
PBE	ch1	9.65	20.69	9.97	–
	ch2	8.52	10.03	8.86	–
	sbm2	11.81	7.73	10.79	–
PBE0	ch1	9.77	19.61	9.96	–
	ch2	9.03	10.24	9.33	–
	sbm2	8.97	8.70	9.00	–
mPWPW	ch1	11.08	22.21	11.35	–
	ch2	8.78	9.89	9.05	–
	sbm2	9.48	9.14	9.52	–
MPW1K	ch1	10.44	19.93	11.03	–
	ch2	9.02	10.33	9.02	–
	sbm2	7.36	7.16	7.36	–
M06-L	ch1	0.62	10.86	1.21	–
	ch2	6.63	7.60	6.63	–
	sbm2	9.11	9.13	9.11	–
M06	ch1	1.48	12.73	2.08	–
	ch2	6.69	8.50	6.69	–
	sbm2	7.76	7.37	7.76	–
MPW3LYP	ch1	7.92	15.79	8.51	–
	ch2	8.54	9.56	8.54	–
	sbm2	6.49	7.12	6.49	–
TPSS	ch1	10.36	21.06	10.96	–
	ch2	9.00	10.76	9.00	–
	sbm2	10.83	10.53	10.83	–

adding a dispersion correction[260,261] to the BP86 and B3LYP results, barrier ch1 was reduced to 1.8 kcal·mol^{-1} (BP86) and 4.4 kcal·mol^{-1} (B3LYP), deviating from the M06–L and M06 results by only 1–2 kcal mol^{-1} (Table 5.5).

In case of the SBM mechanism, five of the six semi-local functionals (except for BLYP) predict the metathesis step sbm2 (Figure 5.6) to be the HRB instead of sbm1 = ch2 (Table 5.4 and Table 5.5). One of the six hybrid functionals, M06, also favors sbm2, just as the semi-local functionals, whereas the other five hybrid functionals all favor sbm1 as the HRB (Table 5.4 and Table 5.5). In summary, the majority of functionals predict ch1 as HRB of the CH mechanism and sbm2 as HRB of the SBM mechanism.

Next the HRBs of the CH and SBM mechanisms are compared to each other. All hybrid functionals, except M06 and MPW3LYP, slightly favor SBM over CH. The differences $\Delta H_a = H_a(CH) - H_a(SBM)$ of enthalpy barriers are 0.7 kcal·mol^{-1} for B3LYP and PBE0, 3.1 kcal·mol^{-1} for B3PW91, 1.4 kcal·mol^{-1} for MPW1K, whereas these differences ΔH_a are −1.1 kcal·mol^{-1} for M06 and 0 kcal·mol^{-1} for MPW3LYP (Table 5.4). Among the semi-local functionals, BP86, BLYP, and mPWPW also result in the SBM to be favored, with ΔH_a = 2.3, 0.7, and 1.6 kcal·mol^{-1}, respectively (Table 5.4). In contrast, the functionals PBE, M06-L and TPSS yield the opposite preference, CH over SBM, with values of ΔH_a = −2.2, −2.5, and −0.5 kcal·mol^{-1}, respectively. In total, seven functionals favor the SBM mechanism and five functionals the CH mechanism. However, the relative barrier heights of CH and SBM are in most cases quite close to each other (Tables 5.5). The highest relative enthalpy barriers differed by more than 2 kcal·mol^{-1} only in four cases: BP86, B3PW91, PBE, and M06-L (Table 5.4). In summary, all functionals agree that the CH and SBM mechanisms are competing in the catalytic hydrosilylation of ethylene by the Rh(I) complex under study.

5.3.2 A Closer Look at the Barrier gt2

All functionals but M06 yield a lower value for the activation barrier gt2 than B3LYP (Figure 5.7); the M06 calculations predict the enthalpy barrier gt2 slightly higher, by 0.4 kcal·mol^{-1} (Table 5.6). Relatively small deviations ΔH_a, within 2 kcal·mol^{-1} of the B3LYP result, were

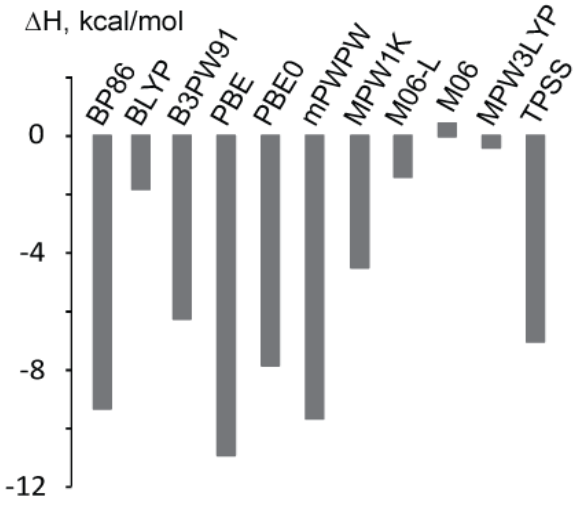

Figure 5.7. Changes ΔHa of the barrier gt2 (kcal·mol−1) calculated with 11 functionals, relative to the corresponding B3LYP result. Adapted from Ref.221.

also obtained with the two semi-local functionals BLYP and M06-L as well as the hybrid functional MPW3LYP (Figure 5.7, Table 5.6). In other words, the smallest deviations ΔH_a from the B3LYP result were determined within the M06 family of functionals and for the two other functionals also containing the LYP correlation part (BLYP, MPW3LYP).

The effect of the LYP functional contribution becomes even more apparent when the results of functionals with the same exchange part are compared to each other: BP86 vs. BLYP as well as B3LYP vs. B3PW91. Despite the same exchange functional, Becke88, the activation enthalpies calculated by BP86 and BLYP differ by more than 7 kcal·mol^{-1} (Figure 5.7, Table 5.6). B3PW91 results predict the barrier to be more than 6 kcal·mol^{-1} lower than with B3LYP (Figure 5.7, Table 5.6). In fact, the activation enthalpies calculated by functionals involving a correlation part other than LYP (except for M06-L and M06) all show relatively large deviations ΔH_a (in absolute terms) from the B3LYP results obtained, −4 to −11 kcal·mol^{-1} (Table 5.6). In comparison to the correlation part, the exact exchange affects the barrier height of gt2 to a smaller extent. This weaker influence can be observed by comparing the results of the functional pairs PBE/PBE0 (25% EEX) and M06-L/M06 (27% EEX) where the activation barrier increases by 3.1 kcal·mol^{-1} and 1.8 kcal·mol^{-1},

Table 5.6. Energetics and structures involved in the activation barrier gt2 calculated with 12 functionals: (*i*) change ΔH_X of the enthalpies H_X (kcal·mol^{-1}) of the intermediate igt2 and the transition state gt2 relative to the corresponding B3LYP results,[a] (*ii*) resulting change ΔH_a in the activation enthalpy relative to the B3LYP result,[a] (*iii*) imaginary frequencies ν_{gt2} (cm^{-1}) of the transition state structures, and (iv) crucial distances (Å) in the intermediate and the transition state structures. Adapted from Ref. 221.

	ΔH_X		ΔH_a	ν_{gt2}	C−Si		C−H		C−C		Si−H	
	igt2	gt2			igt2	gt2	igt2	gt2	igt2	gt2	igt2	gt2
B3LYP	−	−	−	737i	3.47	2.06	3.09	1.70	1.34	1.41	1.47	1.57
BP86	−6.5	−15.8	−9.3	628i	3.24	2.07	2.89	1.73	1.35	1.42	1.49	1.58
BLYP	1.9	0.1	−1.8	702i	3.54	2.07	3.15	1.70	1.35	1.43	1.49	1.58
B3PW91	−4.0	−10.2	−6.2	677i	3.32	2.06	2.96	1.72	1.34	1.41	1.48	1.56
PBE	−10.0	−20.9	−10.9	610i	3.15	2.07	2.89	1.74	1.35	1.42	1.49	1.57
PBE0	−8.8	−16.7	−7.8	668i	3.17	2.06	2.88	1.73	1.34	1.40	1.48	1.56
mPWPW	−6.7	−16.4	−9.7	628i	3.24	2.07	2.89	1.73	1.35	1.42	1.49	1.57
MPW1K	−6.0	−10.4	−4.4	724i	3.23	2.05	2.91	1.71	1.33	1.40	1.47	1.55
M06-L	−6.5	−7.9	−1.4	718i	3.31	2.06	2.90	1.72	1.33	1.41	1.47	1.55
M06	−9.3	−8.9	0.4	752i	3.21	2.06	2.91	1.72	1.33	1.41	1.47	1.56
MPW3LYP	−2.8	−3.1	−0.4	739i	3.41	2.06	3.03	1.70	1.33	1.41	1.48	1.57
TPSS	−6.4	−13.4	−7.0	693i	3.17	2.06	2.88	1.69	1.34	1.42	1.48	1.57

[a]Formation enthalpies H_X relative to the separated reactants Rh(I) *bis*−NHC complex, silane, and ethylene.

respectively, when going from the semi-local to the corresponding hybrid functional (Figure 5.7, Table 5.6). The activation barrier gt2 increases remarkably, by 5.3 kcal·mol^{-1}, in the functional pair mPWPW/MPW1K, likely due to the large contribution, 42.8% EEX, of exact exchange in MPW1K (Figure 5.7, Table 5.6).

All structures of igt2 and gt2, agree very well among the various functionals (Table 5.6). Within the pairs of semi-local and their corresponding hybrid functionals (BLYP/B3LYP, PBE/PBE0, mPWPW/MPW1K, M06-L/M06), the distances C−Si and C−H, characterizing the two bonds being formed during the reaction step, were predicted consistently. Varying the correlation part resulted in larger changes in the non-bonding distances C−Si and C−H of igt2; see the results for BP86/BLYP, B3LYP/B3PW91 and MPW1K/MPW3LYP in Table 5.6. The energy results of the functionals M06-L and M06 are very similar to those of B3LYP, but the non-bonding distances, C−Si and C−H in the initial state igt2, between the ethylene and the silane moieties, are by ~0.2 Å shorter (Table 5.6). In contrast, all functionals consistently describe (Table 5.6) the lengths of the bonds elongated and ultimately cleaved, C−C and Si−H, both in the local minimum (igt2) and the TS structure (gt2). In summary, the correlation functional also seems to have a stronger influence on the structure than the exchange functional, especially regarding bonds to be formed.

Analysis of the HOMO-LUMO gaps of igt2 and gt2, as calculated by the various functionals, showed no correlation with the strong variations of the barrier heights. Furthermore, an NBO charge analysis of all structures gave very similar results for all functionals considered. The higher activation barriers gt2, determined with the functionals B3LYP, BLYP, MPW3LYP, MPW1K, M06L, and M06, correlate with larger absolute values, by 9 to 142 cm^{-1}, of the imaginary frequency (Table 5.6). Thus, as expected, the curvature of the energy profile near the TS gt2 is larger for higher barriers while the reaction coordinate remains similar for all functionals, as discussed above.

5.4 Conclusion

In Chapter 5, barriers of four hydrosilylation mechanisms for a set of density functionals were compared, employing a strategy where the set barriers was restricted to crucial ones while the set of functionals was eventually extended to 12 functionals.

In general, the GT and mCH mechanisms were confirmed to be less favorable than the CH and SBM mechanisms, as predicted in Chapter 4 using the B3LYP function. The CH and SBM mechanisms were calculated to be in general favorable and to have comparable highest relative barriers (HRBs).

Overall the most crucial activation barriers along the CH and SBM pathways differ very little, up to 3 kcal·mol^{-1}, suggesting an intrinsic competitive nature of the two mechanisms in the catalytic cycles studied. The preference among these two mechanisms may well change with the steric demand of the olefin (here: ethylene) and the silane substrate (here: monosilane).

Two functionals, M06-L and M06, predict the HRB along the CH pathway, reductive elimination of the product (ch1), very facile. Thus, for these two functionals, only two crucial barriers sbm1 (= ch2) and sbm2 are to be compared for the mechanisms CH and SBM. These characteristic steps are of the oxidative addition of the first silane to the metal (ch2) and the actual σ-bond metathesis step (sbm2).

Turning to the other functionals, the current study suggests that the differences among the crucial barriers, as obtained by the twelve density functionals, are more affected by the correlation part than the exchange part. Furthermore, for the crucial step (gt2) of the GT mechanism, the LYP functional behaves similar as the functionals M06-L and M06, but notably different from the functionals PBE, PW91, and TPSS. Enthalpy barriers gt2, calculated by these two groups of functionals differ by ~10 kcal·mol^{-1} whereas structures remained relatively similar.

6 Regioselectivity Induced by Catalyst Modification

In general, hydrosilylation of terminal aliphatic olefins follows the anti-Markovnikov (*aM*) selectivity, whereas hydrosilylation of aromatic olefins leads to the formation of Markovnikov (*M*) products, due to the stabilization of the Lewis-acidic or electrophilic metal center by the π-electrons of aromatics, which promotes the formation of α-phenylalkyl intermediates.[86,262,263] For aliphatic 1-olefins, a Markovnikov regioselectivity can be promoted by specific ligand systems [264,265] or by varying the size or the substitution sides of the transition metal.[266] The regioselectivity of the hydrosilylation of aromatic olefins can also be tuned by choosing the ligand[73] or controlling the conditions of the catalytic process.[267] Regarding theoretical work done in this area, computational studies rather focused on the hydrosilylation of alkynes, C−C triple bonds, instead of alkenes.[268,269] In the previous chapters, the potential catalytic activity of a *bis*-NHC-Rh(I) complex in the hydrosilylation of alkenes has been revealed.[93 221] In the current chapter, possible regioselective control of a series of complexes featuring the same basic framework as the one explored before will be tested, in a model reaction for the hydrosilylation of a terminal aliphatic alkene. 1-butene, monosilane, and later dimethylsilane were chosen as reactants, to remain comparable with the experimental investigations.[270]

Rhodium complexes of the same ligand type have been applied to the hydrosilylation of ketone,[243] leading to unselective formation of silyl ether (desired product) and silyl enol ether (side product). Experimentalists have modified the catalyst ligand and analyzed the evoked changes in selectivity for the silyl ether.[243] Bulky ligands of reduced σ-donor ability were found to improve the catalytic activity.[243] However, the chemistry behind this finding was not understood.[243] In a sequel to this study, a mechanism based on a Rh-silylene complex was proposed[27] which actually suggests the *bis*-NHC ligand being remote from the catalytic active center. This proposal was not able to rationalize the previously observed impact of ligand modification on the catalytic activity.[243] In this regard, although the problem of hydrosilylation of an alkene will be addressed here instead of a ketone, it might still be possible to shed some light onto this unsolved problem and to gain a better understanding of the catalytic properties of the *bis*-NHC Rh(I) complexes.

6.1 Location and Energetic Features of the Regioselective Step

In this section, the crucial steps which are relevant for the regioselectivity of the studied model catalysis will be located. With respect to the two silanes applied, the models are denoted as S (monosilane) and DS (dimethylsilane). Both of them differ only to a minor extent from the previous model, ethylene + monosilane.[93] Recalling the results from the Chapter 4 and 5, the two most favored mechanisms, Chalk-Harrod and σ-bond metathesis, initially proceed through three identical steps, generating a crucial intermediate, an ethyl-complex, labeled "**CH4**" in Chapter 4,[93] after the (endothermic) hydrogenation of the olefin,[93] and then continue with the (exothermic) silylation of the ethyl complex via different pathways to form the final product ethylsilane.[93] As shown in Figure 6.1 and Table 6.1, the energy profiles of the CH pathways with ethylene and 1-butene, a model reactant for terminal aliphatic alkenes which can also isomerize to an internal alkene, are essentially parallel to each other. In other words, being independent of the reactant chosen, the catalysis proceeds along the same pathway (CH), passing through the same sequence of catalysis stages: first the hydrogenation of alkene and then the silylation of alkyl moiety (Figure 6.1).

The first stage of the catalytic process, the 3-step hydrogenation, referred to as the "*IOA*" in Chapter 4,[93] will predetermine the regioselectivity of the hydrosilylation of 1-butene. The hydrogen transfer can also proceed in a concerted way, being described as "*COA*" in the previous work, because it is coupled with the oxidative addition of silane.[93] In the current chapter, both "*IOA*" and "*COA*" will be studied with respect to their effect on the regioselectivity, as will be explained in the next paragraph. The intermediates and transition states will be denoted according to the corresponding regioselective pathway, on which they

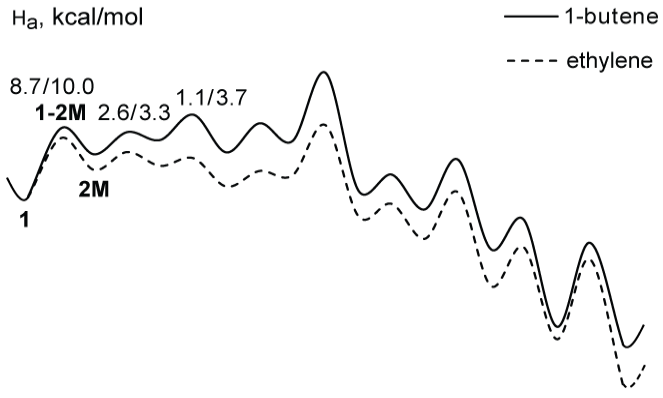

Figure 6.1. Enthalpy profile of the CH pathway, calculated for the hydrosilylation of 1-butene (solid line) and ethylene (dashed line). Relative barriers in the stepwise hydrogenation of olefin (*M* pathway) are given in kcal·mol^{-1} (1-butene/ethene). Detailed energetic data of the full pathways are given in Table 6.1.

are located. For instance, **1−2_aM** denotes the transition state **1–2** along the *aM* pathway.

The catalytically active species consists of both silane and olefin coordinated in an η^2-manner to Rh (CH1 in Chapter 4).[93] Starting from this complex, two different H atoms of the silane can be transferred to the ethylene, either the initially activated one (*COA*), or another one that is still bound to the silyl group (*IOA*).[93] An alteration from *COA* to *IOA* needs a change in the relative position between the migrating H atom and the olefin, enabling the former to bind to either end of the double bond.[93] Whereas the two C atoms in the double bond cannot be discriminated in ethylene, they are different in 1-butene, generating two regioselective reactions (Figure 6.2). Hence, altering the preference of these two reactions for the C−H bond formation implies a redirection of the regioselectivity. In the following, the main part of the discussion will focus on the comparison between the *COA–aM*, and *IOA–M* pathways in various models, abbreviated as *aM* and *M* pathways, respectively. Besides this factor, side effects caused by a possible reorganization of the reactants, e.g., the rotation of 1-butene will be addressed in addition at the end of this chapter.

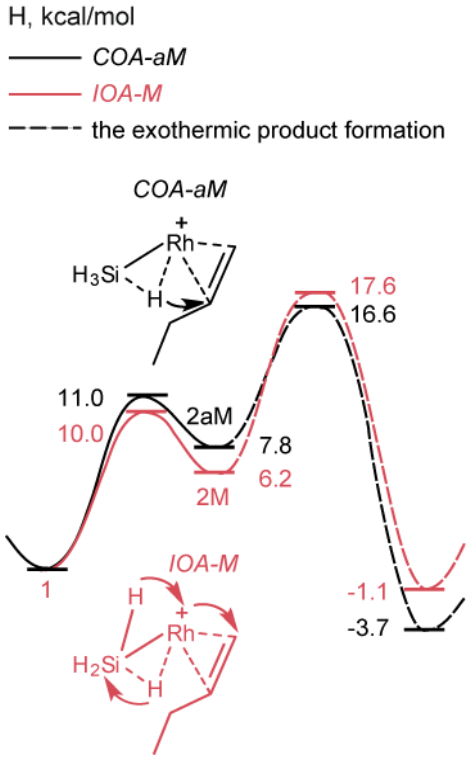

Figure 6.2. Enthalpy profile of the pathways for the hydrogenation of 1-butene, leading to the formation of *aM* or *M* intermediates, illustrated are *aM* (black) and *M* (red) pathways, and the subsequent exothermic product formation (dashed). Relative enthalpies of the TSs and the intermediates are given in kcal·mol^{-1}, with respect to the initial state **1**.

The *IOA–M* (stepwise hydrogenation) starts with the activation of one Si−H bond via a rotation of silane (Figure 6.2). This step exhibits the highest RB for the *M* pathway

(**1/1−2M/2M**); see Figure 6.1 and Table 6.1. This rotation of silane, featuring the highest barrier as mentioned before, prepares the position of H atom relative to the olefin double bond, generating a favorable arrangement for the bond formation between the two atoms (C and H) located in proximity. The regioselectivity can be controlled by this step, as explained in previous paragraph. To make it easier for the reader, extensions **aM** and **M** will be added to the label of the next intermediate **2**. Due to the simultaneous cleavage and formation of the Si−H and Rh−H bonds, the rotation of silane destabilizes **2M** with respect to complex **1** substantially, H(**2M**) − H(**1**) = 6.2 kcal·mol^{-1} (Figure 6.2).

Table 6.1. Relative enthalpies H of the intermediates and TSs shown in Figure 6.1 in kcal·mol^{-1}. Zero-point references are the seperated bare catalyst and reactants (*bis*-NHC-Rh(I)/C_2H_4/SiH_3 and *bis*-NHC-Rh(I)/C_4H_8/SiH_3). The labels of the structures are consistent with those in Chapter 4.

C_2H_4/SiH_3	H	C_4H_8/SiH_3	H
CH1	-51.36	**CH1** (**1**)	-51.24
1–2	-42.65	**1–2** (**1-2M**)	-41.21
CH2	-47.32	**CH2** (**M**)	-45.04
CH2–3	-44.69	**CH2–3**	-41.78
CH3	-46.73	**CH3**	-42.93
CH3–4	-45.60	**CH3–4**	-39.23
CH4	-49.77	**CH4**	-44.75
CH4–5	-47.47	**CH4–5**	-40.49
CH5	-48.12	**CH5**	-43.09
CH5–6	-40.77	**CH5–6**	-33.09
CH6	-54.13	**CH6**	-50.38
CH6–7	-52.29	**CH6–7**	-48.00
CH7	-57.42	**CH7**	-53.11
CH7–GT3	-50.57	**CH7–GT3**	-45.79
GT3	-64.31	**GT3**	-58.92
GT3–4	-58.67	**GT3–4**	-54.62
GT4	-72.13	**GT4**	-70.30
GT4–CH1	-60.41	**GT4–CH1**	-58.00
CH1+prod.	-78.83	**CH1+prod.**	-72.85

Comparing the first steps of the *M* and *aM* pathways, along the concerted pathway *aM* the system has to overcome a higher RB: H_a = 11.0 kcal·mol^{-1} (**1/1−2aM/2aM**) (Figure 6.2).

As shown by a NBO analysis, a radical is formed on the carbon atom to which the hydrogen atom is migrating. Note that the direct hydrogen transfer is considered here only for the nearest carbon atom. For the distant carbon atom, test calculations showed that only the *M* pathway is possible. One reaction, **1** → **2**, with the highest relative barrier in the crucial step of the regioselectivity, is described here to determine the ratio of reactions forming **2**. Starting in the basic model S with ethylene bridged, N-methyl-substituted *bis*-NHC ligand (1,1'-dimethyl-3,3'-ethylenediimidazolium) from **1**, the *M* pathway is by 1 kcal·mol^{-1} more favored, corresponding to an *aM* fraction of 16 %.

6.2 Modification of the Catalyst Ligand

In order to vary the structural and electronic properties of the catalyst, the *bis*-NHC ligand was modified as follows. (*i*) The linker connecting the two NHC moieties was varied in length (methylene or ethylene bridge). (*ii*) The wingtip nitrogen atoms were functionalized by a methyl group or a chlorine atom, representing an electron-donating and an electron-withdrawing substituent. Unsubstituted NHCs (−H at the nitrogen atom) will be examined for comparison. (*iii*) The C−C double bond of the imidazole ring is saturated (imidazoline) or chlorinated (4,5-dichloroimidazole) (Figure 6.3). From a systematic combination of these three types of modifications 14 catalyst models are generated which were applied to the catalytic systems S and DS (Table 6.2).

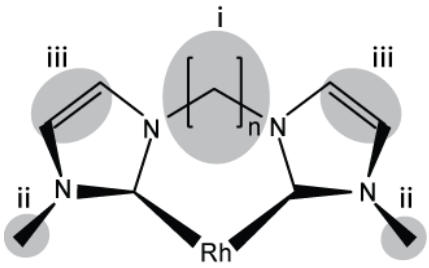

Figure 6.3. Modifications on the *bis*-NHC ligand: (*i*) variation of the linkage length, n=1,2; (*ii*) substitution at the wingtip nitrogen atom; (*iii*) saturation/chlorination of the C−C double bond.

For convenience, abbreviations will be introduced for each modification. In group (*i*), the methylene bridge is denoted with **1**, and the ethylene bridge with **2**. In group (*ii*), the methyl, hydrogen, and chlorine N-substituents are denoted by **m**, **h**, and **c**, respectively. In group (*iii*), **u** denotes the unsaturated (imidazole), **s** the saturated (imidazoline), and **c** the chlorinated (4,5-dichloroimidazole) NHC ligands on both sites of the bridge (Table 6.2). The label of each catalyst model is composed of the abbreviations of these three groups, in that order (Table 6.2). For instance, label **1mu** denotes the catalyst with a NHC ligand that features a methylene bridge (**1**), is N-methyl substituted (**m**), and C−C unsaturated (**u**). These same labels are also used as extensions to specify the intermediate and TS structures, as well as the relative barriers in the corresponding models. For example, **1−2aM_1mu** refers to the TS **1−2aM** in the model **1mu**, and H_a(aM_1mu) refers to the RB H_a(aM) in the same model.

Table 6.2. Notations for modifications *i*-*iii* in Figure 6.3. The full label of a catalyst model is composed in the form *i*+*ii*+*iii*. For modification *i*, **1** = methylene bridge, and **2** = ethylene bridge. For modification *ii*, **m** = methyl, **h** = hydrogen, and **c** = chlorine. For modification *iii*, **u** = unsaturated-, **s** = saturated-, and **c** = chlorinated NHCs.

i	Alteration of the bridge length						
	1						
	2						
ii	Substitution at N atoms of the ligand						
	$N-CH_3$			N−H		N−Cl	
	1m			**1h**		**1c**	
	2m			**2h**		**2c**	
iii	Saturation and chlorination of the C−C backbone						
	−	C−H	C−Cl	−	C−H	−	C−H
	1mu	**1ms**	**1mc**	**1hu**	**1hs**	**1cu**	**1cs**
	2mu	**2ms**	**2mc**	**2hu**	**2hs**	**2cu**	**2cs**

6.3 Impact of the Modifications

In this section, the impact of the modifications (*i*) to (*iii*) on the regioselectivity will be analyzed based on the difference ΔH_a between the two RBs H_a(aM) and H_a(M) (Table 6.3, Figures 6.4–6.6). Within each group of modifications, the models will be also compared among themselves: (*i*): methylene vs. ethylene; (*ii*): $-CH_3$ vs. −H vs. −Cl; and (*iii*): unsaturated vs. saturated vs. chlorinated (Figure 6.4). The corresponding ratio of the *aM* and *M* product (aM%, M%), which is calculated according to the equation detailed in the Chapter 3, is given in Table 6.3 at the end of this section. Crucial electronic and structural properties of selected intermediates and TSs will be analyzed at the end of this section to rationalize the change in regioselectivity evoked by the modifications.

6.3.1 Length of the Linkage

The analysis starts with modifications in position (*i*), which generates two types of catalyst models: first the methylene-linked *bis*-NHC ligands and second the ethylene linked congener (Figure 6.4). The first type of ligand favors the formation of the aM product in both S and DS systems (H_a(aM) < H_a(M)), while the second type yields various regioselectivities depending on other factors in the system S and a consistent reversed regioselectivity (H_a(M) < H_a(aM)) in the system DS (Figure 6.4, Table 6.3). In Section 6.4, the connection between this modification and the *M* and. *aM* regioselectivities will be analyzed.

In general, the regioselectivity promoted by the methylene bridge is sufficiently high (ΔH_a(aM-M) = −2.5 to −6.4 kcal·mol^{-1} in S and −5.0 to −7.3 kcal·mol^{-1} in DS, except for **1mc**, Figure 6.4, Table 6.3), the corresponding ratio of the aM product being hundred percent (Table 6.3). In comparison, the regioselectivity caused by the ethylene bridge is less pronounced (ΔH_a(aM-M) = −0.5 to 1.4 kcal·mol^{-1} in S, except for **2hu** (−7.6 kcal·mol^{-1}), and ΔH_a(aM-M) = 0.8 to 4.3 kcal·mol^{-1} in DS, except for **2mc** (9.0 kcal·mol^{-1}), predicting a dominant ratio of one regioisomer in five cases (**2hu** in S (aM) and DS (M), **2mu**, **2ms** and **2mc** in DS (all *M* regioselectivity, Figure 6.4, Table 6.3).

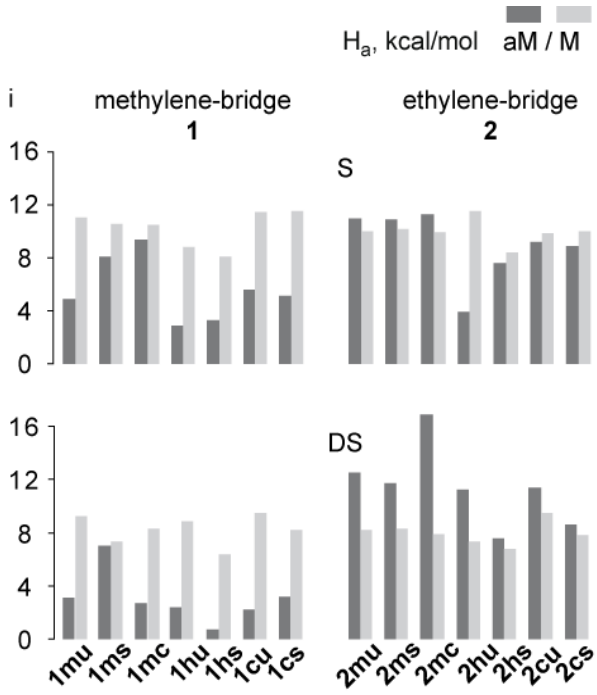

Figure 6.4. Comparison of the relative activation barriers H_a(aM) and H_a(M) (in kcal·mol^{-1}) in group (*i*), models with methylene and ethylene linkers. Each catalyst model was tested for two systems: 1-butene/monosilane (S, first row), and 1-butene/dimethylsilane (DS, second row).

6.3.2 Substitution on the Nitrogen Atoms

Regarding modifications at the wingtip nitrogen centers, i.e. modifications of type (*ii*), the models can be sorted into three sets according to the substitution on the N atom, −CH_3, −H, and –Cl (Figure 6.5,). Only in two sets one observes consistent regioselectivity induced by these modifications, i.e. dominating over the other effects, when applied to the system S: −H, −Cl (Figure 6.5, Table 6.3). Overall the differences in activation barriers (ΔH_a) correlate less well with the N-substitution than the length of the ligand linkage. In other words, in general modification (*i)* dominates over modifications of type (*ii*).

Comparing the three subsets **1mu/1ms/1mc**, **1hu/1hs**, and **1cu/1cs** to each other, one notes that the chlorine substituent increases ΔH_a most notably: ΔH_a(aM-M) = −5.7 kcal·mol^{-1} (**1cu**) and −6.4 kcal·mol^{-1} (**1cs**) in S; ΔH_a(aM-M) = −7.3 kcal·mol^{-1} (**1cu**) and −5.0 kcal·mol^{-1} (**1cs**) in DS. Also the non-substituted models are apparently appropriate choices for enhancing the regioselectivity: ΔH_a(aM-M) = −5.9 kcal·mol^{-1} (**1hu**) and −4.7 kcal·mol^{-1} (**1hs**) in S; ΔH_a(aM-M) = −6.4 kcal·mol^{-1} (**1hu**) and −5.7 kcal·mol^{-1} (**1hs**) in DS. The methyl-substituted models are more regioselective when the NHC moieties are unsaturated, i.e., when the modifications (*ii*) and (*iii*) are combined: ΔH_a(aM-M) = −6.1 kcal·mol^{-1} (**1mu**) in S; ΔH_a(aM-M) = −6.2 kcal·mol^{-1} (**1mu**) in DS. For saturated NHC ligands, methyl substituents on N hardly induce any differences in the two RBs: ΔH_a(aM-M) = −2.5 kcal·mol^{-1} (**1ms**) in S, and ΔH_a(aM-M) = −0.3 kcal·mol^{-1} (**1ms**) in DS.

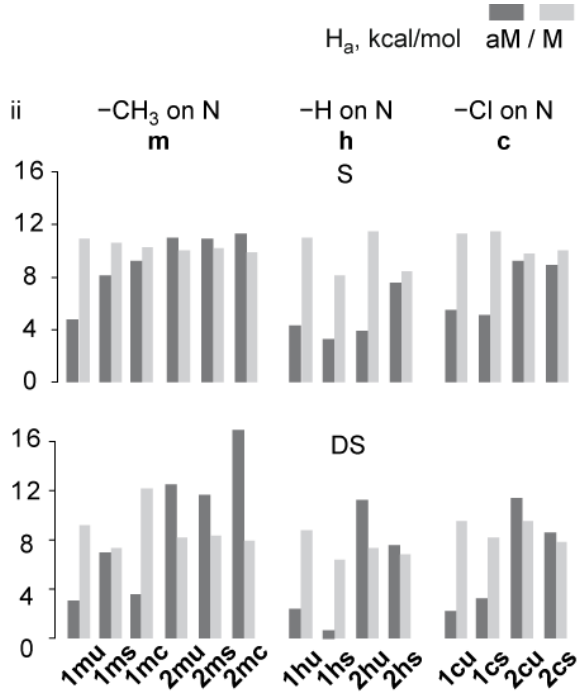

Figure 6.5. Comparison of the relative activation barriers H_a(aM) and H_a(M) (in kcal·mol^{-1}) in group (*ii*), models with various N-substituents: −CH_3, −H, and −Cl. Each catalyst model was tested for two systems: 1-butene/monosilane (S, first row), and 1-butene/dimethylsilane (DS, second row).

Turning to the remaining subsets **2mu/2ms/2mc**, **2hu/2hs**, and **2cu/2cs**, the N-methyl-substituted models obviously promote a reversed regioselectivity (formation of the *M* product preferred) in both catalysis systems S and DS (H_a(M) < H_a(aM), Figure 6.5), while the N-non-substituted and N-chlorine-substituted models switch the regioselectivity, when applied to the systems S, *aM*, and DS, *M*.

6.3.3 Modification of the C−C backbone

In the last group of modifications (*iii*) – saturation/chlorination of the C−C double bond – no dominant regioselectivity can be observed within any set of models. Apparently, this modification has a smaller influence on the regioselectivity than the other two types of modifications.

In most cases, the saturated NHC ligands decrease the values $|\Delta H_a|$ compared to the unsaturated NHC: **1mu**/**1ms**, **2mu**/**2ms**, **1hu**/**1hs**, **2hu**/**2hs**, in S and DS; **1mu**/**1ms**, **2mu**/**2ms**, **1hu**/**1hs**, **2hu**/**2hs**, **1cu**/**1cs,** and **2cu**/**2cs** in DS, reducing the corresponding ratio of the dominant product (Figure 6.6, Table 6.3). In contrast, chlorination of C−C double bond hardly changes the yield of the aM product, except for **1mu**/**1mc** in the model S (Table 6.3).

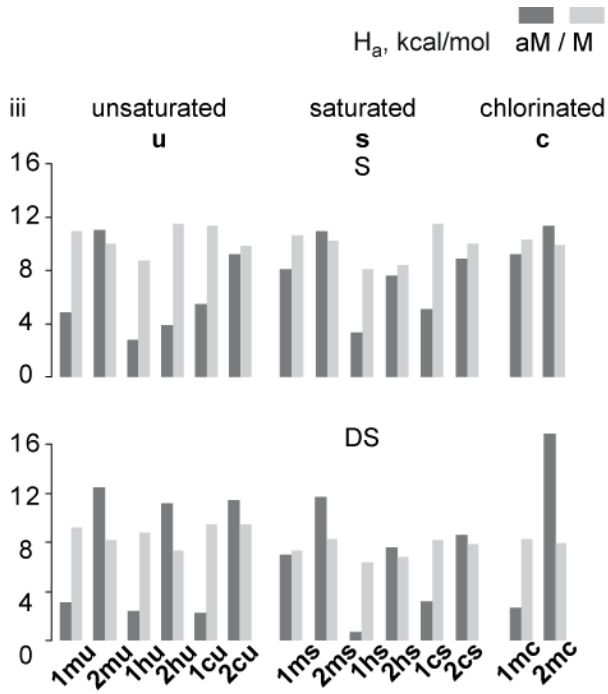

Figure 6.6. Comparison of the relative activation barriers H_a(aM) and H_a(M) (in kcal·mol^{-1}) in group (*iii*), models with differently modified C−C backbones: unsaturated, saturated, and chlorinated. Each catalyst model was tested for two systems: 1-butene/monosilane (S, first row), and 1-butene/dimethylsilane (DS, second row).

Table 6.3. Relative activation barriers H_a(aM) and H_a(M), and their differences, ΔH_a = H_a(aM) − H_a(M), in kcal·mol^{-1}. The corresponding ratio of the *aM* and *M* product (aM%) are predicted according to the equations given in Chapter 3.

	H_a(aM)		H_a(M)		aM%	M%
n=	**1**	**2**	**1**	**2**	**1**	**2**
S						
mu	4.8	11.0	10.9	10.0	100	84
ms	8.1	10.9	10.6	10.2	99	77
mc	9.2	11.3	10.3	9.9	75	91
hu	2.8	3.9	8.7	11.5	100	0
hs	3.3	7.6	8.1	8.4	100	18
cu	5.5	9.2	11.3	9.8	100	29
cs	5.1	8.9	11.5	10.0	100	12
DS						
mu	3.1	12.5	9.2	8.2	100	100
ms	7.0	11.7	7.3	8.3	64	100
mc	2.7	16.9	8.3	7.9	100	100
hu	2.4	11.2	8.8	7.3	100	100
hs	0.7	7.6	6.4	6.8	100	78
cu	2.2	11.4	9.5	9.5	100	97
cs	3.2	8.6	8.2	7.8	100	79

6.4 Analyses of the Reaction Kinetics

In total, there are seven models predicting a selective formation of the *aM* product in S (**1mu**, **1ms**, **1hu**, **2hu**, **1hs**, **1cu**, and **1cs**), and six in DS (**1mu**, **1mc**, **1hu**, **1hs**, **1cu**, and **1cs**, Table 6.3). Considering that the reaction **1→1−2aM→2aM** is endothermic (Figure 6.2), the backward RBs in the abovementioned models are also checked (Figure 6.7, Table 6.4).

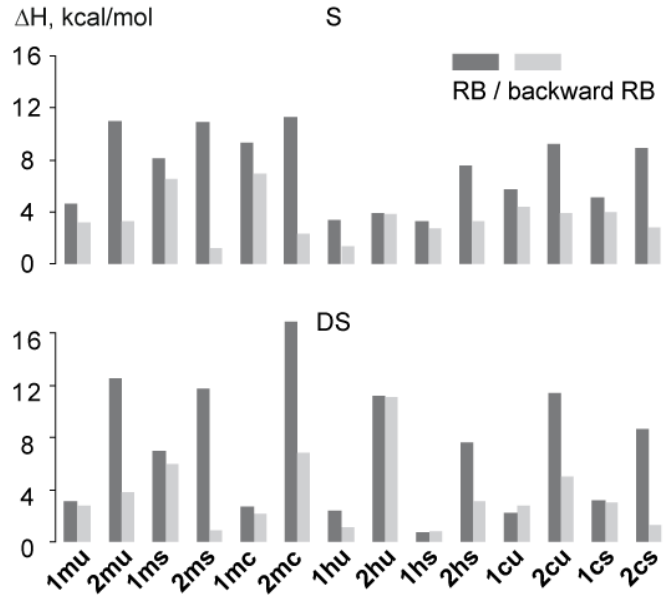

Figure 6.7. Comparison of the forward and backward relative activation barriers along the *aM* pathway for all models, kcal·mol^{-1}.

Among the models listed for S, **1mu**, **1hu**, and **1hs** involve relatively low backward RBs: 3.2 kcal·mol^{-1}, 1.4 kcal·mol^{-1}, and 2.7 kcal·mol^{-1}, respectively (Table 6.4). All six models involving DS as reactant have low backward barriers (0.8−3.0 kcal·mol−1, Table 6.4). Besides, the reaction **1→1−2aM→2aM** is less endothermic in the methylene models than in the corresponding ethylene models, except for **1hu/2hu** (Figure 6.7, Table 6.4). In order to check if there is a correlation between the enthalpy H_R(aM) of reaction and the activation barrier Ha(aM), one examines their potential for a (linear) correlation, in the spirit of the Brønsted-Evans-Polanyi principle.[271-273] In the present case, no such correlation was discovered (Figure 6.8).

This result indicates that the explored elementary step **1→1−2aM→2aM** does not only include the basic reaction **AB + C → A + BC** (corresponding to SiH + C → Si + HC), but very likely also other parts of a chemical reaction. To study the case in detail, one aims to rationalize the impact of modifications on the regioselectivity by analyzing each involved complex individually.

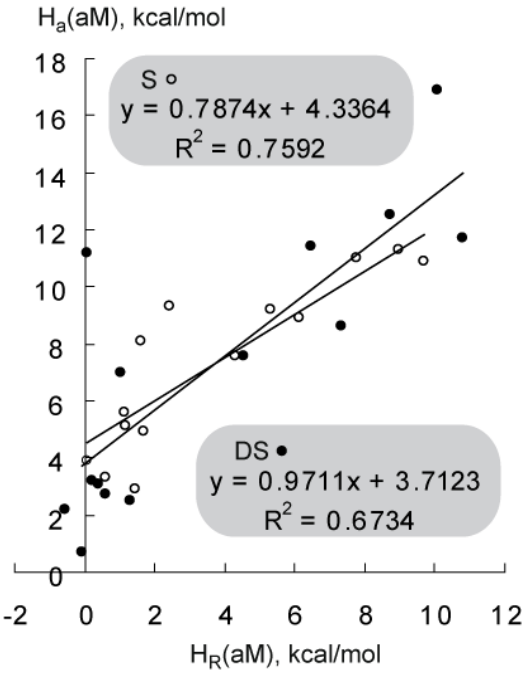

Figure 6.8. Investigation of the Brønsted-Evans-Polanyi relationship on the *aM* reaction in both S (butene/monosilane) and DS (butene/dimethylsilane) systems, as catalyzed by 14 catalyst models. Relative barriers H_a are plotted against the enthalpies of reaction H_R (kcal·mol^{-1}).

Seven of the eight catalyst models that show a good regioselectivity contain a methylene bridged *bis*-NHC ligand, one an ethylene bridge (**2hu**). By comparing the reaction barriers for *aM* and *M* with the two bridge lengths, H_a(aM, n=1) with H_a(aM, n=2), and the RBs H_a(M, n=1) with H_a(M, n=2), one concludes that complexes with the shorter bridge in general have lower barriers H_a(aM) (−13.3 kcal·mol^{-1} < H_a(aM, n=1) − H_a(aM, n=2) < −2.0 kcal·mol^{-1}, Table 6.5), but the corresponding barriers H_a(M) change to a lesser extent with the linkage length, up to 4.9 kcal·mol^{-1} (Table 6.5).

Apparently, the main reason for the increase of ΔH_a in the methylene models is the change in the relative barrier height H_a(aM), whereas the fluctuations of H_a(M) play a minor role. In consequence, the following analysis focuses on the electronic structures and geometries of the intermediates and TSs involved in the *aM* pathway, **1/1−2aM/2aM**. The influence of the modifications on the *M* pathway will be discussed subsequently.

First seven regioselective models will be investigated, **1mu**, **1ms**, **1hu**, **2hu**, **1hs**, **1cu**, and **1cs** for S, in order to search for the difference in electronic structure caused by the methylene bridge. Starting with the models **1mu** and **2mu**, the results of the NBO analysis are compared. In the initial state **1_1mu**, Rh and H of the activated Si−H bond form a weak covalent bond Rh−H (1.62 e, 50% from Rh and 50% from H), which then donates one

Table 6.4. Forward and backward relative activation barriers (RB, BRB) along the *aM* pathway, and the corresponding reaction enthalpies (H_R) in kcal·mol^{-1}, as well as the NBO charge on Rh (e) in the initial state **1** and the TS **1−2aM**.

					charge on Rh	
		RB	BRB	H_R	**1**	**1−2aM**
S	**1mu**	4.8	3.2	1.4	−0.58	−0.56
	2mu	11.0	3.2	7.8	−0.56	−0.55
	1ms	8.1	6.5	1.6	−0.51	−0.54
	2ms	10.9	1.2	9.7	−0.54	−0.54
	1mc	9.2	6.9	2.4	−0.58	−0.55
	2mc	11.3	2.3	9.0	−0.56	−0.56
	1hu	2.8	1.4	2.9	−0.60	−0.56
	2hu	3.9	3.8	0.1	−0.54	−0.59
	1hs	3.3	2.7	0.6	−0.49	−0.52
	2hs	7.6	3.3	4.3	−0.51	−0.54
	1cu	5.5	4.4	1.3	−0.58	−0.56
	2cu	9.2	3.9	5.3	−0.55	−0.57
	1cs	5.1	4.0	1.1	−0.50	−0.53
	2cs	8.9	2.8	6.1	−0.53	−0.55
DS	**1mu**	3.1	2.8	0.8	−0.61	−0.59
	2mu	12.5	3.8	8.7	−0.54	−0.61
	1ms	7.0	6.0	1.0	−0.51	−0.56
	2ms	11.7	0.9	10.8	−0.54	−0.57
	1mc	2.7	2.1	1.5	−0.61	−0.59
	2mc	16.9	6.8	10.1	−0.53	−0.60
	1hu	2.4	1.1	2.8	−0.62	−0.60
	2hu	11.2	11.1	0.1	−0.52	−0.60
	1hs	0.7	0.8	−0.1	−0.46	−0.54
	2hs	7.6	3.1	4.5	−0.48	−0.58
	1cu	2.2	2.8	0.2	−0.61	−0.59
	2cu	11.4	5.0	6.4	−0.53	−0.61
	1cs	3.2	3.0	0.2	−0.49	−0.56
	2cs	8.6	1.3	7.3	−0.50	−0.57

electron to the half-filled (0.89 e) p orbital of the carbon radical in the TS **1−2aM_1mu**. In contrast, no metal hydride is formed in the initial state **1_2mu**. Rather, the 1s orbital of the loosened H atom donates one electron to a vacant sp-hybrid orbital of Rh. In the TS **1−2aM_2mu**, the half-filled (0.93 e) p orbital of the carbon radical donates one electron to this H 1s orbital (donation in the reverse direction compared to **1−2aM_1mu**). Because the H transfer process is coupled with the activation of the Si−H bond, one also has to examine the Si−H distances in the initial states **1_1mu** and **1_2mu**. In the methylene model, the activated Si−H bond is 1.91 Å, i.e., in the range of a secondary interaction[94] (Table 6.5). In the ethylene model, the Si−H distance is 1.75 Å, corresponding to a bond of a three-centered agostic type of interaction[94] (Si−H−Rh), Table 6.5).

In consequence, the hydrogenation of the olefin in the latter case (**2mu**) is associated with the cleavage of a rather stable agostic bond, thus requiring more activation energy than

the standard hydrometalation process in the methylene model (**1mu**). The same electronic features are also observed in **1mc**/**2mc** and **1cu**/**2cu** for reaction model S.

Next the changes Δd(C−H) in the crucial distances C−H, from the TS **1−2aM** to the product **2aM** ("late" transition states of endothermic reactions) were checked. For the models **1mu**/**2mu**, and **1cu**/**2cu**, Δd(C−H) is greater in the methylene models (lower TS) than in the ethylene models (higher TS) where Δd(C−H, n=1)/Δd(C−H, n=2) = 0.48/0.27 Å, and 0.47/0.30 Å. The corresponding RBs are H_a(aM, n=1)/H_a(aM, n=2) = 4.8/11.0 kcal·mol^{-1}, and 5.5/9.2 kcal·mol^{-1}, respectively (Table 6.5). This finding is in consistent with the Hammond postulate: in an endothermic reaction, the more similar the TS structure and the product structure are, the less stable is the TS.[274]

Table 6.5. The lengths of the activated Si−H bond in **1** (d(Si−H), Å) and the change in the crucial distance C−H from **1−2aM** to **2aM** (Δd(C−H), Å).

	d(Si−H)		Δd(C−H)	
n=	**1**	**2**	**1**	**2**
S				
mu	1.91	1.75	0.48	0.27
ms	1.87	1.74	0.44	0.26
mc	1.93	1.75	0.48	0.25
hu	2.63	1.78	0.37	0.93
hs	1.79	1.75	0.40	0.59
cu	1.91	1.78	0.47	0.30
cs	1.88	1.77	0.47	0.32
DS				
mu	1.84	1.71	0.51	0.45
ms	1.76	1.69	0.54	0.31
mc	1.92	1.69	0.43	0.45
hu	2.71	1.71	0.49	0.44
hs	1.70	1.69	0.39	0.59
cu	1.86	1.72	0.50	0.45
cs	1.82	1.71	0.54	0.34

Likewise, in **1ms**/**2ms** and **1cs**/**2cs**, the metal hydride and the agostic bond are determined in the starting species **1** in the methylene and ethylene models, respectively (Table 6.5). A change in the C−H distance from TS to the product correlates with the height of the relative barrier: Δd(C−H)(n=1)/Δd(C−H)(n=2) = 0.44/0.26 Å, and H_a(aM, n=1)/H_a(aM, n=2) = 8.1/10.9 kcal·mol^{-1} for **1ms**/**2ms** and S; and Δd(C−H)(n=1)/Δd(C−H)(n=2) =0.47/0.32 Å, and H_a(aM, n=1)/H_a(aM, n=2) = 5.1/8.9 kcal·mol^{-1} for **1cs**/**2cs** and S (Tables 6.3 and 6.5). A minor difference between these two pairs and the models discussed in the preceding paragraph (**1mu**, **1cu**) is the extent of Si−H bond activation. As shown in Table 6.3, the Si−H distances are 1.87 Å in **1_1ms** and 1.88 Å in **1_1cs**. Thus these models S have shorter Si−H bonds than the model S **1_1mu**, and **1_1cu** (both 1.91 Å, Table 6.5). Apparently, the Si−H

bond is activated to a greater extent in models with unsaturated NHC ligands due to the more electronegative metal center. For instance, the charges on Rh according to a natural population analysis are −0.58e in **1_1mu** and −0.51e in **1_1ms** (Table 6.4).

The group of models consisting of unsubstituted NHCs (**1hu**, **2hu**, **1hs** and **2hs** model S) exhibits some particularities. First, the agostic bond is determined not only with the two ethylene bridged models, but also with **1hs** (Table 6.5); second, the models **2hu** and **1hs** in S feature more similar reaction enthalpies (0.1 kcal·mol^{-1} and 0.6 kcal·mol^{-1}, Table 6.4) and activation barriers (3.9 kcal·mol^{-1} and 3.3 kcal·mol^{-1}, Table 6.4) than the models of the same bridge length. In the exceptional case **2hu**, the C−H distance in the TS is less similar to the one in the product than in **1hu**, model S (Δd(C−H, n=1)/Δd(C−H, n=2) = 0.37/0.93 Å, Table 6.5).

So far, the intermediates and TSs in the seven ligands that provide high regioselectivity for reaction model S have been analyzed (**1mu**, **1ms**, **1hu**, **2hu**, **1hs**, **1cu**, and **1cs**). For the other catalytic system DS, the results are similar, except for **1ms**, **1mc**, and **2hu**. Note that the activation barrier along the *M* pathway H_a(M) is in general lower with DS than with S as reactant. This lowering of H_a(M) is one of the factors which are responsible for the decrease of ΔH_a in **1ms** and **2hu**: H_a(M, S) = 10.6 kcal·mol^{-1} and 11.5 kcal·mol^{-1} (**1ms**, **2hu**); and H_a(M, DS) = 7.3 kcal·mol^{-1} in both cases, Table 6.3. In system **2hu**, the barrier H_a(aM) increases at the same time, H_a(aM, S) = 3.9 kcal·mol^{-1}, H_a(aM, DS) = 11.2 kcal·mol^{-1}, possibly because the TS is closer to the product structure in DS than in S (Δd(C−H, S) = 0.93 Å, Δd(C−H, DS) = 0.44 Å, Table 6.3).

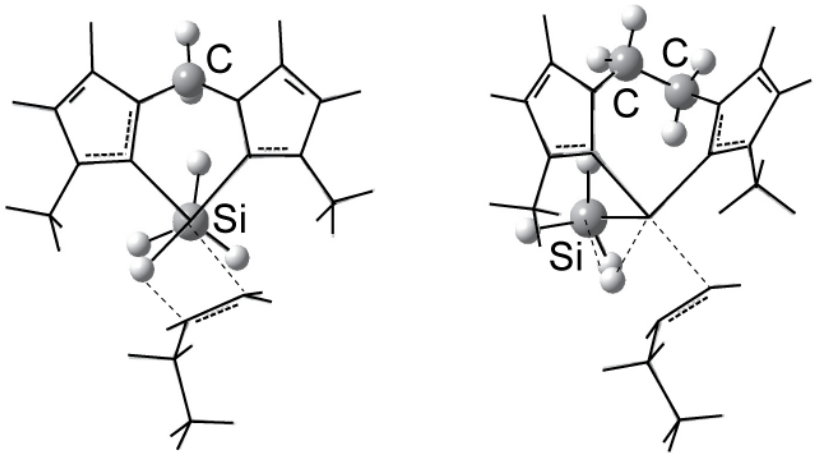

Figure 6.9. Two types of hydrogenation of 1-butene catalyzed by the Rh(I)-*bis*-NHC complex: hydrometalation (**1−2aM_1mu**, left), and agostic bond mediated H transfer (**1−2aM_2mu**, right).

Up to this point, the decrease of the activation barrier H_a(aM) along the *aM* pathway in the methylene models has been traced back to a better Si−H activation in the initial state. Yet the charge analysis does not show a correlation between the degree of this bond activation and the electronegativity of the metal center. Neither does this observation correlate with the type of silane. By comparing the geometries of these two groups of models (methylene vs. ethylene), one notices an increased symmetry around the metal center in the methylene models, compared to the ethylene models. For example, in the TS **1−2aM_1mu**, the two carbon atoms of the Rh−NHC bonds, the hydrogen atom from the activated Si−H bond, and the terminal carbon atom of the olefin are arranged approximately in a square-planar manner, and the silyl group is positioned perpendicular to this plane (Figure 6.9). Likewise this spatial arrangement is less favored in the ethylene model due to steric repulsion. As the ethylene linkage is able to "rotate", this moiety prefers a staggered conformation and blocks the backside of the catalyst complex, so that the silyl group cannot migrate further from the H atom after the Si−H bond activation (Figure 6.9).

It is possible that not only the silane, but also the η^2-coordinated 1-butene can rotate in the coordination sphere. Such a rotation will cause an additional change in the position of the reactants relative to each other. Test calculations showed that the ethylene bridge facilitates the rotation of 1-butene more than the methylene bridge. In addition, the correlation between one type of oxidative addition and one regioselective pathway will be reversed due to this rotation, see Figure 6.10: left side: *COA-M*, *IOA-aM*, and right side: *COA-aM*, *IOA-M*. Note that the TS along the *COA-M* pathway is by 3.0 kcal·mol^{-1} higher than the TS along the

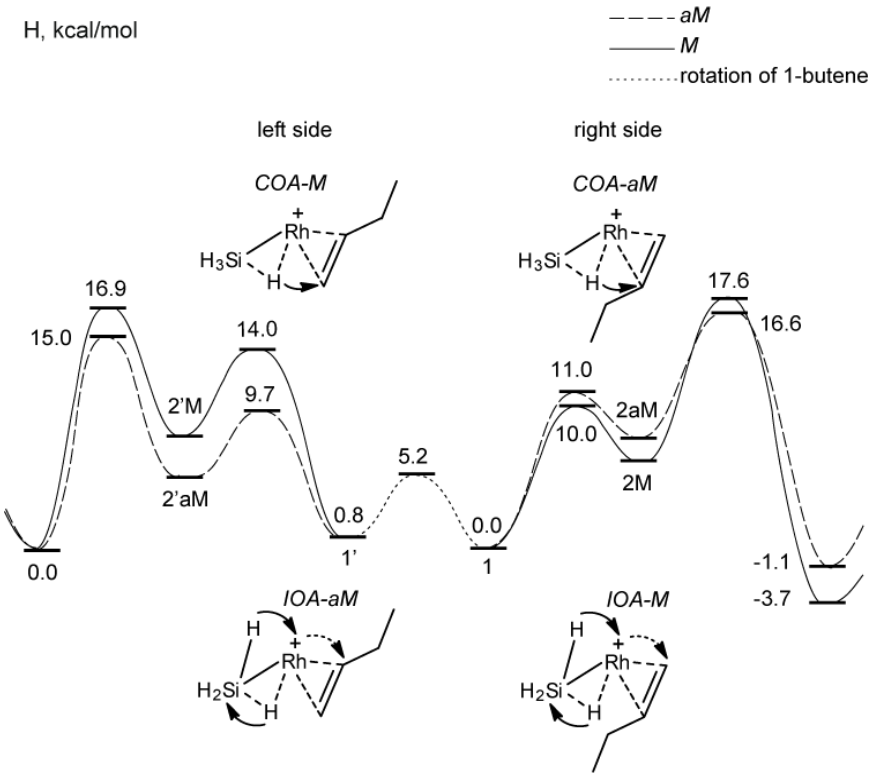

Figure 6.10. Enthalpy profile of the different pathways (exemplified by model **2mu** in S) for the hydrogenation of 1-butene, starting from two energetically comparable initial states **1** and **1'**, ending in the formation of *aM* or *M* intermediates. Dashed line, solid line, and dotted lines are used to mark the *aM* and *M* pathways, as well as the rotation of 1-butene. Relative enthalpies of the TSs and the intermediates are given in kcal·mol^{-1}, with respect to the initial state **1**. In case of the corresponding methylene model (**1mu**), **1'** is higher than **1** in enthalpy by 2 kcal·mol^{-1}; and the rotation of 1-butene occur via two steps, each TS has a relative enthalpy of 8 − 9 kcal·mol^{-1}. Besides, in case of a methylene model, the *aM* pathways are below the *M* pathways on both sides.

COA-aM pathway. The reason is that the carbon radical in the TS is better stabilized on a higher substituted position (*COA-aM*). This observation agrees with the *aM* rule, which is typical for a catalyzed hydrosilylation of alkenes.[1]

From this point of view, the actual regioselectivity for the *M* product in the DS system, observed among the ethylene models, as presented in Table 6.3, is under the premise that the olefin does not re-orient (Figure 6.10). In ethylene models, the *M* pathway on the right hand side is slightly below the *aM* pathway at one point (10.0 vs. 11.0 kcal·mol^{-1}), while exhibiting one TS of very similar height to the TS along the *aM* pathway on the left hand side (10.0 vs. 9.7 kcal·mol^{-1}). This may downgrade the regioselectivity noticeably. In contrast, the regioselectivity induced by a methylene bridge is unlikely to be affected by olefin rotation, because the rotation is kinetically less favored than the hydrogenation: $H_{a,}$(rotation) ≥ 8

kcal·mol^{-1} vs. H_a (hydrogenation) ≤ 6 kcal·mol^{-1}. Besides, in this case, the *aM* pathways are below the *M* pathways on both sides.

6.5 Conclusion

The impact of three types of ligand modifications on the regioselectivity was studied by applying 14 bis-NHC Rh(I) catalyst models in two catalytic cycles, hydrosilylation of 1-butene by monosilane and dimethylsilane. The regioselectivity for the *aM* product can be effectively improved by using NHC ligands linked by a methylene group. The models with ethylene linked ligands tend to cause the reversed regioselectivity. However, this preference may be reduced by a possible reorganization of the reactants. The change in the relative barrier height was related to various types of Si−H activation (metal hydride vs. agostic bond formation) and the coupled or step-wise hydrogenation of 1-butene. Compared to the bridge length, substitutions at the wingtip nitrogen centers do not cause a noticeable change in the relative barriers, except for the unsubstituted models. When applying the larger silane (dimethylsilane), the impact of most modifications remains unchanged.

The current chapter contains the main content of a manuscript in preparation, entitled "Controlling Regioselectivity of Olefin Hydrosilylation by Modifying a *Bis*-NHC Rhodium Catalyst: A DFT Study".[275]

7 Summary

In this thesis, hydrosilylation of alkenes catalyzed by a series of *bis*-N-heterocyclic carbene-Rh(I) complexes was studied using density functional methods. Model reactions and model catalysts were applied to explore (*i*) the full catalytic pathways of the four most studied mechanisms, (*ii*) the method dependency of the preferred mechanisms, and (*iii*) the influence of catalyst modifications on the regioselectivity of the catalyzed reactions.

In the first part of the study, all possible pathways of the four mechanisms were explored, namely the Glaser-Tilley (GT),[21,37] Chalk-Harrod (CH),[38] modified Chalk-Harrod (mCH),[39-44] and σ-Bond metathesis (SBM) mechanisms,[45,46] using the density functional B3LYP.[212-214] Full pathways of the Chalk-Harrod and σ-Bond metathesis mechanisms are energetically favored over those of the Glaser-Tilley and modified Chalk-Harrod mechanisms, with respect to the highest relative barriers – 9.3 kcal·mol^{-1} (CH), 8.6 kcal·mol^{-1} (SBM), 37.3 kcal·mol^{-1} (GT), and 22.3 kcal·mol^{-1} (mCH) – as well as the highest absolute barriers – 10.6 kcal·mol^{-1} (CH), 12.5 kcal·mol^{-1} (SBM), 16.3 kcal·mol^{-1} (GT), and 26.0 kcal·mol^{-1} (mCH).[93] The initial- and final stages, the oxidative addition of silane and reductive elimination of the product, were determined to be crucial for the catalytic process.[93] In total six variants were studied for the first, and two variants for the latter process.[93] The two favored enthalpy profiles CH and SBM present rate-determining steps in the stepwise oxidative addition of silane and the reactant assisted displacement of product (~ 9 kcal·mol^{-1}).[93] The concerted oxidative addition of silane along the mCH pathway and the product elimination without additional reactant in the GT mechanism are also the rate-determining steps in each case, however, requiring much higher activation enthalpies (14–28 kcal·mol^{-1} more) than in the cases of CH and SBM mechanisms.[93] The four mechanisms are interrelated. The CH, mCH, and SBM mechanisms share the same starting species **CH1**, in which both reactants are coordinated to the bare catalyst. The GT mechanism starts and ends with the formation of the silylene complex **GT1**, which consists of the bare catalyst and the reactant monosilane. Although **GT1** is by 17 kcal·mol^{-1} less stable than **CH1**, as the catalysis proceeds further, the intermediates of the various mechanisms become comparable in energetics so that the CH, mCH, and the GT mechanisms are connected by the isomerization between conformational isomers. On the other side, because of the under-coordinated nature of the metal center in several intermediates, crucial bond formations not only occur consecutively (CH and mCH) but also in a concerted way (SBM).

With respect to the structural specialty of the bidentate NHC ligand, a steric descriptor (dihedral angle γ between the two imidazole planes) was introduced to classify the conformation of the chelate ligand. For each mechanism, the conformational change in the *bis*-NHC ligand was studied along the energetically most favored pathway. The reaction energetics and the ligand conformation are correlated. In fact, the conformational isomerization of the *bis*-NHC was estimated to facilitate crucial bond formation steps considerably, reducing a selected key barrier by 17 kcal·mol^{-1}.

In the second part of the study, an extended set of DF functionals was applied to explore crucial barriers selected from the energetically favored pathways of each mechanism. The 12 chosen functionals are: semi-local functionals BP86,[212,231] BLYP,[212,214] PBE,[222,223] mPWPW,[225-227,232,233] M06-L,[235] and TPSS;[230] and hybrid functionals B3LYP,[212-214] B3PW91,[212,213,225,226,232,233] PBE0,[222-224] MPW1K,[225-228,232,233] M06,[235] and MPW3LYP.[225-227,229,232,233] The examined relative enthalpy barriers were selected from crucial elementary steps. For the purpose of examining both the structural and energetic changes caused by the varied density functionals, all selected intermediates and transition states were optimized with each chosen functional. In some cases, the structural changes resulting from the geometry optimization have notable influence on the height of the corresponding relative barrier, varying it by up to 3 kcal·mol^{-1}. This result suggested that the changes in geometries caused by the alternation of functionals are correlated with the changes in the energy.

Furthermore, it can be concluded that among the selected barriers, the correlation part of the functional plays a more important role than the exchange part in estimating the barrier heights.[221] Density functionals consisting of the same exchange part but different correlation part predicted the same relative barrier by 6–7 kcal·mol^{-1} differently, while adding the exact exchange in a normal range (~25%) brought about much less change in relative barrier (< 3 kcal·mol^{-1}).[221]

In the current work, the mechanism preference did not change with the density functional applied.[221] All chosen density functionals predicted the CH and SBM mechanisms to be strongly favored over the GT and mCH mechanisms.[221] The results also suggested that these two mechanisms are intrinsically competitive.[221] Nevertheless, with respect to particular elementary steps, the choice of a density functional can change the predicted reaction kinetics to a large extent, by up to 11 kcal·mol^{-1}.[221] This calls attention to the sensitivity of theoretical results to the chosen computational methods, especially in cases such as the current one, where more than one pathway is energetically conceivable and the highest barriers along these pathways are of similar height.

The final part of the study deals with the problem of regioselectivity. The reaction model was extended from the hydrosilylation of ethylene to the hydrosilylation of 1-butene, which models terminal aliphatic alkenes. Besides monosilane, dimethylsilane was also considered as one of the reactants. The catalyst model was modified on the *bis*-NHC ligand in three different positions: the linkage was varied in length, the C−C backbone of the NHC moiety was saturated or substituted, and the substituents on the wingtip nitrogen atom of the imidazole were varied. Calculations were carried out with the semi-local DF functional BP86.

The regioselectivity was assessed by evaluating the yield of the regioisomers on the basis of the Erying equation.[241] It was studied as related to the systematical combinations of different modifications. Among the three types of ligand modifications, the tuning of the linkage length was determined to be the most effective one. Based on the current reaction models, the selective formation of the anti-Markovnikov product will be promoted by using ligands bridged with a methylene group. The ethylene bridged bis-NHC ligands have a potential to reverse the regioselectivity (to Markovnikov) – especially in reaction models involving larger silane. Comparing to the bridge length, other modifications have only minor influences on the regioselectivity. In general, for the chosen *bis*-NHC framework, the impact of modifications decreases as following: variation of linkage length > substitution on the wingtip nitrogen atoms > modifications at the C−C backbone.

In order to rationalize the regioselectivity induced by the ligand modification, charge and geometry analyses were carried out for the intermediates and transition states, which were involved in the models of promising regioselectivity. Crucial distances which are directly related to the chemical process in the regioselective steps were analyzed. It was determined that the switch of the two regioselectivities is controlled by the population of anti-Markovnikov and Markovnikov types of intermediates via the modification of catalyst ligand. The root of the matter was estimated to be the different bond order of certain bonds, especially which of one activated Si−H bond in the reactant substrates, which can be induced by the ligand modification and then cause energetic difference in the two types of intermediates.

It was also noted that the inversion of regioselectivity can occur in case of an isomerization of the key intermediate. Yet the catalyst models involving a methylene bridge were not prone to such isomerizations, according to the calculations.

In summary, this thesis is the first theoretical attempt to examine the adaptability of a series of *bis*-NHC-Rh(I) catalytic active complexes for the hydrosilylation of alkenes. The results indicated that these compounds are efficient catalysts, as lately confirmed by

experiments on a family of closely related *mono*-NHC-Rh(I) catalysts.[32] This work also pointed out the importance of choosing an appropriate computational method. With respect to the optimization of the catalyst model, regioselectivity of reaction models catalyzed by complexes bearing different ligands was studied. The results hinted at utilization of methylene-bridged *bis*-NHC ligands for a better anti-Markovnikov regioselectivity in the hydrosilylation of terminal aliphatic alkenes. Based on the current work, future studies can be envisaged to explore the catalytic efficiency of other reaction models, as well as the potential enantioselectivity of the catalyst by entailing further modifications.

8 List of Abbreviation

ASE	Aromatic stabilization energy
a.u.	Atomic unit
aM	anti-Markovnikov
aNHC	Abnormal NHC, in this thesis: imidazol-4-ylidenes
B3LYP	Hybrid functional consisting of the Becke88 three parameter exchange functional and the correlation functional of Lee-Yang-Parr, containing 20% exact exchange
B3PW91	Hybrid functional consisting of the three parameter Becke88 exchange functional and the correlation functional of Perdew-Wang, containing 20% exact exchange
BP86	Becke's 1988 functional combined with the gradient corrected local correlation functional of Perdew
CH	Chalk-Harrod mechanism
COA	Coupled oxidative addition
COD	η^4-cycloocta-1,5-diene
Cp*	1,2,3,4,5-Pentamethylcyclopentadienyl
DCM	Dichloromethane
DFT	Density functional theory
DI	Delocalization index
DOA	Direct oxidative addition
ε	Dielectric constant
ECP	Effective core potential
FTIR	Fourier transform infrared spectroscopy
γ	Dihedral angle between two NHC moieties
G03/G09	Software package Gaussian03 and Gaussian09
GGA	Generalized gradient approximation
GT	Glaser-Tilley mechanism
HOMO	Highest occupied molecular orbital
IHI	interligand hypervalent interactions
IM	intermediate
IMID	The most stable tautomer of imidazole
IOA	Indirect oxidative addition
IR	Infrared spectroscopy
LSD	Local spin density
LUMO	Lowest unoccupied molecular orbital
M	Markovnikov
M06-L	A new local density functional developed by Truhlar's group
M06	The hybrid counterpart of M06, containing 27% exact exchange
mCH	Modified Chalk-Harrod mechanism
Me	Methyl
MO	Molecular orbital
mPWPW	The modified Perdew-Wang 1991 exchange functional combined with the Perdew and Wang's 1991 gradient-corrected correlation functional
MPW1K	Hybrid counterpart of mPWPW containing 42.8% exact exchange
MPW3LYP	Hybrid functional consisting of the modified Perdew-Wang 1991 exchange functional and the Lee-Yang-Parr correlation functional, containing 21.8% exact exchange

NBO	Natural bond orbital
NHC	N-heterocyclic carbene
nNHC	Normal NHC, in this thesis: imidazol-2-ylidenes
NICS	Nucleus-independent chemical shifts
NMR	Nuclear magnetic resonance spectroscopy
PBE	The 1996 functional of Perdew, Burke and Ernzerhof, including the gradient-corrected correlation functional PBE
PBE0	The hybrid functional made from the pure functional of Perdew, Burke and Ernzerhof 1996, containing 25% exact exchange
SBM	σ-Bond metathesis mechanism
SISHA	Secondary interactions between a silicon and a hydrogen atom
STQN	Synchronous Transit-Guided Quasi-Newton method
THF	Tetrahydrofuran
TM	Transition metal
TPSS	Tao-Perdew- Staroverov-Scuseria general gradient approximation
Vi	Vinyl
XRD	X-ray diffraction

9 Appendix

Table A1. Formation enthalpies and energies[a] H (kcal·mol^{-1}) of all intermediates (IM) and transition states (TS) along the pathways of the mechanisms GT, CH, mCH and SBM, calculated with B3LYP and BP86. The resulting enthalpy differences[b] ΔH and differences in enthalpy barriers[c] ΔH_a are given for method comparison. Note that some steps are shared by several pathways. Single point energies E(BP86//B3LYP) are provided for comparison. The repeated structures of such steps are marked by an asterisk.

	IM/TS		H(B3LYP)	H(BP86)	E(BP86)	E(BP86//B3LYP)	ΔH	ΔH_a
GT		1	–23.61	–30.01	–31.06	–29.30	–6.40	
	igt2	2	–25.85	–32.76	–34.23	–32.06	–6.91	
	gt2	2–3	–7.27	–23.48	–23.66	–22.29	–16.21	–9.30
		3	–55.70	–64.28	–64.89	–66.26	–8.58	
		3–4	–48.00	–58.67	–59.02	–58.59	–10.67	–2.09
		4	–58.95	–72.13	–72.29	–74.03	–13.18	
		4–5	–53.52	–67.52	–67.37	–68.51	–14.00	–0.82
		5	–60.87	–74.62	–75.00	–76.72	–13.75	
		5–6	–53.68	–67.92	–67.86	–68.67	–14.24	–0.49
	igt1	6	–60.96	–75.02	–75.24	–77.42	–14.06	
	gt1	6–1	–23.66	–41.79	–41.66	–43.50	–18.13	–4.07
CH	ich2	1	–40.14	–51.36	–51.93	–51.90	–11.22	
	ch2	1–2	–31.52	–42.65	–42.95	–41.01	–11.13	0.09
		2	–36.41	–47.32	–47.79	–47.23	–10.91	
		2–3	–31.97	–44.69	–44.53	–44.46	–12.72	–1.81
		3	–33.71	–46.73	–46.90	–47.27	–13.02	
		3–4	–31.91	–45.60	–43.29	–43.36	–13.69	–0.67
		4	–37.57	–49.77	–50.24	–51.12	–12.20	
		4–5	–35.28	–47.47	–47.06	–48.76	–12.19	0.01
	ich3	5	–35.81	–48.12	–51.93	–50.21	–12.31	
	ch3	5–6	–29.52	–40.78	–42.95	–41.07	–11.26	1.05
		6	–45.39	–54.13	–54.53	–55.58	–8.74	
		6–7	–43.91	–52.29	–52.49	–53.46	–8.38	0.36
		7	–49.15	–57.42	–58.52	–60.09	–8.27	
		7–8	–42.86	–50.57	–50.89	–51.59	–7.71	0.56
		8*	–55.70	–64.28	–64.89	–66.26	–8.58	
		8–9*	–48.00	–58.67	–59.02	–58.59	–10.67	–2.09
	ich1	9*	–58.95	–72.13	–72.29	–74.03	–13.18	
	ch1	9–1	–49.60	–60.41	–60.35	–61.19	–10.81	2.37
mCH	imch3	1*	–40.14	–51.36	–51.93	–51.90	–11.22	
	mch3	1–2*	–31.52	–42.65	–42.95	–41.01	–11.13	0.09
	imch1	2*	–36.41	–47.32	–47.79	–47.23	–10.91	
	mch1	2–3	–14.17	–27.05	–47.79	–27.07	–12.88	–1.97
		3	–29.90	–41.09	–27.22	–41.22	–11.19	
		3–4	–27.83	–40.62	–40.68	–39.67	–12.79	–1.60
		4*	–45.39	–54.13	–54.53	–55.58	–8.74	
		4–5*	–43.91	–52.29	–52.49	–53.46	–8.38	0.36
		5*	–49.15	–57.42	–58.52	–60.09	–8.27	
		5–6*	–42.86	–50.57	–50.89	–51.59	–7.71	0.56

		6*	–55.70	–64.28	–64.89	–66.26	–8.58	
		6–7*	–48.00	–58.67	–59.02	–58.59	–10.67	–2.09
	imch2	7*	–58.95	–72.13	–72.29	–74.03	–13.18	
	mch2	7–1*	–49.60	–60.41	–60.35	–61.19	–10.81	2.37
SBM	isbm1	1*	–40.14	–51.36	–51.93	–51.90	–11.22	
	sbm1	1–2*	–31.52	–42.65	–42.95	–41.01	–11.13	0.09
		2*	–36.41	–47.32	–47.79	–47.23	–10.91	
		2–3*	–31.97	–44.69	–44.53	–44.46	–12.72	–1.81
		3*	–33.71	–46.73	–46.90	–47.27	–13.02	
		3–4*	–31.91	–45.60	–43.29	–43.36	–13.69	–0.67
		4*	–37.57	–49.77	–50.24	–51.12	–12.20	
		4–5	–31.08	–44.34	–44.73	–44.65	–13.26	–1.06
	isbm2	5	–33.97	–54.20	–53.60	–56.75	–20.23	
	sbm2	5–6	–27.59	–44.82	–44.16	–47.59	–17.23	3.00
	isbm3	6	–55.34	–70.07	–70.15	–72.65	–14.73	
	sbm3	6–1	–51.30	–62.43	–62.75	–64.13	–11.13	3.60

[a]Formation enthalpies relative to the separated reactants Rh(I)-*bis*-NHC complex, silane, and ethylene.

[b]$\Delta H = H(BP86) - H(B3LYP)$

[c]$\Delta H_a = \Delta H(TS) - \Delta H(IM)$

Table A2. B3LYP and BP86 calculated crucial distances[a] d (Å) in all intermediates (IM) and transition states (TS).

	IM/TS			B3LYP	BP86	Δd	Type[b]
GT		1	Rh–Si1	2.31	2.29	–0.02	u0–u1
			Rh–H1	1.86	1.84	–0.02	u0–u1
			Rh–H2	1.83	1.81	–0.02	u0–u1
			Si1–H1	1.59	1.62	0.03	u0–u1
			Si1–H2	1.59	1.63	0.04	u0–u1
	igt2	2	Rh–Si1	2.31	2.28	–0.03	u0–u1
			Rh–H1	1.84	1.81	–0.03	u0–u1
			Rh–H2	1.80	1.77	–0.03	u0–u1
			Si1–H1	1.59	1.63	0.04	u0–u1
			Si1–H2	1.61	1.66	0.05	u0–u1
			Si1–H3	1.48	1.49	0.01	u1
			C1–H3	3.09	2.89	–0.20	u1–u2
			C2–Si1	3.47	3.24	–0.23	u1–u2
			C1–C2	1.34	1.35	0.01	u2
	gt2	2–3	Rh–Si1	2.19	2.20	0.01	u0–u1
			Rh–H1	1.65	1.66	0.01	u0–u1
			Rh–H2	1.63	1.64	0.01	u0–u1
			Si1–H1	1.93	1.96	0.03	u0–u1
			Si1–H2	1.93	1.94	0.01	u0–u1
			Si1–H3	1.57	1.58	0.01	u1–u2
			C1–H3	1.70	1.73	0.03	u1–u2
			C2–Si1	2.06	2.07	0.01	u1–u2
			C1–C2	1.41	1.42	0.01	u2

	3	Rh–Si1	2.32	2.29	–0.03	u0–u1
		Rh–H1	1.84	1.82	–0.02	u0–u1
		Rh–H2	1.81	1.79	–0.02	u0–u1
		Si1–H1	1.60	1.63	0.03	u0–u1
		Si1–H2	1.61	1.64	0.03	u0–u1
		C2–Si1	1.87	1.88	0.01	u3
		C1–H3	1.09	1.10	0.01	u3
		C1–C2	1.54	1.55	0.01	u3
	3–4	Rh–Si1	2.47	2.40	–0.07	u0–u3
		Rh–Si2	3.64	3.32	–0.32	u0–u1
		Rh–H1	1.76	1.75	–0.01	u0–u3
		Rh–H5	2.19	1.92	–0.03	u0–u1
		Si1–H1	1.61	1.66	0.05	u0–u3
		Si2–H5	1.51	1.56	0.05	u0–u1
ich1 [c]	4	Rh–Si1	2.82	2.57	–0.25	u0–u3
		Rh–Si2	2.41	2.37	–0.04	u0–u1
		Rh–H1	1.75	1.69	–0.06	u0–u3
		Rh–H5	1.63	1.63	0.00	u0–u1
		Si1–H1	1.57	1.67	0.10	u0–u3
		Si2–H5	1.78	1.90	0.12	u0–u1
	4–5	Rh–Si1	2.75	2.61	–0.14	u0–u3
		Rh–Si2	2.45	2.43	–0.02	u0–u1
		Rh–H1	2.09	1.95	–0.14	u0–u3
		Rh–H5	1.63	1.63	0.00	u0–u1
		Si1–H1	1.52	1.57	0.00	u0–u3
		Si2–H5	1.74	1.80	0.06	u0–u1
	5	Rh–Si1	2.67	2.51	–0.16	u0–u3
		Rh–Si2	2.46	2.44	–0.02	u0–u1
		Rh–H1	1.71	1.66	–0.05	u0–u3
		Rh–H5	1.63	1.63	0.00	u0–u1
		Si1–H1	1.60	1.71	0.11	u0–u3
		Si2–H5	1.72	1.77	0.05	u0–u1
	5–6	Rh–Si1	2.50	2.46	–0.04	u0–u3
		Rh–Si2	2.68	2.57	–0.11	u0–u1
		Rh–H1	1.66	1.65	–0.01	u0–u3
		Rh–H5	2.03	1.89	–0.14	u0–u1
		Si1–H1	1.70	1.77	0.07	u0–u3
		Si2–H5	1.53	1.57	0.04	u0–u1
igt1	6	Rh–Si1	2.52	2.45	–0.07	u0–u3
		Rh–Si2	2.48	2.44	–0.04	u0–u1
		Rh–H1	1.67	1.65	–0.02	u0–u3
		Rh–H5	1.66	1.65	–0.01	u0–u1
		Si1–H1	1.68	1.78	0.10	u0–u3
		Si2–H5	1.68	1.74	0.06	u0–u1
gt1	6–1	Rh–Si1	3.02	3.04	0.02	u0–u3
		Rh–Si2	2.28	2.27	–0.01	u0–u1
		Rh–H1	1.63	1.63	0.00	u0–u3
		Rh–H5	1.63	1.65	0.02	u0–u1
		Si1–H1	2.45	2.53	0.08	u0–u3
		Si2–H5	1.74	1.77	0.03	u0–u1

			Si1–H6	1.69	1.69	0.00	u1–u3
			Si2–H6	1.59	1.62	0.03	u1–u3
CH	ich2[c]	1	Rh–H1	1.65	1.64	–0.01	u0–u1
			Rh–H2	2.98	3.01	0.03	u0–u1
			Si1–H1	1.70	1.76	0.06	u0–u1
			Si1–H2	1.49	1.51	0.02	u0–u1
	ch2[c]	1–2	Rh–H1	2.21	2.05	–0.16	u0–u1
			Rh–H2	2.08	1.92	–0.16	u0–u1
			Si1–H1	1.51	1.54	0.03	u0–u1
			Si1–H2	1.52	1.56	0.04	u0–u1
	imch1	2	Rh–H1	2.98	2.98	0.00	u0–u1
			Rh–H2	1.65	1.69	0.04	u0–u1
			Si1–H1	1.48	1.50	0.02	u0–u1
			Si1–H2	1.60	1.70	0.10	u0–u1
			Rh–Si1	2.62	2.48	–0.14	u0–u1
			Rh–C1	2.24	2.23	–0.01	u0–u2
			Rh–C2	2.28	2.26	–0.02	u0–u2
		2–3	Rh–C1	2.26	2.22	–0.04	u0–u2
			Rh–C2	2.30	2.26	–0.04	u0–u2
			H2–C1	2.43	2.42	–0.01	u1–u2
		3	Rh–C1	2.25	2.21	–0.04	u0–u2
			Rh–C2	2.26	2.22	–0.04	u0–u2
			H2–C1	2.28	2.26	–0.02	u1–u2
		3–4	Rh–C1	2.25	2.23	–0.02	u0–u2
			Rh–C2	2.16	2.15	–0.01	u0–u2
			H2–C1	1.61	1.60	–0.01	u1–u2
		4	Rh–C1	2.41	2.38	–0.03	u0–u2
			Rh–C2	2.08	2.09	0.01	u0–u2
			H2–C1	1.17	1.19	0.02	u1–u2
			Si1–C2	3.39	3.47	0.08	u1–u2
			Rh–Si1	2.31	2.31	0.00	u0–u1
			Rh–C2	2.08	2.09	0.01	u0–u2
		4–5	Si1–C2	2.80	2.79	–0.01	u1–u2
			Rh–Si1	2.32	2.32	0.00	u0–u1
			Rh–C2	2.09	2.10	0.01	u0–u2
	ich3	5	Si1–C2	2.63	2.61	–0.02	u1–u2
			Rh–Si1	2.34	2.34	0.00	u0–u1
			Rh–C2	2.09	2.10	0.01	u0–u2
	ch3	5–6	Si1–C2	2.03	2.01	–0.02	u1–u2
			Rh–Si1	2.68	2.69	0.01	u0–u3
			Rh–C2	2.28	2.26	–0.02	u0–u3
		6	Si1–C2	1.90	1.90	0.00	u3
			Rh–Si1	2.78	2.63	–0.15	u0–u3
			Rh–C2	3.27	3.21	–0.06	u0–u3
			Rh–C1	2.60	2.55	–0.05	u0–u3
		6–7	Rh–C1	3.22	3.13	–0.09	u0–u3
			Rh–C2	2.99	2.90	–0.09	u0–u3
		7	Rh–C1	3.67	3.66	–0.01	u0–u3
			Rh–C2	2.56	2.53	–0.03	u0–u3
			Rh–Si1	2.49	2.43	–0.06	u0–u3

		7–8	Rh–C1	5.00	5.04	0.04	u0–u3
			Rh–C2	3.64	3.72	0.08	u0–u3
			Rh–Si1	2.66	2.51	–0.15	u0–u3
	ch1[c]	9–1[d]	Rh–Si1	3.76	2.97	–0.79	u0–u3
			Rh–Si2	2.40	2.41	0.01	u0–u1
			Rh–H1	2.30	1.90	–0.40	u0–u3
			Rh–H5	1.63	1.62	–0.01	u0–u1
			Si1–H1	1.51	1.57	0.06	u0–u3
			Si2–H5	1.77	1.81	0.04	u0–u3
			Rh–C3	3.46	3.01	–0.45	u0–u2
			Rh–C4	3.28	2.90	–0.38	u0–u2
mCH	mch1	2–3	Rh–C1	2.05	2.05	0.00	u0–u2
			Rh–Si1	2.76	2.88	0.12	u0–u1
			C1–Si1	2.09	2.02	–0.07	u1–u2
		3	Rh–C1	2.12	2.14	0.02	u0–u3
			Rh–Si1	2.84	2.71	–0.13	u0–u3
			C1–Si1	1.88	1.88	0.00	u3
			Rh–H1	1.81	1.76	–0.05	u0–u3
			Si–H1	1.56	1.61	0.05	u0–u3
		3–4	Rh–C1	2.17	2.18	0.01	u0–u3
			Rh–Si1	2.82	2.69	–0.13	u0–u3
			C1–Si1	1.88	1.88	0.00	u3
			Rh–H1	1.81	1.75	–0.06	u0–u3
			Si–H1	1.56	1.61	0.05	u0–u3
SBM		4–5	Rh–Si2	3.90	3.82	–0.08	u0–u1
			Rh–H5	2.46	2.32	–0.14	u0–u1
			Si2–H4	1.50	1.53	0.03	u0–u1
			Rh–C1	2.59	2.52	–0.07	u0–u2
			Rh–H1	2.23	2.11	–0.12	u0–u2
			Rh–C2	2.09	2.10	0.01	u0–u2
	isbm2	5	Rh–Si2	2.47	2.42	–0.05	u0–u1
			Si2–H5	1.78	1.89	0.11	u0–u1
			Rh–H2	1.63	1.63	0.00	u0–u1
			Rh–C1	2.56	2.52	–0.04	u0–u2
			Rh–H1	2.15	2.08	–0.07	u0–u2
			Rh–C2	2.14	2.15	0.01	u0–u2
			Si2–C2	2.72	2.69	–0.03	u1–u2
	sbm2	5–6	Rh–Si2	2.69	2.75	0.06	u0–u1
			Si2–H5	2.32	2.40	0.08	u0–u1
			Rh–H5	1.58	1.59	0.01	u0–u1
			Rh–C1	2.64	2.63	–0.01	u0–u2
			Rh–H1	2.18	2.12	–0.06	u0–u2
			Rh–C2	2.38	2.46	0.08	u0–u2
			Si2–C2	2.09	2.04	–0.05	u1–u2
	isbm3	6	Rh–Si2	2.59	2.48	–0.11	u0–u1
			Si2–H5	1.63	1.73	0.1	u0–u1
			Rh–H5	1.68	1.65	–0.03	u0–u3
			Rh–C1	3.72	3.79	0.07	u0–u3
			Rh–C2	3.35	3.33	–0.02	u0–u3
			Si2–C2	1.90	1.91	0.01	u3

sbm3	6–1	Rh–Si2	2.59	2.48	–0.11	u0–u3
		Si2–H5	1.53	1.56	0.03	u0–u3
		Rh–H5	1.95	1.85	–0.10	u0–u3
		Rh–C3	3.95	3.67	–0.28	u0–u2
		Rh–C4	3.90	3.63	−0.27	u0–u2

[a]Si and C atoms are numbered in the order of bond formation. C1 and C2, C3 and C4 refer to the carbon atoms of the first and second ethylene moieties, respectively. H1−H4 denote hydrogen atoms of the first silane, and H5−H8 those of the second silane.

[b]The reactants Rh(I) *bis*-NHC catalyst, silane, and ethylene, as well as the product ethylsilane are denoted by the labels u0, u1, u2, and u3, respectively, thus indicating inter– (e.g. u0−u1) or intramolecular (e.g. u1) quantities.

[c]ch1 = mch2, and ch2 = mch3 = sbm1.

[d]Repeated IM and TS structures are presented only once. For example, in CH, the omitted IMs and TS 8, 8−9, and 9 were already given for GT, equal to 3, 3−4, and 4 on page 114.

Table A3. Crucial distances d (Å) in the intermediates (IM) and transition states (TM) involved in the selected barriers, calculated by five chosen density functionals. Labels of atoms, molecular units, and IM/TS structures as introduced in Table A2.

	IM/TS	B3LYP	BP86	mPWPW	PBE	PBE0	Type
Rh−Si2	igt1	2.48	2.44	2.43	2.43	2.43	u0−u1
	gt1	2.28	2.27	2.27	2.26	2.25	u0−u1
Si2−H5	igt1	1.68	1.74	1.74	1.74	1.69	u0−u1
	gt1	1.74	1.77	1.77	1.78	1.75	u0−u1
Rh−Si1	igt1	2.52	2.45	2.45	2.43	2.43	u0−u3
	gt1	3.02	3.04	3.04	3.03	2.99	u0−u3
Si1−H1	igt1	1.68	1.78	1.77	1.80	1.75	u0−u3
	gt1	1.69	1.69	1.69	1.69	1.67	u0−u3
Si1−H3	igt2	1.48	1.49	1.49	1.49	1.48	u1
	gt2	1.57	1.58	1.57	1.57	1.56	u1−u2
C1−H3	igt2	3.09	2.89	2.89	2.89	2.88	u1−u2
	gt2	1.70	1.73	1.73	1.74	1.73	u1−u2
C2−Si1	igt2	3.47	3.24	3.24	3.15	3.17	u1−u2
	gt2	2.06	2.07	2.07	2.07	2.06	u1−u2
Rh−Si1	ich1	2.82	2.57	2.56	2.48	2.57	u0−u3
	ch1	3.76	2.97	2.93	2.93	2.94	u0−u3
Rh−H1	ich1	1.75	1.69	1.69	1.70	1.70	u0−u3
	ch1	2.30	1.90	1.89	1.81	1.90	u0−u3
Si1−H1	ich1	1.57	1.67	1.67	1.70	1.64	u0−u3
	ch1	1.51	1.57	1.57	1.61	1.55	u0−u3
Rh−H1	ich2	1.65	1.64	1.65	1.65	1.64	u0−u1
	ch2	2.21	2.05	2.05	2.03	2.05	u0−u1
Rh−H2	ich2	2.98	3.01	3.01	3.01	2.96	u0−u1
	ch2	2.08	1.92	1.92	1.91	1.96	u0−u1
Si1−H1	ich2	1.70	1.76	1.76	1.77	1.73	u0−u1
	ch2	1.51	1.54	1.54	1.55	1.53	u0−u1
Si1−H2	ich2	1.49	1.51	1.51	1.51	1.50	u0−u1
	ch2	1.52	1.56	1.56	1.57	1.54	u0−u1
Rh−Si1	ich3	2.34	2.34	2.34	2.34	2.32	u0−u1
	ch3	2.68	3.19	3.17	2.84	2.71	u0−u1
Rh−C2	ich3	2.09	2.10	2.10	2.10	2.07	u0−u2
	ch3	2.28	2.26	2.61	2.34	2.26	u0−u2
Si1−C2	ich3	2.63	2.61	2.60	2.60	2.53	u1−u2
	ch3	2.03	1.92	1.92	1.97	1.98	u1−u2
Si1−C1	imch1	3.23	3.17	3.11	3.10	3.09	u1−u2
	mch1	2.09	2.02	2.02	2.01	2.01	u1−u2
Rh−Si1	imch1	2.62	2.48	2.48	2.47	2.48	u0–u1
	mch1	2.76	2.88	2.87	2.88	2.83	u0–u1
Rh–C2	imch1	2.28	2.26	2.26	2.25	2.24	u0–u2
	mch1	2.38	2.46	2.45	2.45	2.40	u0–u2
Rh–H2	isbm2	1.63	1.63	1.63	1.63	1.61	u0–u1
	sbm2	1.58	1.59	1.59	1.59	1.58	u0–u1
Si2–H5	isbm2	1.78	1.89	1.88	1.89	1.87	u0–u1
	sbm2	2.32	2.40	2.39	2.41	2.40	u0–u1
Rh–C2	isbm2	2.14	2.15	2.15	2.14	2.12	u0–u2
	sbm2	2.38	2.46	2.46	2.47	2.41	u0–u2

C2–Si2	isbm2	2.72	2.69	2.68	2.67	2.62	u1–u2
	sbm2	2.09	2.04	2.03	2.03	2.02	u1–u2
Rh–Si2	isbm3	2.59	2.48	2.48	2.46	2.52	u0–u1
	sbm3	3.27	2.99	2.87	2.99	3.25	u0–u1
Si2–H5	isbm3	1.63	1.73	1.73	1.74	1.70	u0–u1
	sbm3	1.53	1.56	1.58	1.56	1.53	u0–u1
Rh–C4	isbm3	–	–	–	–	–	–
	sbm3	3.90	3.63	3.65	3.60	3.85	u0–u2
Rh–H5	isbm3	1.68	1.65	1.65	1.65	1.65	u0–u3
	sbm3	1.95	1.85	1.83	1.85	1.95	u0–u3

Table A4. Change $\Delta H_X = H_X - H(B3LYP)$ (kcal·mol^{-1}) in the formation enthalpies of selected intermediates (IM) and the corresponding transition states (TS), relative to the B3LYP results, calculated with 11 functionals.

IM/TS	B3LYP	BP86	BLYP	B3PW91	PBE	PBE0
igt2	−	−6.48	1.92	−4.00	−9.97	−8.84
gt2	−	−15.80	0.12	−10.23	−20.87	−16.67
ich1	−	−12.76	5.01	−10.28	−21.50	−20.74
ch1	−	−10.39	5.00	−7.30	−21.20	−20.32
ich2	−	−10.80	1.73	−13.30	−15.77	−13.82
ch2	−	−10.71	1.76	−6.55	−15.87	−13.40
isbm2	−	−19.82	2.96	−14.17	−29.51	−26.56
sbm2	−	−16.81	3.74	−12.40	−24.08	−23.97

IM/TS	mPWPW	MPW1K	M06−L	M06	MPW3LYP	TPSS
igt2	−6.70	−6.01	−6.51	−9.32	−2.75	−6.42
gt2	−16.36	−10.39	−7.89	−8.91	−3.15	−13.43
ich1	−14.35	−16.47	−12.95	−16.59	−5.20	−11.66
ch1	−12.61	−15.38	−21.68	−24.45	−6.64	−10.65
ich2	−11.57	−15.70	−17.93	−20.38	−9.86	−19.01
ch2	−11.40	−9.12	−13.74	−16.13	−3.76	−12.45
isbm2	−21.73	−18.85	−23.86	−22.07	−6.02	−22.11
sbm2	−18.63	−17.87	−21.13	−20.69	−5.91	−17.66

Table A5. Characteristic bond distances d (Å) of the intermediates (IM) and transition states (TM) involved in the selected barriers, calculated by 12 density functionals. Labels of atoms, molecular units, and IM/TS structures as introduced in Table A2.

	IM/TS	BP86	BLYP	B3LYP	B3PW91	PBE	PBE0	Type
Si1–H3	igt2	1.49	1.49	1.48	1.48	1.49	1.48	u1
	gt2	1.58	1.58	1.57	1.56	1.57	1.56	u1–u2
C1–H3	igt2	2.89	3.15	3.09	2.96	2.89	2.88	u1–u2
	gt2	1.73	1.70	1.70	1.72	1.74	1.73	u1–u2
C2–Si1	igt2	3.24	3.54	3.47	3.32	3.15	3.17	u1–u2
	gt2	2.07	2.07	2.06	2.06	2.07	2.23	u1–u2
Rh–Si1	ich1	2.57	2.85	2.82	2.62	2.48	2.57	u0−u3
	ch1	2.97	3.85	3.76	3.23	2.73	2.94	u0−u3
Rh−H1	ich1	1.69	1.76	1.75	1.70	1.70	1.70	u0−u3
	ch1	1.90	2.36	2.30	2.05	1.81	1.90	u0−u3
Si1–H1	ich1	1.67	1.59	1.57	1.63	1.70	1.64	u0–u3
	ch1	1.57	1.52	1.51	1.53	1.61	1.55	u0–u3
Rh–H1	ich2	1.64	1.66	1.65	1.64	1.65	1.64	u0–u1
	ch2	2.05	2.20	2.21	2.08	2.03	2.05	u0–u1
Rh–H2	ich2	3.01	3.03	2.98	2.98	3.01	2.96	u0–u1
	ch2	1.92	2.07	2.08	1.97	1.91	1.96	u0–u1
Si1–H1	ich2	1.76	1.74	1.70	1.72	1.77	1.73	u0–u1
	ch2	1.54	1.52	1.51	1.52	1.55	1.53	u0–u1
Si1–H2	ich2	1.51	1.51	1.49	1.50	1.51	1.50	u0–u1
	ch2	1.56	1.53	1.52	1.54	1.57	1.54	u0–u1
Rh–H2	isbm2	1.63	1.64	1.63	1.61	1.63	1.61	u0–u1
	sbm2	1.58	1.60	1.58	1.58	1.59	1.58	u0–u1
Si2–H5	isbm2	1.78	1.80	1.78	1.86	1.89	1.87	u0–u1
	sbm2	2.32	2.34	2.32	2.37	2.41	2.40	u0–u1
Rh–C2	isbm2	2.14	2.18	2.14	2.13	2.14	2.12	u0–u2
	sbm2	2.38	2.44	2.38	2.41	2.47	2.41	u0–u2
C2–Si2	isbm2	2.72	2.78	2.72	2.64	2.67	2.62	u1–u2
	sbm2	2.09	2.11	2.09	2.03	2.03	2.02	u1–u2

	IM/TS	mPWPW	MPW1K	M06-L	M06	MPW3LYP	TPSS	Type
Si1–H3	igt2	1.49	1.47	1.48	1.47	1.48	1.48	u1
	gt2	1.57	1.55	1.55	1.56	1.57	1.57	u1–u2
C1–H3	igt2	2.89	2.91	2.91	2.87	3.03	2.88	u1–u2
	gt2	1.73	1.71	1.69	1.68	1.70	1.69	u1–u2
C2–Si1	igt2	3.24	3.23	3.21	3.28	3.41	3.17	u1–u2
	gt2	2.07	2.05	2.03	2.04	2.06	2.06	u1–u2
Rh–Si1	ich1	2.93	2.64	2.65	2.76	2.80	2.52	u0–u3
	ch1	2.93	3.10	3.27	3.17	3.57	2.99	u0–u3
Rh–H1	ich1	1.69	1.71	1.79	1.78	1.75	1.73	u0–u3
	ch1	1.89	2.01	2.15	2.08	2.18	1.93	u0–u3
Si1–H1	ich1	1.67	1.60	1.59	1.57	1.58	1.65	u0–u3
	ch1	1.57	1.52	1.51	1.52	1.51	1.55	u0–u3
Rh–H1	ich2	1.65	1.64	1.68	1.70	1.65	1.65	u0–u1
	ch2	2.05	2.10	2.23	2.20	2.19	2.07	u0–u1

Rh–H2	ich2	3.01	2.92	2.93	2.89	2.97	2.99	u0–u1
	ch2	1.92	2.00	2.11	2.09	2.07	1.97	u0–u1
Si1–H1	ich2	1.76	1.68	1.68	1.65	1.69	1.74	u0–u1
	ch2	1.54	1.51	1.50	1.51	1.51	1.52	u0–u1
Si1–H2	ich2	1.51	1.49	1.49	1.49	1.49	1.50	u0–u1
	ch2	1.56	1.52	1.51	1.52	1.51	1.54	u0–u1
Rh–H2	isbm2	1.63	1.60	1.65	1.65	1.63	1.63	u0–u1
	sbm2	1.59	1.57	1.60	1.60	1.58	1.60	u0–u1
Si2–H5	isbm2	1.88	1.84	1.82	1.83	1.79	1.88	u0–u1
	sbm2	2.39	2.35	2.38	2.47	2.32	2.42	u0–u1
Rh–C2	isbm2	2.15	2.10	2.13	2.13	2.14	2.14	u0–u2
	sbm2	2.46	2.36	2.43	2.41	2.38	2.46	u0–u2
C2–Si2	isbm2	2.68	2.59	2.66	2.69	2.70	2.66	u1–u2
	sbm2	2.03	2.02	2.02	2.02	2.08	2.02	u1–u2

Complete References 211 and 236

(211) M. J. Frisch, G. W. Trucks, H. B. Schlegel, G. E. Scuseria, M. A. Robb, J. R. Cheeseman, J. A. Montgomery, Jr., T. Vreven, K. N. Kudin, J. C. Burant, J. M. Millam, S. S. Iyengar, J. Tomasi, V. Barone, B. Mennucci, M. Cossi, G. Scalmani, N. Rega, G. A. Petersson, H. Nakatsuji, M. Hada, M. Ehara, K. Toyota, R. Fukuda, J. Hasegawa, M. Ishida, T. Nakajima, Y. Honda, O. Kitao, H. Nakai, M. Klene, X. Li, J. E. Knox, H. P. Hratchian, J. B. Cross, V. Bakken, C. Adamo, J. Jaramillo, R. Gomperts, R. E. Stratmann, O. Yazyev, A. J. Austin, R. Cammi, C. Pomelli, J. W. Ochterski, P. Y. Ayala, K. Morokuma, G. A. Voth, P. Salvador, J. J. Dannenberg, V. G. Zakrzewski, S. Dapprich, A. D. Daniels, M. C. Strain, O. Farkas, D. K. Malick, A. D. Rabuck, K. Raghavachari, J. B. Foresman, J. V. Ortiz, Q. Cui, A. G. Baboul, S. Clifford, J. Cioslowski, B. B. Stefanov, G. Liu, A. Liashenko, P. Piskorz, I. Komaromi, R. L. Martin, D. J. Fox, T. Keith, M. A. Al-Laham, C. Y. Peng, A. Nanayakkara, M. Challacombe, P. M. W. Gill, B. Johnson, W. Chen, M. W. Wong, C. Gonzalez, and J. A. Pople, Gaussian, Inc., Wallingford CT, 2004.

(236) M. J. Frisch, G. W. Trucks, H. B. Schlegel, G. E. Scuseria, M. A. Robb, J. R. Cheeseman, G. Scalmani, V. Barone, B. Mennucci, G. A. Petersson, H. Nakatsuji, M. Caricato, X. Li, H. P. Hratchian, A. F. Izmaylov, J. Bloino, G. Zheng, J. L. Sonnenberg, M. Hada, M. Ehara, K. Toyota, R. Fukuda, J. Hasegawa, M. Ishida, T. Nakajima, Y. Honda, O. Kitao, H. Nakai, T. Vreven, J. A. Montgomery, Jr., J. E. Peralta, F. Ogliaro, M. Bearpark, J. J. Heyd, E. Brothers, K. N. Kudin, V. N. Staroverov, T. Keith, R. Kobayashi, J. Normand, K. Raghavachari, A. Rendell, J. C. Burant, S. S. Iyengar, J. Tomasi, M. Cossi, N. Rega, J. M. Millam, M. Klene, J. E. Knox, J. B. Cross, V. Bakken, C. Adamo, J. Jaramillo, R. Gomperts, R. E. Stratmann, O. Yazyev, A. J. Austin, R. Cammi, C. Pomelli, J. W. Ochterski, R. L. Martin, K. Morokuma, V. G. Zakrzewski, G. A. Voth, P. Salvador, J. J. Dannenberg, S. Dapprich, A. D. Daniels, O. Farkas, J. B. Foresman, J. V. Ortiz, J. Cioslowski, and D. J. Fox, Gaussian, Inc., Wallingford CT, 2010.

10 References

(1) *Hydrosilylation: A Comprehensive Review on Recent Advances*; Marciniec, B., Ed.; Springer: Milton Keynes, 2009; Vol. 1.

(2) Auner, N.; Weis, J. In *Organosilicon Chemistry I: From Molecules to Materials*; Wiley: 2011, p 253.

(3) Craig, P. J. In *Organometallic Compounds in the Environment*; Wiley: 2003, p 305.

(4) Bains, W.; Tacke, R. *Curr. Opin. Drug. Discov. Devel.* **2003**, *6*, 526.

(5) Heying, M. D.; Moline, P. K.; Watson, M. J.; Lutz, M. A.; Dow Corning Corp.

(6) Grisworld, R. M.; General Electric Co Ltd.

(7) Sato, S.; Shinetsu Chem Ind Co Ltd; Nikkiso Co Ltd.

(8) Igarashi, M.; Nakamura, T.; Ito, A.; Furihata, T.; Kim, H.; Kim, H. B.; Ikarashi, M.; Kutahata, C.; Shinetsu Chem Ind Co Ltd.

(9) Irifune, S.; Shinetsu Chem Ind Co Ltd.

(10) Geisberger, G.; Lautenschlager, H.; Gesbegel, G.; Wacker Chem AG; Wacker Chem GmbH.

(11) Xiang, Y.; Fu, C.; Breiding, T.; Sasmal, P. K.; Liu, H.; Shen, Q.; Harms, K.; Zhang, L.; Meggers, E. *Chem. Commun.* **2012**, *48*, 7131.

(12) Karamouzi, S.; Maniadaki, A.; Nasiopoulou, D. A.; Kotali, E.; Kotali, A.; Harris, P. A.; Raftery, J.; Joule, J. A. *Synth.-Stuttgart* **2013**, *45*, 2150.

(13) Hoffmann, R. W. In *Elements of Synthesis Planning*; Springer: 2009, p 121.

(14) Marciniec, B. *Silicon Chem.* **2002**, *1*, 155.

(15) Marciniec, B. *Coord. Chem. Rev.* **2005**, *249*, 2374.

(16) Cesar, V.; Bellemin-Laponnaz, S.; Gade, L. H. *Chem. Soc. Rev.* **2004**, *33*, 619.

(17) Gade, L. H.; Cesar, V.; Bellemin-Laponnaz, S. *Angew. Chem., Int. Ed.* **2004**, *43*, 1014.

(18) Trost, B. M.; Ball, Z. T. *J. Am. Chem. Soc.* **2001**, *123*, 12726.

(19) Trost, B. M.; Ball, Z. T. *J. Am. Chem. Soc.* **2003**, *125*, 30.

(20) Trost, B. M.; Ball, Z. T. *J. Am. Chem. Soc.* **2005**, *127*, 17644.

(21) Glaser, P. B.; Tilley, T. D. *J. Am. Chem. Soc.* **2003**, *125*, 13640.

(22) Tuttle, T.; Wang, D.; Thiel, W. *Organometallics* **2006**, *25*, 4504.

(23) Tuttle, T.; Wang, D.; Thiel, W.; Köhler, J.; Hofmann, M.; Weis, J. *J. Organomet. Chem.* **2007**, *692*, 2282.

(24) Tuttle, T.; Wang, D.; Thiel, W.; Köhler, J.; Hofmann, M.; Weis, J. *Dalton Trans.* **2009**, 5894.

(25) van Leeuwen, P. W. N. M. In *Homogeneous Catalysis: Understanding the Art*; Kluwer Academic Publishers: 2006.

(26) Maseras, F.; Lledós, A. In *Computational Modeling of Homogeneous Catalysis*; Springer: 2002.

(27) Gigler, P.; Bechlars, B.; Herrmann, W. A.; Kühn, F. E. *J. Am. Chem. Soc.* **2011**, *133*, 1589.

(28) Jimenez, M. V.; Perez-Torrente, J. J.; Bartolome, M. I.; Gierz, V.; Lahoz, F. J.; Oro, L. A. *Organometallics* **2008**, *27*, 224.

(29) Busetto, L.; Cassani, M. C.; Femoni, C.; Mancinelli, M.; Mazzanti, A.; Mazzoni, R.; Solinas, G. *Organometallics* **2011**, *30*, 5258.

(30) Nolan, S. P. In *N-Heterocyclic Carbenes in Synthesis*; Wiley: 2006, p 185.

(31) Steinbeck, M.; Frey, G. D.; Schoeller, W. W.; Herrmann, W. A. *J. Organomet. Chem.* **2011**, *696*, 3945.
(32) Truscott, B. J.; Slawin, A. M. Z.; Nolan, S. P. *Dalton Trans.* **2013**, *42*, 270.
(33) Speier, J. L.; Webster, J. A.; Barnes, G. H. *J. Am. Chem. Soc.* **1957**, *79*, 974.
(34) Karstedt, B. D.; Offen.: Ger., 1970; Vol. DE 1941411.
(35) Karstedt, B. D.; Offen.: Ger., 1973; Vol. DE 2307085.
(36) Marko, I. E.; Sterin, S.; Buisine, O.; Berthon, G.; Michaud, G.; Tinant, B.; Declercq, J. P. *Adv. Synth. Catal.* **2004**, *346*, 1429.
(37) Beddie, C.; Hall, M. B. *J. Am. Chem. Soc.* **2004**, *126*, 13564.
(38) Chalk, A. J.; Harrod, J. F. *J. Am. Chem. Soc.* **1965**, *87*, 16.
(39) Schroeder, M. A.; Wrighton, M. S. *J. Org. Chem.* **1977**, *128*, 345.
(40) Onopchenko, A.; Sabourin, E. T.; Beach, D. L. *J. Org. Chem.* **1983**, *48*, 5101.
(41) Ojima, I.; Fuchikami, T.; Yatabe, M. *J. Org. Chem.* **1984**, *260*, 335.
(42) Fernandez, M. J.; Esteruelas, M. A.; Jimenez, M. S.; Oro, L. A. *Organometallics* **1986**, *5*, 1519.
(43) Randolph, C. L.; Wrighton, M. S. *J. Am. Chem. Soc.* **1986**, *108*, 3366.
(44) Seitz, F.; Wrighton, M. S. *Angew. Chem., Int. Ed.* **1988**, *27*, 289.
(45) Crabtree, R. H. *Chem. Rev.* **1995**, *95*, 987.
(46) Arndtsen, B. A.; Bergman, R. G.; Mobley, T. A.; Peterson, T. H. *Acc. Chem. Res.* **1995**, *28*, 154.
(47) Wu, Y. Diploma thesis, Technische Universität München, 2010.
(48) Marciniec, B.; Gulinski, J. *J. Organomet. Chem.* **1993**, *446*, 15.
(49) *Modern Synthetic and Application Aspects of Polysilanes: An Underestimated Class of Materials*; Aziz M. Muzafarov ed.; A. Feigl, A. B., J. Weis, and B. Rieger, Ed.; Springer, 2010.
(50) Hirao, T.; Fujii, T.; Ohshiro, Y. *Tetrahedron* **1994**, *50*, 10207.
(51) Ho, T. L.; Jana, G. H. *J. Chin. Chem. Soc.* **1999**, *46*, 639.
(52) Takahashi, K.; Minami, T.; Ohara, Y.; Hiyama, T. *Tetrahedron Lett.* **1993**, *34*, 8263.
(53) Effenberger, F.; Krebs, A. *J. Org. Chem.* **1984**, *49*, 4687.
(54) Giraud, A.; Provot, O.; Harnze, A.; Brion, J.-D.; Alami, M. *Tetrahedron Lett.* **2008**, *49*, 1107.
(55) Jeges, G.; Skoda-Foldes, R.; Kollar, L.; Pinter, Z.; Horvath, J.; Tuba, Z. *J. Mol. Catal. A: Chem.* **2001**, *165*, 89.
(56) Murai, S.; Chatani, N. *Journal of Synthetic Organic Chemistry Japan* **1993**, *51*, 421.
(57) Sommer, L. H.; Pietrusza, E. W.; Whitmore, F. C. *J. Am. Chem. Soc.* **1947**, *69*, 188.
(58) Sommer, L. H.; Goldberg, G. M.; Gold, J.; Whitmore, F. C. *J. Am. Chem. Soc.* **1947**, *69*, 980.
(59) Fujiki, M.; Mori, T.; Univ Nara.
(60) Brenner, M.; Carreira, E. M.; Chinkov, N.; Lorenzi, M.; Warm, A.; Zimmermann, L.; Lonza Ltd.
(61) Ojima, I.; Nihonyan.M; Nagai, Y. *J. Chem. Soc., Chem. Commun.* **1972**, 938.
(62) Ojima, I.; Kogure, T. *Chem. Lett.* **1973**, 541.
(63) Zheng, G. Z.; Chan, T. H. *Organometallics* **1995**, *14*, 70.
(64) Eisenstein, O.; Hoffmann, R. *J. Am. Chem. Soc.* **1981**, *103*, 4308.
(65) Schneider, N.; Finger, M.; Haferkemper, C.; Bellemin-Laponnaz, S.; Hofmann, P.; Gade, L. H. *Chem.-Eur. J.* **2009**, *15*, 11515.

(66) Schneider, N.; Finger, M.; Haferkemper, C.; Bellemin-Laponnaz, S.; Hofmann, P.; Gade, L. H. *Angew. Chem., Int. Ed.* **2009**, *48*, 1609.

(67) Maruyama, Y.; Yamamura, K.; Nakayama, I.; Yoshiuchi, K.; Ozawa, F. *J. Am. Chem. Soc.* **1998**, *120*, 1421.

(68) Shearer, G.; Tzoganakis, C. *J. Appl. Polym. Sci.* **1997**, *65*, 439.

(69) Song, Y. S.; Yoo, B. R.; Lee, G. H.; Jung, I. N. *Organometallics* **1999**, *18*, 3109.

(70) Sudo, T.; Asao, N.; Gevorgyan, V.; Yamamoto, Y. *J. Org. Chem.* **1999**, *64*, 2494.

(71) Fuchter, M. J. *Chem.-Eur. J.* **2010**, *16*, 12286.

(72) Schwieger, S.; Herzog, R.; Wagner, C.; Steinborn, D. *J. Organomet. Chem.* **2009**, *694*, 3548.

(73) Taige, M. A.; Ahrens, S.; Strassner, T. *J. Organomet. Chem.* **2011**, *696*, 2918.

(74) Peng, J. J.; Bai, Y.; Li, J. Y.; Lai, G. Q. *Curr. Org. Chem.* **2011**, *15*, 2802.

(75) Kesti, M. R.; Waymouth, R. M. *Organometallics* **1992**, *11*, 1095.

(76) Brookhart, M.; Grant, B. E. *J. Am. Chem. Soc.* **1993**, *115*, 2151.

(77) LaPointe, A. M.; Rix, F. C.; Brookhart, M. *J. Am. Chem. Soc.* **1997**, *119*, 906.

(78) Bart, S. C.; Lobkovsky, E.; Chirik, P. J. *J. Am. Chem. Soc.* **2004**, *126*, 13794.

(79) Tondreau, A. M.; Lobkovsky, E.; Chirik, P. J. *Org. Lett.* **2008**, *10*, 2789.

(80) Kandepi, V.; Cardoso, J. M. S.; Peris, E.; Royo, B. *Organometallics* **2010**, *29*, 2777.

(81) Kakiuchi, F.; Nogami, K.; Chatani, N.; Seki, Y.; Murai, S. *Organometallics* **1993**, *12*, 4748.

(82) Sakaki, S.; Sumimoto, M.; Fukuhara, M.; Sugimoto, M.; Fujimoto, H.; Matsuzaki, S. *Organometallics* **2002**, *21*, 3788.

(83) Wechsler, D.; Myers, A.; McDonald, R.; Ferguson, M. J.; Stradiotto, M. *Inorg. Chem.* **2006**, *45*, 4562.

(84) Cipot, J.; McDonald, R.; Ferguson, M. J.; Schatte, G.; Stradiotto, M. *Organometallics* **2007**, *26*, 594.

(85) Hesp, K. D.; Wechsler, D.; Cipot, J.; Myers, A.; McDonald, R.; Ferguson, M. J.; Schatte, G.; Stradiotto, M. *Organometallics* **2007**, *26*, 5430.

(86) Fu, P. F.; Brard, L.; Li, Y. W.; Marks, T. J. *J. Am. Chem. Soc.* **1995**, *117*, 7157.

(87) Roy, A. K. In *Advances in Organometallic Chemistry Vol 55*; West, R., Hill, A. F., Fink, M. J., Eds.; Elsevier Academic Press Inc: San Diego, 2008; Vol. 55, p 1.

(88) Riant, O.; Mostefai, N.; Courmarcel, J. *Synth.-Stuttgart* **2004**, 2943.

(89) Osborn, J. A.; Wilkinson, G. *Inorg. Synth.* **1990**, *28*, 77.

(90) Gustafsson, M.; Frejd, T. *J. Organomet. Chem.* **2004**, *689*, 438.

(91) Li, J. Y.; Peng, J. J.; Li, X. N.; Ma, L.; Bai, Y.; Zhang, G. D.; Lai, G. Q. *Chin. J. Org. Chem.* **2010**, *30*, 1468.

(92) Normand, A. T.; Cavell, K. J. *Eur. J. Inorg. Chem.* **2008**, 2781.

(93) Wu, Y.; Karttunen, V. A.; Parker, S.; Genest, A.; Rösch, N. *Organometallics* **2013**, *32*, 2363.

(94) Corey, J. Y. *Chem. Rev.* **2011**, *111*, 863.

(95) Duckett, S. B.; Perutz, R. N. *Organometallics* **1992**, *11*, 90.

(96) Brinkman, K. C.; Blakeney, A. J.; Kroneschmidt, W.; Gladysz, J. A. *Organometallics* **1984**, *3*, 1325.

(97) Reichel, C. L.; Wrighton, M. S. *Inorg. Chem.* **1980**, *19*, 3858.

(98) Millan, A.; Fernandez, M. J.; Bentz, P.; Maitlis, P. M. *J. Mol. Catal.* **1984**, *26*, 89.

(99) Watson, P. L.; Parshall, G. W. *Acc. Chem. Res.* **1985**, *18*, 51.
(100) Woo, H. G.; Tilley, T. D. *J. Am. Chem. Soc.* **1989**, *111*, 3757.
(101) Corey, J. Y.; Zhu, X. H. *Organometallics* **1992**, *11*, 672.
(102) Gountchev, T. I.; Tilley, T. D. *Organometallics* **1999**, *18*, 5661.
(103) Ryan, J. W.; Speier, J. L. *J. Am. Chem. Soc.* **1964**, *86*, 895.
(104) Bergens, S. H.; Noheda, P.; Whelan, J.; Bosnich, B. *J. Am. Chem. Soc.* **1992**, *114*, 2121.
(105) Corey, J. Y.; Braddock-Wilking, J. *Chem. Rev.* **1999**, *99*, 175.
(106) Lachaize, S.; Sabo-Etienne, S. *Eur. J. Inorg. Chem.* **2006**, 2115.
(107) Nikonov, G. I. *J. Organomet. Chem.* **2001**, *635*, 24.
(108) Schöllkopf, U. *Angew. Chem.* **1965**, *77*, 819.
(109) Fischer, E. O.; Maasbol, A. *Angew. Chem., Int. Ed.* **1964**, *3*, 580.
(110) Feldman, J.; Schrock, R. R. *Prog. Inorg. Chem.* **1991**, *39*, 1.
(111) Tebbe, F. N.; Parshall, G. W.; Reddy, G. S. *J. Am. Chem. Soc.* **1978**, *100*, 3611.
(112) Dötz, K. H. *Angew. Chem., Int. Ed.* **1975**, *14*, 644.
(113) Dötz, K. H.; Dietz, R.; von Imhof, A.; Lorenz, H.; Huttner, G. *Chem. Ber.* **1976**, *109*, 2033.
(114) Grubbs, R. H. *Handbook of metathesis: Applications in organic synthesis*; Wiley-VCH, 2003.
(115) Grubbs, R. H.; Trnka, T. M. In *Ruthenium in Organic Synthesis*; Wiley-VCH Verlag GmbH & Co. KGaA: 2005, p 153.
(116) Wanzlick, H. W.; J., S. H. *Angew. Chem., Int. Ed.* **1968**, *7*, 141.
(117) Öfele, K. *J. Organomet. Chem.* **1968**, *12*, 42.
(118) Cardin, D. J.; Cetinkay.B; Lappert, M. F. *Chem. Rev.* **1972**, *72*, 545.
(119) Cardin, D. J.; Cetinkay.B; Lappert, M. F.; Manojlov.L; Muir, K. W. *J. Chem. Soc. D - Chem. Commun.* **1971**, 400.
(120) Arduengo, A. J.; Harlow, R. L.; Kline, M. *J. Am. Chem. Soc.* **1991**, *113*, 361.
(121) Lachmann, B.; Steinmau.H; Wanzlick, H. W. *Tetrahedron* **1971**, *27*, 4085.
(122) Albert, A. *Chemie der Heterocyclen*; Verlag Chemie, 1962.
(123) Herrmann, W. A. *Angew. Chem., Int. Ed.* **2002**, *41*, 1290.
(124) Huang, J. K.; Schanz, H. J.; Stevens, E. D.; Nolan, S. P. *Organometallics* **1999**, *18*, 2370.
(125) Tafipolsky, M.; Scherer, W.; Ofele, K.; Artus, G.; Pedersen, B.; Herrmann, W. A.; McGrady, G. S. *J. Am. Chem. Soc.* **2002**, *124*, 5865.
(126) Herrmann, W. A.; Elison, M.; Fischer, J.; Kocher, C.; Artus, G. R. J. *Angew. Chem., Int. Ed.* **1995**, *34*, 2371.
(127) Gstottmayr, C. W. K.; Bohm, V. P. W.; Herdtweck, E.; Grosche, M.; Herrmann, W. A. *Angew. Chem., Int. Ed.* **2002**, *41*, 1363.
(128) Huang, J.; Grasa, G.; Nolan, S. P. *Org. Lett.* **1999**, *1*, 1307.
(129) Stauffer, S. R.; Lee, S. W.; Stambuli, J. P.; Hauck, S. I.; Hartwig, J. F. *Org. Lett.* **2000**, *2*, 1423.
(130) Cheng, J.; Trudell, M. L. *Org. Lett.* **2001**, *3*, 1371.
(131) Weskamp, T.; Schattenmann, W. C.; Spiegler, M.; Herrmann, W. A. *Angew. Chem., Int. Ed.* **1998**, *37*, 2490.
(132) Weskamp, T.; Kohl, F. J.; Herrmann, W. A. *J. Organomet. Chem.* **1999**, *582*, 362.
(133) Weskamp, T.; Bohm, V. P. W.; Herrmann, W. A. *J. Organomet. Chem.* **2000**, *600*, 12.

(134) Caddick, S.; Cloke, F. G. N.; Clentsmith, G. K. B.; Hitchcock, P. B.; McKerrecher, D.; Titcomb, L. R.; Williams, M. R. V. *J. Organomet. Chem.* **2001**, *617*, 635.
(135) Gardiner, M. G.; Herrmann, W. A.; Reisinger, C. P.; Schwarz, J.; Spiegler, M. *J. Organomet. Chem.* **1999**, *572*, 239.
(136) Bohm, V. P. W.; Weskamp, T.; Gstottmayr, C. W. K.; Herrmann, W. A. *Angew. Chem., Int. Ed.* **2000**, *39*, 1602.
(137) Grasa, G. A.; Nolan, S. P. *Org. Lett.* **2000**, *3*, 119.
(138) Lee, H. M.; Smith, D. C.; He, Z.; Stevens, E. D.; Yi, C. S.; Nolan, S. P. *Organometallics* **2001**, *20*, 794.
(139) Chen, A. C.; Ren, L.; Decken, A.; Crudden, C. M. *Organometallics* **2000**, *19*, 3459.
(140) Schramm, M. P.; Reddy, D. S.; Kozmin, S. A. *Angew. Chem., Int. Ed.* **2001**, *40*, 4274.
(141) Cetinkaya, B.; Özdemir, I.; Dixneuf, P. H. *J. Organomet. Chem.* **1997**, *534*, 153.
(142) Furstner, A.; Krause, H. *Adv. Synth. Catal.* **2001**, *343*, 343.
(143) Desmarets, C.; Kuhl, S.; Schneider, R.; Fort, Y. *Organometallics* **2002**, *21*, 1554.
(144) Louie, J.; Grubbs, R. H. *Chem. Commun.* **2000**, 1479.
(145) Enders, D.; Gielen, H. *J. Organomet. Chem.* **2001**, *617*, 70.
(146) Crabtree, R. H. *J. Organomet. Chem.* **2005**, *690*, 5451.
(147) Perrin, L.; Clot, E.; Eisenstein, O.; Loch, J.; Crabtree, R. H. *Inorg. Chem.* **2001**, *40*, 5806.
(148) Kühl, O. *Chem. Soc. Rev.* **2007**, *36*, 592.
(149) Spencer, L. P.; Fryzuk, M. D. *J. Organomet. Chem.* **2005**, *690*, 5788.
(150) Steiner, G.; Kopacka, H.; Ongania, K. H.; Wurst, K.; Preishuber-Pflugl, P.; Bildstein, B. *Eur. J. Inorg. Chem.* **2005**, *7*, 1325.
(151) Shi, M.; Qian, H. X. *Appl. Organomet. Chem.* **2005**, *19*, 1083.
(152) Perry, M. C.; Burgess, K. *Tetrahedron: Asymm.* **2003**, *14*, 951.
(153) Cioslowski, J. *Int. J. Quantum Chem.* **1993**, 309.
(154) Cioslowski, J. *Int. J. Quantum Chem.* **1990**, 15.
(155) Cioslowski, J.; Mixon, S. T. *J. Am. Chem. Soc.* **1991**, *113*, 4142.
(156) Heinemann, C.; Müller, T.; Apeloig, Y.; Schwarz, H. *J. Am. Chem. Soc.* **1996**, *118*, 2023.
(157) Heinemann, C.; Thiel, W. *Chem. Phys. Lett.* **1994**, *217*, 11.
(158) Bader, R. F. W. *Atoms in Molecules: A Quantum Theory*; Oxford University Press, Incorporated, 1994.
(159) Fernandez, I.; Dyker, C. A.; DeHope, A.; Donnadieu, B.; Frenking, G.; Bertrand, G. *J. Am. Chem. Soc.* **2009**, *131*, 11875.
(160) Bourissou, D.; Guerret, O.; Gabbai, F. P.; Bertrand, G. *Chem. Rev.* **2000**, *100*, 39.
(161) Hahn, F. E. *Angew. Chem., Int. Ed.* **2006**, *45*, 1348.
(162) Tonner, R.; Frenking, G. *Angew. Chem., Int. Ed.* **2007**, *46*, 8695.
(163) Tonner, R.; Frenking, G. *Chem.-Eur. J.* **2008**, *14*, 3260.
(164) Hückel, E. *Z. Phys.* **1931**, *70*, 204.
(165) Streitwieser, A. *Molecular Orbital Theory for Organic Chemists*; John Wiley & Sons, 1967.
(166) Sauers, R. R. *Tetrahedron Lett.* **1996**, *37*, 149.
(167) Hückel, E. *Z. Elektrochem. Angew. Phys. Chem.* **1937**, *43*, 752.
(168) Hess, B. A.; Schaad, L. J. *J. Am. Chem. Soc.* **1971**, *93*, 305.

(169) Gutman, I.; Milun, M.; Trinajstic, N. *J. Am. Chem. Soc.* **1977**, *99*, 1692.
(170) Aihara, J. *J. Am. Chem. Soc.* **1976**, *98*, 2750.
(171) Zhou, Z. X.; Parr, R. G.; Garst, J. F. *Tetrahedron Lett.* **1988**, *29*, 4843.
(172) Schleyer, P. v. R.; Maerker, C.; Dransfeld, A.; Jiao, H. J.; Hommes, N. *J. Am. Chem. Soc.* **1996**, *118*, 6317.
(173) Grimme, S. *J. Am. Chem. Soc.* **1996**, *118*, 1529.
(174) Giambiagi, M.; de Giambiagi, M. S.; Silva, C. D. D.; de Figueiredo, A. P. *Phys. Chem. Chem. Phys.* **2000**, *2*, 3381.
(175) Herges, R.; Geuenich, D. *J. Phys. Chem. A* **2001**, *105*, 3214.
(176) Poater, J.; Fradera, X.; Duran, M.; Sola, M. *Chem.-Eur. J.* **2003**, *9*, 400.
(177) Matito, E.; Duran, M.; Sola, M. *Journal of Chemical Physics* **2005**, *122*.
(178) Viciu, M. S.; Navarro, O.; Germaneau, R. F.; Kelly, R. A.; Sommer, W.; Marion, N.; Stevens, E. D.; Cavallo, L.; Nolan, S. P. *Organometallics* **2004**, *23*, 1629.
(179) Diez-Gonzalez, S.; Nolan, S. P. *Coord. Chem. Rev.* **2007**, *251*, 874.
(180) Tolman, C. A. *Chem. Rev.* **1977**, *77*, 313.
(181) Dorta, R.; Stevens, E. D.; Scott, N. M.; Costabile, C.; Cavallo, L.; Hoff, C. D.; Nolan, S. P. *J. Am. Chem. Soc.* **2005**, *127*, 2485.
(182) Crudden, C. M.; Allen, D. P. *Coord. Chem. Rev.* **2004**, *248*, 2247.
(183) Danopoulos, A. A.; Tsoureas, N.; Green, J. C.; Hursthouse, M. B. *Chem. Commun.* **2003**, 756.
(184) Nielsen, D. J.; Magill, A. M.; Yates, B. F.; Cavell, K. J.; Skelton, B. W.; White, A. H. *Chem. Commun.* **2002**, 2500.
(185) Nielsen, D. J.; Cavell, K. J.; Skelton, B. W.; White, A. H. *Inorg. Chim. Acta* **2002**, *327*, 116.
(186) Denk, M. K.; Rodezno, J. M.; Gupta, S.; Lough, A. J. *J. Organomet. Chem.* **2001**, *617*, 242.
(187) Nielsen, D. J.; Cavell, K. J.; Skelton, B. W.; White, A. H. *Inorg. Chim. Acta* **2003**, *352*, 143.
(188) Titcomb, L. R.; Caddick, S.; Cloke, F. G. N.; Wilson, D. J.; McKerrecher, D. *Chem. Commun.* **2001**, 1388.
(189) Jacobsen, H.; Correa, A.; Poater, A.; Costabile, C.; Cavallo, L. *Coord. Chem. Rev.* **2009**, *253*, 687.
(190) Hillier, A. C.; Sommer, W. J.; Yong, B. S.; Petersen, J. L.; Cavallo, L.; Nolan, S. P. *Organometallics* **2003**, *22*, 4322.
(191) Lord, R. L.; Wang, H.; Vieweger, M.; Baik, M.-H. *J. Organomet. Chem.* **2006**, *691*, 5505.
(192) Winkelmann, O. H.; Riekstins, A.; Nolan, S. P.; Navarro, O. *Organometallics* **2009**, *28*, 5809.
(193) Fu, C.-F.; Lee, C.-C.; Liu, Y.-H.; Peng, S.-M.; Warsink, S.; Elsevier, C. J.; Chen, J.-T.; Liu, S.-T. *Inorg. Chem.* **2010**, *49*, 3011.
(194) Boehme, C.; Frenking, G. *Organometallics* **1998**, *17*, 5801.
(195) Tonner, R.; Heydenrych, G.; Frenking, G. *Chem-Asian J.* **2007**, *2*, 1555.
(196) Frenking, G.; Sola, M.; Vyboishchikov, S. F. *J. Organomet. Chem.* **2005**, *690*, 6178.
(197) Antonova, N. S.; Carbo, J. J.; Poblet, J. M. *Dalton Trans.* **2011**, *40*, 2975.
(198) Penka, E. F.; Schlaepfer, C. W.; Atanasov, M.; Albrecht, M.; Daul, C. *J. Organomet. Chem.* **2007**, *692*, 5709.
(199) Arnold, P. L.; Pearson, S. *Coord. Chem. Rev.* **2007**, *251*, 596.
(200) Praetorius, J. M.; Crudden, C. M. *Dalton Trans.* **2008**, 4079.
(201) Normand, A. T.; Nechaev, M. S.; Cavell, K. J. *Chem.-Eur. J.* **2009**, *15*, 7063.

(202) Binobaid, A.; Iglesias, M.; Beetstra, D.; Dervisi, A.; Fallis, I.; Cavell, K. J. *Eur. J. Inorg. Chem.* **2010**, 5426.

(203) Ashley, J. M.; Farnaby, J. H.; Hazari, N.; Kim, K. E.; Luzik, E. D., Jr.; Meehan, R. E.; Meyer, E. B.; Schley, N. D.; Schmeier, T. J.; Tailor, A. N. *Inorg. Chim. Acta* **2012**, *380*, 399.

(204) Poyatos, M.; McNamara, W.; Incarvito, C.; Clot, E.; Peris, E.; Crabtree, R. H. *Organometallics* **2008**, *27*, 2128.

(205) Chianese, A. R.; Crabtree, R. H. *Organometallics* **2005**, *24*, 4432.

(206) Wolf, J.; Labande, A.; Daran, J.-C.; Poli, R. *Eur. J. Inorg. Chem.* **2007**, 5069.

(207) Liu, L.-j.; Wang, F.; Shi, M. *Organometallics* **2009**, *28*, 4416.

(208) Faller, J. W.; Fontaine, P. P. *Organometallics* **2006**, *25*, 5887.

(209) Burling, S.; Field, L. D.; Li, H. L.; Messerle, B. A.; Turner, P. *Eur. J. Inorg. Chem.* **2003**, 3179.

(210) Grasa, G. A.; Guveli, T.; Singh, R.; Nolan, S. P. *J. Org. Chem.* **2003**, *68*, 2812.

(211) Frisch, M. J. T., G. W.; Schlegel, H. B.; et al. Gaussian03; revision B.4; Gaussian, I., Pittsburgh, PA, 2003; see Appendix.

(212) Becke, A. D. *Phys. Rev. A* **1988**, *38*, 3098.

(213) Becke, A. D. *J. Chem. Phys.* **1993**, *98*, 5648.

(214) Lee, C.; Yang, W.; Parr, R. G. *Phys. Rev. B* **1988**, *37*, 785.

(215) Andrae, D.; Häußermann, U.; Dolg, M.; Stoll, H.; Preuß, H. *Theor. Chim. Acta* **1990**, *77*, 123.

(216) Peng, C. Y.; Schlegel, H. B. *Isr. J. Chem.* **1993**, *33*, 449.

(217) Peng, C. Y.; Ayala, P. Y.; Schlegel, H. B.; Frisch, M. J. *J. Comput. Chem.* **1996**, *17*, 49.

(218) Barone, V.; Cossi, M. *J. Phys. Chem. A* **1998**, *102*, 1995.

(219) Cossi, M.; Rega, N.; Scalmani, G.; Barone, V. *J. Comput. Chem.* **2003**, *24*, 669.

(220) Barone, V.; Cossi, M.; Tomasi, J. *J. Chem. Phys.* **1997**, *107*, 3210.

(221) Wu, Y.; Genest, A.; Rösch, N. *J. Phys. Chem. A* **2014**, DOI: 10.1021/jp5010677.

(222) Perdew, J. P.; Burke, K.; Ernzerhof, M. *Phys. Rev. Lett.* **1996**, *77*, 3865.

(223) Perdew, J. P.; Burke, K.; Ernzerhof, M. *Phys. Rev. Lett.* **1997**, *78*, 1396.

(224) Adamo, C.; Barone, V. *J. Chem. Phys.* **1999**, *110*, 6158.

(225) *Electronic Structure of Solids '91*; Perdew, J. P., Ed.; Akademie Verlag: Berlin, 1991.

(226) Perdew, J. P.; Chevary, J. A.; Vosko, S. H.; Jackson, K. A.; Pederson, M. R.; Singh, D. *Phys. Rev. B* **1992**, *46*, 6671.

(227) Adamo, C.; Barone, V. *J. Chem. Phys.* **1998**, *108*, 664.

(228) Lynch, B. J.; Fast, P. L.; Harris, M.; Truhlar, D. G. *J. Phys. Chem. A* **2000**, *104*, 4811.

(229) Zhao, Y.; Truhlar, D. G. *J. Phys. Chem. A* **2004**, *108*, 6908.

(230) Tao, J.; Perdew, J. P.; Staroverov, V. N.; Scuseria, G. E. *Phys. Rev. Lett.* **2003**, *91*, 146401.

(231) Perdew, J. P. *Phys. Rev. B* **1986**, *33*, 8822.

(232) Perdew, J. P.; Chevary, J. A.; Vosko, S. H.; Jackson, K. A.; Pederson, M. R.; Singh, D. J.; Fiolhais, C. *Phys. Rev. B* **1993**, *48*, 4978.

(233) Perdew, J. P.; Burke, K.; Wang, Y. *Phys. Rev. B* **1996**, *54*, 16533.

(234) Zhao, Y.; Truhlar, D. G. *J. Chem. Phys* **2006**, *125*, 194101.

(235) Zhao, Y.; Truhlar, D. *Theor. Chem. Acc.* **2008**, *120*, 215.

(236) M. J. Frisch, G. W. T., H. B. Schlegel et al. ; Gaussian09 Revision C.01; Gaussian, I., Wallingford CT, 2009; see Appendix.

(237) Boys, S. F.; Bernardi, F. *Mol. Phys.* **1970**, *19*, 553.

(238) NBO Version 3.1, E. D. G., A. E. Reed, J. E. Carpenter, and F. Weinhold.; NBO 3.1 ed.

(239) Foster, J. P.; Weinhold, F. *J. Am. Chem. Soc.* **1980**, *102*, 7211.

(240) Weinhold, F.; Landis, C. R. *Valency and Bonding: A Natural Bond Orbital Donor-Acceptor Perspective*; Cambridge University Press: Cambridge, 2005.

(241) Eyring, H. *J. Chem. Phys.* **1935**, *3*, 107.

(242) Mata, J. A.; Chianese, A. R.; Miecznikowski, J. R.; Poyatos, M.; Peris, E.; Faller, J. W.; Crabtree, R. H. *Organometallics* **2004**, *23*, 1253.

(243) Riederer, S. K. U.; Gigler, P.; Högerl, M. P.; Herdtweck, E.; Bechlars, B.; Herrmann, W. A.; Kühn, F. E. *Organometallics* **2010**, *29*, 5681.

(244) Burdett, J. K. In *Chemical Bonds : A Dialog*; Wiley: 1997, p 131.

(245) Basch, H.; Gray, H. B. *Inorg. Chem.* **1967**, *6*, 365.

(246) Fernandez, M. J.; Bailey, P. M.; Bentz, P. O.; Ricci, J. S.; Koetzle, T. F.; Maitlis, P. M. *J. Am. Chem. Soc.* **1984**, *106*, 5458.

(247) Ruiz, J.; Bentz, P. O.; Mann, B. E.; Spencer, C. M.; Taylor, B. F.; Maitlis, P. M. *J. Chem. Soc., Dalton Trans.* **1987**, 2709.

(248) Ghadwal, R. S.; Azhakar, R.; Proepper, K.; Holstein, J. J.; Dittrich, B.; Rösky, H. W. *Inorg. Chem.* **2011**, *50*, 8502.

(249) Rotzinger, F. P. *Chem. Rev.* **2005**, *105*, 2003.

(250) Sakaki, S.; Ohnizhi, Y.-Y.; Sato, H. *Chem. Rec.* **2010**, *10*, 29.

(251) Sousa, S. F.; Fernandes, P. A.; Ramos, M. J. *J. Phys. Chem. A* **2007**, *111*, 10439.

(252) Beddie, C.; Hall, M. B. *J. Phys. Chem. A* **2005**, *110*, 1416.

(253) Bernardi, F.; Bottoni, A.; Garavelli, M. *Quant. Struct-Act. Rel.* **2002**, *21*, 128.

(254) Bühl, M.; Kabrede, H. *J. Chem. Theory Comput.* **2006**, *2*, 1282.

(255) Bühl, M.; Reimann, C.; Pantazis, D. A.; Bredow, T.; Neese, F. *J. Chem. Theory Comput.* **2008**, *4*, 1449.

(256) Waller, M. P.; Braun, H.; Hojdis, N.; Bühl, M. *J. Chem. Theory Comput.* **2007**, *3*, 2234.

(257) Quintal, M. M.; Karton, A.; Iron, M. A.; Boese, A. D.; Martin, J. M. L. *J. Phys. Chem. A* **2006**, *110*, 709.

(258) Cramer, C. J. *Essentials of Computational Chemistry: Theories and Models*; Wiley, 2013.

(259) Gritsenko, O. V.; Ensing, B.; Schipper, P. R. T.; Baerends, E. J. *J. Phys. Chem. A* **2000**, *104*, 8558.

(260) Grimme, S.; Antony, J.; Ehrlich, S.; Krieg, H. *J. Chem. Phys.* **2010**, *132*, 1541041.

(261) Grimme, S.; Ehrlich, S.; Goerigk, L. *J. Comput. Chem.* **2011**, *32*, 1456.

(262) Junge, K.; Wendt, B.; Enthaler, S.; Beller, M. *ChemCatChem* **2010**, *2*, 453.

(263) Konkol, M.; Kondracka, M.; Voth, P.; Spaniol, T. P.; Okuda, J. *Organometallics* **2008**, *27*, 3774.

(264) Uozumi, Y.; Hayashi, T. *J. Am. Chem. Soc.* **1991**, *113*, 9887.

(265) Hua, Y.; Nguyen, H. H.; Scaggs, W. R.; Jeon, J. *Org. Lett.* **2013**, *15*, 3412.

(266) Molander, G. A.; Dowdy, E. D.; Noll, B. C. *Organometallics* **1998**, *17*, 3754.

(267) Ura, Y.; Gao, G.; Bao, F.; Ogasawara, M.; Takahashi, T. *Organometallics* **2004**, *23*, 4804.

(268) Chung, L. W.; Wu, Y. D.; Trost, B. M.; Ball, Z. T. *J. Am. Chem. Soc.* **2003**, *125*, 11578.

(269) Ding, S.; Song, L.-J.; Chung, L. W.; Zhang, X.; Sun, J.; Wu, Y.-D. *J. Am. Chem. Soc.* **2013**, *135*, 13835.

(270) Beller, M.; Bolm, C.; Wiley: 2004, p 167.

(271) Brønsted, J. N. *Chem. Rev.* **1928**, *5*, 231.

(272) Bell, R. P. *Proc. R. Soc. London, Ser. A* **1936**, *154*, 414.

(273) Evans, M. G.; Polanyi, M. *Trans. Faraday Soc.* **1938**, *34*, 11.

(274) Hammond, G. S. *J. Am. Chem. Soc.* **1955**, *77*, 334.

(275) Wu, Y.; Genest, A.; Rösch, N. **2014**, in preparation.